Nuclear Safety
NEA/CSNI/R(2016)6/VOL1
March 2016
www.oecd-nea.org

Reactivity Initiated Accident (RIA) Fuel Codes Benchmark Phase-II

Volume 1:
Simplified Cases Results Summary and Analysis

OECD
BETTER POLICIES FOR BETTER LIVES

NEA
NUCLEAR ENERGY AGENCY

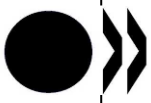

Organisation de Coopération et de Développement Économiques
Organisation for Economic Co-operation and Development

19-Apr-2016

English text only

NUCLEAR ENERGY AGENCY
COMMITTEE ON THE SAFETY OF NUCLEAR INSTALLATIONS

NEA/CSNI/R(2016)6/VOL1
Unclassified

Reactivity Initiated Accident (RIA) Fuel Codes Benchmark Phase-II

Report - Volume 1
Simplified Cases Results
Summary and Analysis

JT03394281

Complete document available on OLIS in its original format

English text only

ORGANISATION FOR ECONOMIC CO-OPERATION AND DEVELOPMENT

The OECD is a unique forum where the governments of 34 democracies work together to address the economic, social and environmental challenges of globalisation. The OECD is also at the forefront of efforts to understand and to help governments respond to new developments and concerns, such as corporate governance, the information economy and the challenges of an ageing population. The Organisation provides a setting where governments can compare policy experiences, seek answers to common problems, identify good practice and work to co-ordinate domestic and international policies.

The OECD member countries are: Australia, Austria, Belgium, Canada, Chile, the Czech Republic, Denmark, Estonia, Finland, France, Germany, Greece, Hungary, Iceland, Ireland, Israel, Italy, Japan, Luxembourg, Mexico, the Netherlands, New Zealand, Norway, Poland, Portugal, the Republic of Korea, the Slovak Republic, Slovenia, Spain, Sweden, Switzerland, Turkey, the United Kingdom and the United States. The European Commission takes part in the work of the OECD.

OECD Publishing disseminates widely the results of the Organisation's statistics gathering and research on economic, social and environmental issues, as well as the conventions, guidelines and standards agreed by its members.

NUCLEAR ENERGY AGENCY

The OECD Nuclear Energy Agency (NEA) was established on 1 February 1958. Current NEA membership consists of 31 countries: Australia, Austria, Belgium, Canada, the Czech Republic, Denmark, Finland, France, Germany, Greece, Hungary, Iceland, Ireland, Italy, Japan, Luxembourg, Mexico, the Netherlands, Norway, Poland, Portugal, the Republic of Korea, the Russian Federation, the Slovak Republic, Slovenia, Spain, Sweden, Switzerland, Turkey, the United Kingdom and the United States. The European Commission also takes part in the work of the Agency.

The mission of the NEA is:

- to assist its member countries in maintaining and further developing, through international co-operation, the scientific, technological and legal bases required for a safe, environmentally friendly and economical use of nuclear energy for peaceful purposes;
- to provide authoritative assessments and to forge common understandings on key issues, as input to government decisions on nuclear energy policy and to broader OECD policy analyses in areas such as energy and sustainable development.

Specific areas of competence of the NEA include the safety and regulation of nuclear activities, radioactive waste management, radiological protection, nuclear science, economic and technical analyses of the nuclear fuel cycle, nuclear law and liability, and public information.

The NEA Data Bank provides nuclear data and computer program services for participating countries. In these and related tasks, the NEA works in close collaboration with the International Atomic Energy Agency in Vienna, with which it has a Co-operation Agreement, as well as with other international organisations in the nuclear field.

COMMITTEE ON THE SAFETY OF NUCLEAR INSTALLATIONS

The NEA Committee on the Safety of Nuclear Installations (CSNI) is an international committee made up of senior scientists and engineers with broad responsibilities for safety technology and research programmes, as well as representatives from regulatory authorities. It was created in 1973 to develop and co-ordinate the activities of the NEA concerning the technical aspects of the design, construction and operation of nuclear installations insofar as they affect the safety of such installations.

The committee's purpose is to foster international co-operation in nuclear safety among NEA member countries. The main tasks of the CSNI are to exchange technical information and to promote collaboration between research, development, engineering and regulatory organisations; to review operating experience and the state of knowledge on selected topics of nuclear safety technology and safety assessment; to initiate and conduct programmes to overcome discrepancies, develop improvements and reach consensus on technical issues; and to promote the co-ordination of work that serves to maintain competence in nuclear safety matters, including the establishment of joint undertakings.

The priority of the CSNI is on the safety of nuclear installations and the design and construction of new reactors and installations. For advanced reactor designs, the committee provides a forum for improving safety-related knowledge and a vehicle for joint research.

In implementing its programme, the CSNI establishes co-operative mechanisms with the NEA Committee on Nuclear Regulatory Activities (CNRA), which is responsible for issues concerning the regulation, licensing and inspection of nuclear installations with regard to safety. It also co-operates with other NEA Standing Technical Committees, as well as with key international organisations such as the International Atomic Energy Agency (IAEA), on matters of common interest.

ACKNOWLEDGEMENTS

This report is prepared by the RIA Benchmark Phase II Task Group of the Working Group of Fuel Safety (WGFS).

Special gratitude is expressed to Olivier Marchand (IRSN, France) for drafting the report, to Pierre Ruyer (IRSN, France) for his efforts in drafting Chapter 0 of the report, as well as to Marco Cherubini (NINE, Italy), Vincent Georgenthum (IRSN, France), Luis Enrique Herranz (CIEMAT, Spain), Lars Olof Jernkvist (Quantum Technologies, Sweden), Marc Petit (IRSN, France), Patrick Raynaud (NRC, USA) and Jinzhao Zhang (TRACTEBEL, Belgium) for reviewing the report.

The following WGFS members and experts performed calculations and provided valuable input to various chapters of the report:

Asko ARKOMA,VTT, Finland
Felix BOLDT, GRS, Germany
Heng BAN, INL, United States
Marco CHERUBINI, NINE, Italy
Adrien DETHIOUX, Tractebel (ENGIE), Belgium
Thomas DRIEU, Tractebel (ENGIE), Belgium
Charles FOLSOM, INL, United States
Vincent GEORGENTHUM, IRSN, France
Patrick GOLDBRONN, CEA, France
Luis Enrique HERRANZ, CIEMAT, Spain
Lars Olof JERNKVIST, Quantum Technologies, Sweden
Hyedong JEONG, KINS, Korea
Jan KLOUZAL, UJV, Czech Republic
Olivier MARCHAND, IRSN, France
István PANKA, MTA EK, Hungary
Patrick RAYNAUD, NRC, United States
José M. REY GAYO, CSN, Spain
Pierre RUYER, IRSN, France
Inmaculada C. SAGRADO GARCIA, CIEMAT, Spain
Jérôme SERCOMBE, CEA, France,
Heinz Günther SONNENBERG, GRS, Germany
Gerold SPYKMAN, TÜV NORD, Germany
Yutaka UDAGAWA, JAEA, Japan
Jinzhao ZHANG, Tractebel (ENGIE), Belgium

LIST OF ABBREVIATIONS AND ACRONYMS

BWR	Boiling-water reactor
CABRI	Test reactor in France
CIEMAT	Centro de Investigaciones Energéticas, Medioambientales y Tecnológicas (Spain)
CSN	Consejo de seguridad nuclear (Spain)
CSNI	Committee on the Safety of Nuclear Installations (NEA)
CZP	Cold Zero Power
DNB	Departure from nucleate boiling
FGR	Fission-gas release
FWHM	Full Width at Half Maximum
GRS	Gesellschaft für Anlagen- und Reaktorsicherheit (Germany)
HZP	Hot Zero Power
INL	Idaho National Laboratory (United States)
IRSN	Institut de radioprotection et de sûreté nucléaire (France)
JAEA	Japan atomic energy agency
KINS	Korean Institute of Nuclear safety
MOX	Mixed oxide fuel (U and Pu)
MTA EK	Centre of Energy Research, Hungarian Academy of Sciences
NEA	Nuclear Energy Agency (OECD)
NINE	Nuclear and INdustrial Engineering (Italy)
NRC	Nuclear Regulatory Commission (United States)
NSRR	Nuclear safety research reactor (Japan)
OECD	Organisation for Economic Co-operation and Development
PCMI	Pellet-cladding mechanical interaction
PWR	Pressurised-water reactor
RIA	Reactivity-initiated accident
SSM	Strålsäkerhetsmyndigheten (Swedish Radiation Safety Authority)
TRACTEBEL	Tractebel Engineering (ENGIE)

TSO	Technical Support Organisation
TUV	Technischer überwachungsverein (Germany)
UJV	Nuclear research institute (Czech Republic), ÚJV Řež
VTT	Valtion Teknillinen Tutkimuskeskus/Technical Research Centre of Finland
WGFS	Working Group on Fuel Safety (NEA/CSNI)
xD	x-dimensional (where x is for 1.5, 2 and 3)

TABLE OF CONTENTS

LIST OF FIGURES 9
LIST OF TABLES 12
EXECUTIVE SUMMARY 13
1. BACKGROUND AND INTRODUCTION 17
2. SUMMARY OF SPECIFICATIONS 21
3. PARTICIPANTS AND CODES USED 25
4. RESULTS SUMMARY AND ANALYSIS 29
4.1 Use of input data 29
4.2 Thermal behaviour 30
4.2.1 Analysis of initial state 30
4.2.2 Analysis of overall transient behaviour 32
4.2.3 Analysis of heat-up phase 42
4.3 Mechanical behaviour 45
4.3.1 Analysis of initial state 46
4.3.2 Analysis of overall transient behaviour 48
4.3.3 Analysis of heat-up phase 58
4.3.4 Influence of clad temperature 63
4.3.5 Influence of clad/fuel modelling 64
5. RIA THERMAL HYDRAULICS – STATE-OF-THE-ART REVIEW 69
5.1 Introduction 69
5.2 High clad temperature transients during a RIA 70
5.2.1 Quantities of interest 70
5.2.2 A high temperature phase that appears for large enthalpy insertion 70
5.2.3 Main difficulties to model the heat transfer coefficient 73
5.2.4 Partial conclusion 75
5.3 Boiling flows of interest for RIA-related heat transfer 75
5.3.1 The onset of boiling 75
5.3.2 Nucleate boiling 75
5.3.3 Departure from Nucleate boiling 76
5.3.4 Film boiling 76
5.3.5 Rewetting 78
5.3.6 Wettability of the fluid onto the wall and boiling 78
5.3.7 Models for the boiling curve 78
5.4 Analysis of the different phases of the RIA-related boiling heat transfer 79
5.4.1 Till the peak heat flux 79
5.4.2 Transition toward film boiling and peak cladding temperature 80
5.4.3 Film boiling till quenching 81

5.5 Conclusion....84
6. CONCLUSIONS AND RECOMMENDATIONS....85
7. REFERENCES....87
8. APPENDIX I: GENERAL DESCRIPTION OF THE CODES....92
8.1 ALCYONE V1.4....93
8.2 BISON....95
8.3 FRAPTRAN....96
8.4 RANNS....98
8.5 SCANAIR....99
8.6 TESPAROD....101
8.7 TRANSURANUS....103
9. APPENDIX II: SPECIFIC DESCRIPTION OF THERMAL HYDRAULICS MODELS USED IN CODES....105
9.1 ALCYONE....105
9.2 BISON....106
9.3 FRAPTRAN....109
9.3.1 Standard Version....109
9.3.2 TRABCO coupling....110
9.4 RANNS....111
9.5 SCANAIR....115
9.5.1 Standard Version....115
9.5.2 QT-COOL Model....124
9.6 TESPAROD....126
9.7 TRANSURANUS....128

LIST OF FIGURES

Figure 2.1: Rod design 21
Figure 4.1: Case No. 8 – Energy Injected..... 30
Figure 4.2: Variation of Radial Average Enthalpy at beginning of transient for all Cases 31
Figure 4.3: Temperature of Fuel Centreline at beginning of transient for all Cases 31
Figure 4.4: Temperature of Clad Outer Surface at beginning of transient for all Cases 32
Figure 4.5: Case No. 4 – Variation of Radial Average Enthalpy 33
Figure 4.6: Case No. 5 – Variation of Radial Average Enthalpy 33
Figure 4.7: Case No. 6 – Variation of Radial Average Enthalpy 34
Figure 4.8: Case No. 7 – Variation of Radial Average Enthalpy 34
Figure 4.9: Case No. 4 – Temperature of Fuel Centreline..... 35
Figure 4.10: Case No. 5 – Temperature of Fuel Centreline..... 35
Figure 4.11: Case No. 6 – Temperature of Fuel Centreline..... 36
Figure 4.12: Case No. 7 – Temperature of Fuel Centreline..... 36
Figure 4.13: Variation of Radial Average Enthalpy – Values of Maximum for all Cases..... 37
Figure 4.14: Temperature of Fuel Centreline – Values of Maximum for all Cases 37
Figure 4.15: Case No. 4 – Temperature of Clad Outer Surface 39
Figure 4.16: Case No. 5 – Temperature of Clad Outer Surface 39
Figure 4.17: Case No. 6 – Temperature of Clad Outer Surface 40
Figure 4.18: Case No. 7 – Temperature of Clad Outer Surface 40
Figure 4.19: Temperature of Clad Outer Surface – Values of Maximum for all Cases 41
Figure 4.20: Boiling Duration – Values for all Cases 41
Figure 4.21: Case No. 2 – Temperature of Fuel Centreline (Heat-up Phase)..... 42
Figure 4.22: Temperature of Fuel Centreline – Values at end of Heat-up Phase for all Cases (Heat-up Phase)..... 43
Figure 4.23: Case No. 1 – Temperature of Fuel Outer Surface (Heat-up Phase) 43
Figure 4.24: Case No. 2- Temperature of Fuel Outer Surface (Heat-up Phase)..... 44
Figure 4.25: Temperature of Fuel Outer Surface – Values at end of Heat-up Phase for all Cases 44
Figure 4.26: Case No. 7 – Temperature of Clad Outer Surface (Heat-up Phase)..... 45
Figure 4.27: Temperature of Clad Outer Surface – Values at end of Heat-up Phase for all Cases..... 45
Figure 4.28: Clad Total Hoop Strain at beginning of transient for all Cases 46
Figure 4.29: Fuel Outer Radius – relative variation at beginning of transient for all Cases 47
Figure 4.30: Clad Total Stress at beginning of transient for all Cases 47
Figure 4.31: Case No. 1 – Clad Total Hoop Strain..... 48
Figure 4.32: Case No. 5 – Clad Total Hoop Strain..... 49
Figure 4.33: Clad Total Hoop Strain – Values of Maximum for all Cases 49
Figure 4.34: Gap Opening Time for all Cases..... 50
Figure 4.35: Fuel outer Radius – Values of Maximum of relative variation for all Cases..... 50
Figure 4.36: Case No. 8 – Free Volume Pressure 51
Figure 4.37: Case No. 1 – Fuel Total Axial Elongation 52
Figure 4.38: Case No. 5 – Fuel Total Axial Elongation 52
Figure 4.39: Fuel Total Axial Elongation – Values of Maximum for all Cases..... 53

Figure 4.40: Case No. 1 – Clad Total Axial Elongation 53
Figure 4.41: Case No. 5 – Clad Total Axial Elongation 54
Figure 4.42: Clad Total Axial Elongation – Values of Maximum for all Cases 54
Figure 4.43: Case No. 1 – Gap Width 55
Figure 4.44: Case No. 5 – Gap Width 55
Figure 4.45: Case No. 3 – Gap Width 56
Figure 4.46: Clad Hoop Stress – Values of Maximum for all Cases 57
Figure 4.47: Case No. 1 – Clad Hoop Stress 57
Figure 4.48: Case No. 2– Clad Hoop Stress 58
Figure 4.49: Case No. 1 – Clad Total Hoop Strain (Heat-up Phase) 59
Figure 4.50: Clad Total Hoop Strain – Values at end of Heat-up Phase for all Cases 59
Figure 4.51: Case No. 2 – Clad Total Axial Elongation (Heat-up Phase) 60
Figure 4.52: Clad Total Axial Elongation – Values at end of Heat-up Phase for all Cases 60
Figure 4.53: Case No. 3 – Fuel Total Axial Elongation (Heat-up Phase) 61
Figure 4.54: Fuel Total Elongation – Values at end of Heat-up Phase for all Cases 61
Figure 4.55: Case No. 2 – Clad Hoop Stress (Heat-up Phase) 62
Figure 4.56: Clad Hoop Stress – Values at end of Heat-up Phase for all Cases 62
Figure 4.57: Case No. 5 – Clad Total Hoop Strain 63
Figure 4.58: Case No. 9 – Clad Total Hoop Strain 64
Figure 4.59: Case No. 10 – Clad Total Hoop Strain 65
Figure 4.60: Case No. 10 – Clad Total Elongation 65
Figure 4.61: Case No. 10 – Fuel Total Elongation 66
Figure 4.62: Case No. 10 – Clad Total Hoop Stress 66
Figure 4.63: Case No. 10 – Clad Total Hoop Stress (Heat-up Phase) 67
Figure 5.1: Maximum cladding surface temperature measurements for different fuel pellet enrichment, stagnant flow [3] 70
Figure5.2: Cladding temperature evolution recorded on NSRR test 103-31-1 (0.1MPa, stagnant water at 90°C) and NSRR power (dashed line centre plot) [3]. 71
Figure 5.3: Schematic view of the experimental boiling curve in the NSRR tests, [4]. 72
Figure 5.4: Variation of the CHF versus the maximum linear heat rate in the NSRR Surface Effect Tests, [4]. 72
Figure 5.5: Comparison of inverse-heat-conduction calculation results with correlation by Shiotsu for forced flow condition, [6] 74
Figure 5.6: Scheme of the different flow boiling regimes for the cooling of hot rods thanks to a bottom-up liquid flooding rate [9]. 77
Figure 5.7: 253-3 (solid line) and 103-31-1 (dashed line) NSRR test cladding to coolant heat flux versus time, [3] 79
Figure 5.8: Peak temperatures at fuel rod surface for test Cases with fresh fuels conducted under the conditions of stagnant coolant, atmospheric coolant pressure, and varied coolant subcoolings. Legends with an asterisk like “Fresh*” denotes the result of the 2nd, 3rd, or the latter pulse irradiation in an iterative pulse-irradiation experiment in which a series of pulse-irradiations had been conducted on an identical test fuel rod, [6]. 81
Figure 5.9: Transient records of cladding surface temperature, [21]. 82
Figure 5.10: Maximum cladding surface temperature measurements for fresh and irradiated fuels [3]. 83
Figure 5.11: Film boiling duration measured for different coolant flow [3]. 83
Figure 8.1: ALCYONE – Different schemes 94
Figure 8.2: FRAPTRAN – Locations at which fuel rod variables are evaluated 98
Figure 8.3: Development overview of fuel analysis code in JAEA 98
Figure 8.4: FEMAXI – RANNS analytical geometry 99
Figure 8.5: Overview diagram of data flow between the different SCANAIR modules 99
Figure 9.1: FRAPTRAN – Relation of surface heat flux to surface temperature 109

Figure 9.2: TRABCO/FRAPTRAN coupling scheme 111
Figure 9.3: Heat transfer regimes assumed in the RANNS model for heat transfer from fuel rod surface to coolant water 111
Figure 9.4: SCANAIR – Standard Clad to coolant heat flux phases 115
Figure 9.5: Heat Transfer modes of TESPAROD shown in a Nukijama curve 126
Figure 9.6: Transuranus – Clad surface and liquid temperature distribution in single-phase, subcooled and saturated boiling. ONB = onset of subcooled nucleate boiling. 130

LIST OF TABLES

Table 2.1: Summary of Cases 23
Table 2.2: List of parameters to be provided 24
Table 3.1: Benchmark collected contributions 27
Table 9.1: FRAPTRAN – Heat transfer mode selection and correlations 110
Table 9.2: SCANAIR – cladding-to-coolant heat transfer correlations available in QT-COOL 125
Table 9.3: SCANAIR – Correlations for critical heat flux available in QT-COOL. 125

EXECUTIVE SUMMARY

Reactivity-initiated accident (RIA) fuel rod codes have been developed for a significant period of time and validated against their own available database. However, the high complexity of the scenarios dealt with has resulted in a number of different models and assumptions adopted by code developers; additionally, databases used to develop and validate codes have been different depending on the availability of the results of some experimental programmes. This diversity makes it difficult to find the source of estimate discrepancies, when these occur.

A technical workshop on "Nuclear Fuel Behaviour during Reactivity Initiated Accidents" was organized by the NEA in September 2009. As a conclusion of the workshop, it was recommended that a benchmark (RIA benchmark Phase I) between these codes be organized in order to give a sound basis for their comparison and assessment. This recommendation was endorsed by the Working Group on Fuel Safety.

The RIA benchmark Phase I was organized in 2010-2013. It consisted of a consistent set of four experiments on very similar highly irradiated fuel rods tested under different experimental conditions (NSRR VA-1, VA-3, CABRI CIP0-1 and CIP3-1). Seventeen organizations from fourteen countries participated in the Phase I, using eight different fuel rod codes.

The main conclusions of this RIA benchmark Phase I were the following:

- With respect to the thermal behaviour, the differences in the evaluation of fuel temperatures remained limited, although significant in some cases. The situation was very different for the cladding temperatures that exhibited considerable scatter, in particular for the cases when water boiling occurred.
- With respect to mechanical behaviour, the parameter of greatest interest was the cladding hoop strain because failure during RIA transient results from the formation of longitudinal cracks. When compared to the results of an experiment that involved only PCMI, the predictions from the different participants appeared acceptable even though there was a factor of 2 between the highest and the lowest calculations. The conclusion was not so favourable for cases where water boiling had been predicted to appear: a factor of 10 for the hoop strain between the calculations was exhibited. Other mechanical results compared during the RIA benchmark Phase I were fuel stack and cladding elongations. The scatter remained limited for the fuel stack elongation, but the cladding elongation was found to be much more difficult to evaluate.
- The fission-gas release evaluations were also compared. The ratio of the maximum to the minimum values appeared to be roughly 2, which is considered to be relatively moderate given the complexity of fission-gas release processes.

As a conclusion of the RIA benchmark Phase I, it was recommended to launch a second-phase exercise with the following specific guidelines:

- The emphasis should be put on deeper understanding of the differences in modelling of the different codes; in particular, looking for simpler cases than those used in the first exercise was expected to reveal the main reasons for the observed large scatter in some conditions such as coolant boiling.
- Due to the large scatter between the calculations that was shown in the RIA benchmark Phase I, it appears that an assessment of the uncertainty of the results should be performed for the different codes. This should be based on a well-established and shared methodology. This also entailed performing a sensitivity study of results to input parameters to assess the impact of initial state of the rod on the final outcome of the power pulse.

The Working Group on Fuel Safety endorsed these recommendations and a second phase of the RIA fuel-rod-code benchmark (RIA benchmark Phase II) was launched early in 2014. This RIA benchmark Phase II has been organized as two complementary activities:

- The first activity is to compare the results of different simulations on simplified cases in order to provide additional bases for understanding the differences in modelling of the concerned phenomena.
- The second activity is focused on the assessment of the uncertainty of the results. In particular, the impact of the initial states and key models on the results of the transient are to be investigated.

The present report provides a summary and documents the conclusions and recommendations from the first activity.

Participation in the RIA benchmark Phase II has been very remarkable: 15 organizations representing 12 countries have provided analyses for some or all the cases that were defined. In terms of computer codes used, the spectrum was also large as analyses were performed with ALCYONE, BISON, FRAPTRAN, RANNS, SCANAIR, TESPAROD, and TRANSURANUS.

Following the recommendations from Phase I, ten simplified cases have been defined with an increasing degree of complexity to assess the different phenomena step by step. To avoid possible differences due to the evaluation of the initial state of an irradiated fuel, the cases have been limited to fresh fuel. The studied cases cover both PWR and BWR typical conditions. More than 20 computed values have been compared between the different codes.

By comparing the results provided by participants, it has been possible to draw the following conclusions:

- With respect to the fuel thermal behaviour, the differences in the estimation of fuel enthalpies and temperatures are rather limited especially for maximum values of these parameters. However, the agreement is worse for BWR thermal-hydraulic conditions than PWR thermal-hydraulic conditions that lead to water boiling. This seems to be mainly driven by uncertainty in the clad-to-coolant heat transfer.
- Concerning cladding temperatures, considerable scatter is obtained for the cases where water boiling occurs. This scatter is clearly related to the clad-to-coolant heat transfer modelling. Boiling in RIA conditions is known to be significantly different than in steady-state conditions. Some codes assume that the steady-state correlations are applicable to RIA conditions while other codes use specific fast-transient correlations (for critical heat flux, heat exchange in film

boiling, rewetting conditions, etc.). Given the lack of sufficient experimental investigation on boiling in RIA conditions, no sound recommendation can be made as for which correlations are the most suitable ones to use.

- From cases devoted to BWR conditions, it is clear that very few (if any) of the applied computer codes are able to handle the thermal-hydraulic conditions expected in a BWR RIA with large energy injection at cold, zero-power conditions. This is not simply a question of uncertainties in the clad-to-coolant heat transfer modelling; the excessive steam generation expected in the fuel assembly at atmospheric pressure can obviously not be handled by the simple thermal-hydraulic models in the codes.
- With respect to mechanical behaviour, the loading mode of the cladding considered during this benchmark exercise is limited to the PCMI one.
- Although the general behaviour is similar from one case to another, and although the agreement between predictions is reasonable during the heating phase, significant discrepancies are obtained for the maxima of different variables of interest (namely clad hoop strain, fuel and clad elongation and clad hoop stress), and for long-term evolution of many parameters. The difference between upper and lower values reaches almost 200% (of the mean value) for the clad hoop stress and is between 25 and 75% for clad hoop strain and fuel and clad elongations.
- The reasons for this disagreement can only be partly attributed to model approaches and specific formulations; dependency on key boundary conditions for clad loading, such as the gap closure/opening, is also heavily involved.

Based on the conclusions of Phases I and II summed up above, some generic recommendations can be made:

- Fuel and clad thermomechanical models (with the associated material properties) should be further improved and validated more extensively against a sound RIA database.
- Build-up of a comprehensive and robust database consisting of both separate-effect tests and integral tests should be pursued in the short term. In this way, both individual model validation and model integration into codes would be feasible.
- An assessment of the uncertainty of fuel thermo-mechanics is of high interest, which is consistent with the second activity of this RIA benchmark Phase II.

Some more specific recommendations can be also added:

- The clad-to-coolant heat transfer in the case of water boiling during very fast transients is of particular interest, and capabilities related to modelling this phenomenon should be improved. To achieve this target regarding clad-to-coolant heat transfer, more separate-effect tests and experiments seem necessary.
- Models related to the evolution of the gap between fuel and clad should be improved and validated in RIA conditions as this has been shown to have a significant effect on fuel rod response. To reach this objective, in-reactor measurements of cladding strain during RIA simulation tests should be done (or at least attempted).

Finally, as RIA fuel codes are more and more likely to be used for reactor accident studies, particularly for those involving safety analyses, the fuel rod failure criteria (generally used in such analyses) will have to be carefully justified and validated.

Such fuel rod failure criteria can in general be described in terms of:

- thermal variables (e.g., fuel enthalpy, variation of fuel enthalpy);
- mechanical variables (e.g., clad hoop strain, clad hoop stress).

The current RIA fuel failure criteria are mainly based on the fuel thermal variables and the verification is based on “conservative” assumptions for the heat transfer conditions. As all codes give rather consistent evaluations of such variables, it appears possible, taking into account adequate provisions, to derive criteria based on thermal variables from experimental values or from an analytical approach.

However, if in the future more mechanistic modelling is ever to be used to establish fuel-failure criteria based on mechanical variables, the codes will have to be further improved and validated for all the aspects identified above.

The assessment of the uncertainty and sensitivity of the results expected in the second task of this RIA benchmark Phase II will provide more insights on the important input parameters and models to be considered.

1 BACKGROUND AND INTRODUCTION

Reactivity-initiated accident (RIA) fuel rod codes have been developed for a significant period of time and validated against their own available database. However, the high complexity of the scenarios dealt with has resulted in a number of different models and assumptions adopted by code developers; additionally, databases used to develop and validate codes have been different depending on the availability of the results of some experimental programmes. This diversity makes it difficult to find the source of estimate discrepancies, when these occur.

A technical workshop on "Nuclear Fuel Behaviour during Reactivity Initiated Accidents" was organized by the NEA in September 2009. A major highlight from the session devoted to RIA safety criteria was that RIA fuel rod codes are now widely used, within the industry as well as the technical safety organizations (TSOs), in the process of setting up and assessing revised safety criteria for the RIA design basis accident. This turns mastering the use of these codes into an outstanding milestone, particularly in safety analyses. To achieve that, a thorough understanding of the codes predictability is mandatory.

As a conclusion of the workshop, it was recommended that a benchmark (RIA benchmark Phase I) between these codes be organized in order to give a sound basis for their comparison and assessment. This recommendation was endorsed by the Working Group on Fuel Safety.

In order to maximize the benefits from this RIA benchmark Phase I exercise, it was decided to use a consistent set of four experiments on very similar highly irradiated fuel rods tested under different experimental conditions:

- low temperature, low pressure, stagnant water coolant, very short power pulse (NSRR VA-1),
- high temperature, medium pressure, stagnant water coolant, very short power pulse (NSRR VA-3),
- high temperature, low pressure, flowing sodium coolant, larger power pulse (CABRI CIP0-1),
- high temperature, high pressure, flowing water coolant, medium width power pulse (CABRI CIP3-1).

The main conclusions of this RIA benchmark Phase I are the following [1]:

- With respect to the thermal behaviour, the differences in the evaluation of fuel temperatures remained limited, although significant in some cases. The situation was very different for the cladding temperatures that exhibited considerable scatter, in particular for the cases when water boiling occurred.
- With respect to mechanical behaviour, the parameter of largest interest was the cladding hoop strain because failure during RIA transient results from the formation of longitudinal cracks. When compared to the results of an experiment that involved only PCMI, the predictions from

the different participants appeared acceptable even though there was a factor of 2 between the highest and the lowest calculations. The conclusion was not so favourable for cases where water boiling had been predicted to appear: a factor of 10 for the hoop strain between the calculations was exhibited. Other mechanical results compared during the RIA benchmark Phase I were fuel stack and cladding elongations. The scatter remained limited for the fuel stack elongation, but the cladding elongation was found to be much more difficult to evaluate.

- The fission-gas release evaluations were also compared. The ratio of the maximum to the minimum values appeared to be roughly 2, which is considered to be relatively moderate given the complexity of fission gas release processes.
- Failure predictions, which may be considered as the ultimate goal of fuel code dedicated to the behaviour in RIA conditions, were compared: it appears that the failure/no failure predictions are fairly consistent between the different codes and with experimental results. However, when assessing the code qualification, one should rather look at predictions in terms of enthalpy at failure because it is a parameter that may vary significantly between different predictions (and is also of interest in practical reactor applications). In the frame of this RIA benchmark Phase I the failure prediction levels among the different codes were within a +/- 50% range. A detailed and complete RIA benchmark Phase I specification was prepared in order to assure as much as possible the comparability of the calculation results submitted.

As a conclusion of the RIA benchmark Phase I, it was recommended to launch a second phase exercise with the following specific guidelines:

- The emphasis should be put on deeper understanding of the differences in modelling of the different codes; in particular, looking for simpler cases than those used in the first exercise was expected to reveal the main reasons for the observed large scatter in some conditions such as coolant boiling.
- Due to the large scatter between the calculations that was shown in the RIA benchmark Phase I, it appears that an assessment of the uncertainty of the results should be performed for the different codes. This should be based on a well-established and shared methodology. This also entailed performing a sensitivity study of results to input parameters to assess the impact of initial state of the rod on the final outcome of the power pulse.

The Working Group on Fuel Safety endorsed these recommendations and a second phase of the RIA fuel-rod-code benchmark (RIA benchmark Phase II) was launched early in 2014. This RIA benchmark Phase II has been organized as two complementary activities:

- The first activity is to compare the results of different simulations on simplified cases in order to provide additional bases for understanding the differences in modelling of the concerned phenomena.
- The second activity is focused on the assessment of the uncertainty of the results. In particular, the impact of the initial states and key models on the results of the transient are to be investigated.

The present report provides a summary and documents the conclusions and recommendations from the first activity.

A detailed and complete RIA benchmark Phase II specification was prepared in order to ensure as much as possible the comparability of the calculation results submitted. The specifications regarding the first activity are compiled in the Volume 2 of the present report.

The complete set of solutions provided by all the participants are compiled in an unpublished WGFS report.

This document is organized as follows:

- Chapter 1 (this Chapter) is a short introduction of this RIA benchmark Phase II;
- Chapter 2 gives a short description of the specifications for this RIA benchmark Phase II;
- Chapter 3 presents the participants and the codes they used;
- Chapter 0 discusses the main findings and is illustrated by selected plots comparing the solutions provided by the participants;
- Chapter 0 is a state of the art review regarding RIA thermal hydraulics;
- Chapter 0 gives the conclusions of the RIA benchmark Phase II exercise and provides some recommendations for follow-up activities;
- APPENDIX I gives a general description of the fuel codes used;
- APPENDIX II presents thermal-hydraulic models used in codes.

2. SUMMARY OF SPECIFICATIONS

The objective of this first part of the RIA benchmark Phase II is to compare the results of different simulations on simplified Cases, in order to better understand the differences in modelling of the concerned specific phenomena.

Ten Cases were defined with an increasing degree of complexity to assess the different phenomena step by step.

The first Case is mainly devoted to the thermal behaviour, the second and third Cases are focused on the thermo-mechanical behaviour, and in the last five Cases the thermal-hydraulics behaviour aspect is added.

For each code, it is recommended to use the standard options for all models except for the failure model, fuel relocation model, and high temperature cladding oxidation model, which must be disabled (considering the proposed problems). In one Case thermal and thermal-mechanical properties/models for clad and fuel should be imposed as close as possible to those of FRAPTRAN.

To limit the differences linked to the initial state of the fuel, the Cases are limited to a fresh 17x17 PWR type fuel rod as described in the Figure 2.1. In all Cases, starting from ambient conditions, a stabilisation phase is simulated before the real transient phase in order to reach the foreseen initial state of the rod.

Two different values for the clad inner radius are used to impose the presence or absence of an initial gap between the fuel and the clad. In most of the Cases, the fuel and the clad are considered bonded (no slipping between the fuel and the clad is assumed) except for one Case where perfect slipping between the fuel and the clad is assumed as contact condition.

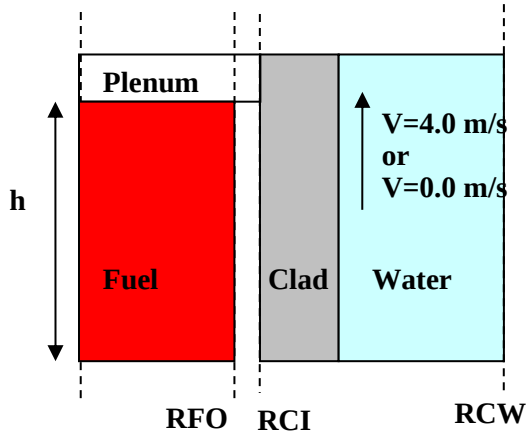

Fuel outer radius (RFO) = 4.13 mm
Clad inner radius (RCI) = 4.13 or 4.18 mm
Clad thickness = 570 µm
Water canal radius (RCW) = 7.5 mm
Upper plenum volume =2 cm^3
Fuel height (h) = 10 cm

Figure 2.1: Rod design

Depending on the Case, the thermal-hydraulics conditions during transient could be:

- water coolant in nominal PWR hot zero power (HZP) conditions (coolant inlet conditions: Pcool=155 bar, Tcool=280°C at Vcool=4 m/s),referred as “PWR conditions”,
- water coolant in BWR cold zero power (CZP) conditions (coolant inlet conditions: Pcool=1 bar, Tcool=20°C at Vcool=0.0 m/s), referred as “BWR conditions”,
- imposed coolant bulk temperature (Tbulk=300°C during the first 5 seconds, then Tbulk=Tcool=280°C till the end of transient); imposed to clad to coolant heat transfer coefficient (Htrans=4000 W/m2/K during the first 5 seconds, then Htrans=Hsteady=40000 W/m2/K till the end of transient) and external pressure at 155 bar (Pcool), referred as “imposed conditions”,
- imposed external clad temperature at 280°C (Tcool) and external pressure at 155 bar (Pcool), referred as “fixed conditions”.

The pulse will start from zero power and it is considered to have a triangular shape, with 30 ms of Full Width at Half Maximum (FWHM) and two values for the rod maximal power in the fuel is considered:

- a low value to avoid DNB occurrence;
- a high value to provoke DNB occurrence.

The axial and radial profiles in the fuel are assumed to be flat.

Finally, the initial helium pressure in free volume is increased in one Case.

Table 2.1 summarizes all Cases and detailed specifications are presented in Volume 2 of the report. All requested variables are presented in Table 2.2.

		Geometry		Contact Conditions		**Thermomechanical Models**		**Thermal Hydraulic Conditions**				**Pmax**		**Helium Pressure**	
		No gap	Open gap	No Slipping	Slipping	Standard	Imposed	Fixed	PWR	BWR	Imposed	Low	High	Low	High
Thermal	Case No. 1	X		X		X		X					X	X	
Mechanical	Case No. 2		X	X		X		X					X	X	
	Case No. 3		X		X	X		X					X	X	
	Case No. 10		X	X			X	X					X	X	
Thermal Hydraulic	Case No. 6	X		X		X				X		X		X	
	Case No. 7	X		X		X				X			X	X	
	Case No. 4	X		X		X			X			X		X	
	Case No. 5	X		X		X			X				X	X	
	Case No. 8	X		X		X			X				X		X
	Case No. 9	X		X		X					X		X	X	

Table 2.1: Summary of Cases

Parameter	Unit	Description
EDR	cal/g	Energy Injected in the whole rodlet as a function of time
DHR	cal/g	Variation of radial average enthalpy with respect to initial conditions of the transient in the rodlet as a function of time (at z=h/2) (NB: DHR(t=0)=0)
TFC	°C	Temperature of fuel centreline as a function of time (at z=h/2)
TFO	°C	Temperature of fuel outer surface as a function of time (at z=h/2)
TCI	°C	Temperature of clad inner surface as a function of time (at z=h/2)
TCO	°C	Temperature of clad outer surface as a function of time (at z=h/2)
ECMH	%	Clad mechanical (elastic + plastic) hoop strain at the outer part of the clad as a function of time (at z=h/2)
ECMZ	%	Clad mechanical (elastic + plastic) axial strain at the outer part of the clad as a function of time (at z=h/2)
ECTH	%	Clad total (thermal + elastic + plastic) hoop strain at the outer part of the clad as a function of time(at z=h/2)
ECTZ	%	Clad total (thermal + elastic + plastic) axial strain at the outer part of the clad as a function of time(at z=h/2)
ECT	mm	Clad total axial elongation as a function of time
EFT1	mm	Fuel column total axial elongation as a function of time
EFT2	mm	Fuel column thermal axial elongation as a function of time
SCH	MPa	Clad hoop stress at outer part of the clad as a function of time (at z=h/2)
SCZ	MPa	Clad axial stress at outer part of the clad as a function of time (at z=h/2)
RFO	mm	Fuel outer radius as a function of time (at z=h/2)
RCI	mm	Clad inner radius as a function of time (at z=h/2)
HFC	$W/m^2/K$	Fuel to clad heat transfer coefficient as a function of time (at z=h/2)
HCW	$W/m^2/K$	Clad to water heat transfer coefficient as a function of time (at z=h/2)
PG	bar	Free volume pressure as a function of time
VOL	mm^3	Free Volume as a function of time (including open porosity)

Table 2.2: List of parameters to be provided

3. PARTICIPANTS AND CODES USED

The participation to the RIA benchmark Phase II has been very important because 15 organizations provided solutions for some or all the Cases that were defined.

The participants originated from 12 countries and are listed below:

- Tractebel Engineering – ENGIE (Tractebel) from Belgium,
- ÚJV Řež (UJV) from the Czech Republic,
- Institut de Radioprotection et de Sûreté Nucléaire (IRSN) and Commissariat à l'énergie atomique et aux énergies alternatives (CEA) from France,
- TÜV NORD Group (TUV) and Gesellschaft für Anlagen- und Reaktorsicherheit mbH (GRS) from Germany,
- Centre of Energy Research, Hungarian Academy of Sciences (MTA-EK) from Hungary,
- Nuclear and INdustrial Engineering (NINE) (initially Università di Pisa) from Italy[1],
- Japan Atomic Energy Agency (JAEA) from Japan,
- Korea Institute of Nuclear Safety (KINS) from Korea,
- Centro de Investigaciones Energéticas, Medioambientales y Tecnológicas (CIEMAT) and Consejo de Seguridad Nuclear (CSN) from Spain,
- Strålsäkerhetsmyndigheten (Swedish Radiation Safety Authority – SSM) represented by Quantum Technologies from Sweden,
- Nuclear Regulatory Commission (USNRC) and Idaho National Laboratory (INL) from the Unites States,
- VTT Technical Research Centre of Finland (VTT) from Finland.

As can be seen, research institutions, utilities, technical safety organizations as well as safety authorities are all represented within the participants.

In terms of computer codes used, the spectrum was also large as solutions were provided with ALCYONE, BISON, FRAPTRAN, RANNS, SCANAIR, TESPAROD and TRANSURANUS.

Table 3.1 summarizes all the contributions provided by the participants.

1. Marked as "UNIPI" in the figures

Organisation	Codes	Case No. 1	Case No. 2	Case No. 3	Case No. 4	Case No. 5	Case No. 6	Case No. 7	Case No. 8	Case No. 9	Case No. 10
SSM	SCANAIR	X	X	X	X	X	X	X	X	X	--
	SCANAIR + TH-2P	X	X	X	X	X	X	Failed	X	---	---
VTT	SCANAIR	X	X	X	X	X	X	X	X	X	X
IRSN	SCANAIR	X	X	X	X	X	X	X	X	X	X
CIEMAT	SCANAIR	X	X	X	X	X	X	X	X	X	X
	FRAPTRAN	X	X	X	X	X	Stopped at 101 s	Failed	X	X	X
USNRC	FRAPTRAN	X	X	X	X	X	X	X	X	X	X
UJV	FRAPTRAN	X	X	X	X	X	Failed	Failed	X	X	X
KINS	FRAPTRAN	X	X	X	X	X	X	X	X	X	X
TRACTEBEL	FRAPTRAN	X	X	X	X	X	---	---	X	X	X
MTA-EK	FRAPTRAN	X	X	X	X	X	---	---	X	X	X
NINE	TRANSURANUS	X	X	X	X	X	---	---	X	X	X
TUV	TRANSURANUS	X	X	X	X	X	X	X	X	X	X
JAEA	RANNS	X	X	X	X	X	X	X	X	X	X
GRS	TESPAROD	X	X	X	X	X	X	X	X	X	---
CEA	ALCYONE	X	X	X	X	X	X	X	X	X	---
INL	BISON	---	X	X	X	X	---	---	X	X	---

Table 3.1: Benchmark collected contributions

4. RESULTS SUMMARY AND ANALYSIS

This Chapter provides a general discussion of the results obtained during the RIA benchmark Phase II to identify the main conclusions that can be drawn. Because of the very large amount of data generated during the exercise, not all the results are presented here. Instead, selected comparison plots (parameters evolution versus time and syntheses data) are used. The complete results (all variables, all Cases and syntheses) are presented in an unpublished WGFS report.

One has to note that all the provided results are reported in figures showing evolutions of parameters versus time and that the two extremes values (lower and upper values) are suppressed in figures showing syntheses.

4.1 Use of input data

As a conclusion of the RIA benchmark Phase I, it was recommended that the code developers carefully examine the way the input data are used because this source of difference, that appeared to be significant, should be completely removed.

Three groups of input data that are necessary for performing a RIA calculation should be checked: the initial state of the fuel before the transient, the power pulse definition and boundaries conditions used for the transient calculation, and the modelling options used.

Regarding the first group of inputs, as simplified Cases with fresh fuel were used, no differences were observed (except numerical errors for fuel or clad initial radius, which were all corrected).

Concerning the second group of inputs, in contrast to the RIA benchmark Phase I, participants carefully defined the power pulse and boundaries conditions so that no differences were observed. For example, Figure 4.1 shows the injected energy as a function of time for Case No. 8. It appears that the difference between the minimum and the maximum values in the different codes is very low (less than 1%) compared to the RIA benchmark Phase I exercise in which the difference reached 10%.

With regard to the third group of inputs, it was recommended in the specifications to use the standard options for all models except for the failure model, fuel relocation model, and high temperature cladding oxidation model, which must all be disabled. Those recommendations were well respected by participants, thus avoiding unexpected results like clad temperature escalation due to oxidation or fuel relocation during the stabilisation phase of the simulation, prior to the power pulse.

In conclusion, it appears that each participant carefully defined their input decks to conform to the specifications, and that no discrepancies coming from bad input decks were observed.

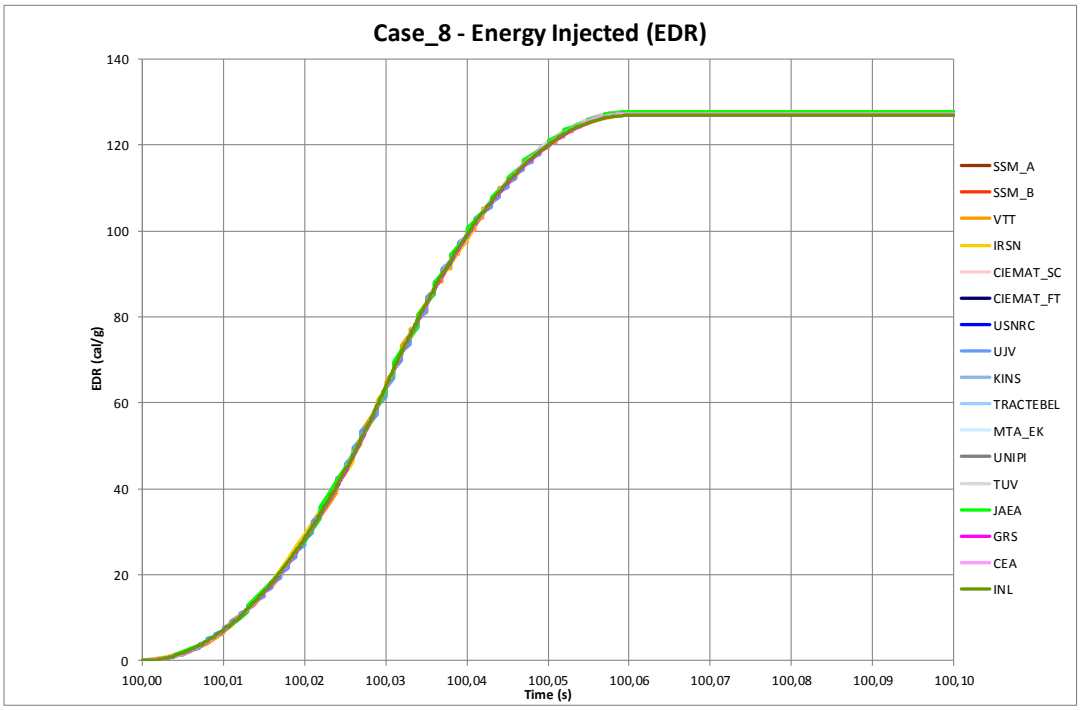

Figure 4.1: Case No. 8 – Energy Injected

4.2 Thermal behaviour

The thermal behaviour was evaluated by comparing different parameters: the fuel enthalpy, the fuel temperature, and the cladding temperature at the beginning of the transient (end of stabilization phase of simulation), during the whole transient, and during the heat-up phase of the transient together with boiling duration for Cases in which DNB occurs.

4.2.1 *Analysis of initial state*

Figure 4.2, Figure 4.3, and Figure 4.4 provide lower, upper, and mean values (extracted from different codes simulations) for fuel enthalpy, fuel centreline temperature, and cladding temperature respectively, for all Cases at the beginning of the transient. As expected, the differences are very small, showing that the stabilization phase of all Cases is well simulated and that transient phases are starting from very similar thermal conditions for all Cases and all simulations.

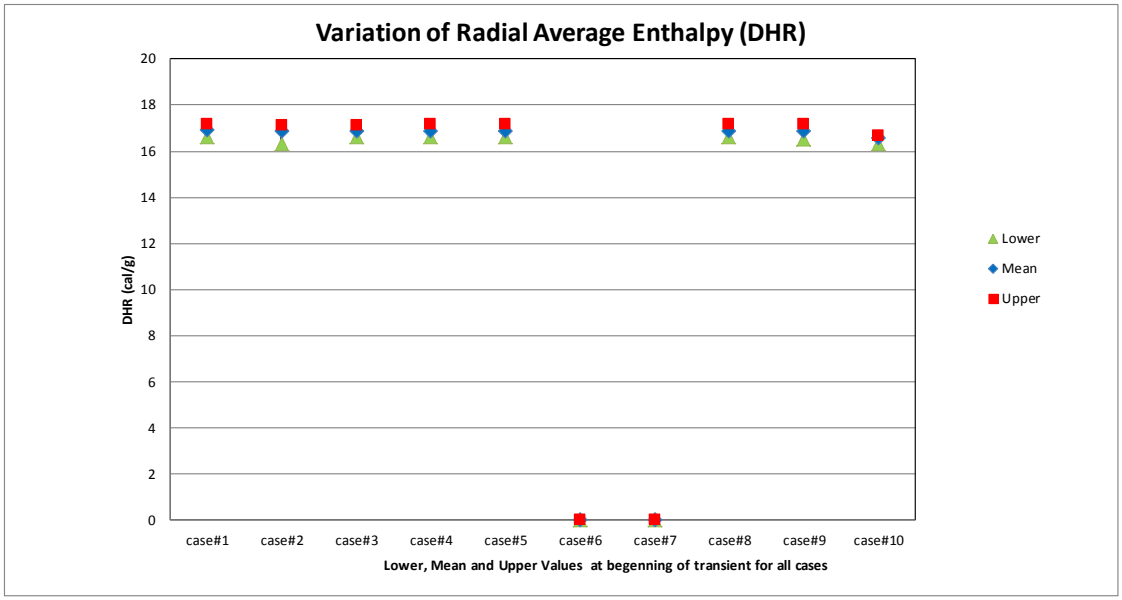

Figure 4.2: Variation of Radial Average Enthalpy at beginning of transient for all Cases

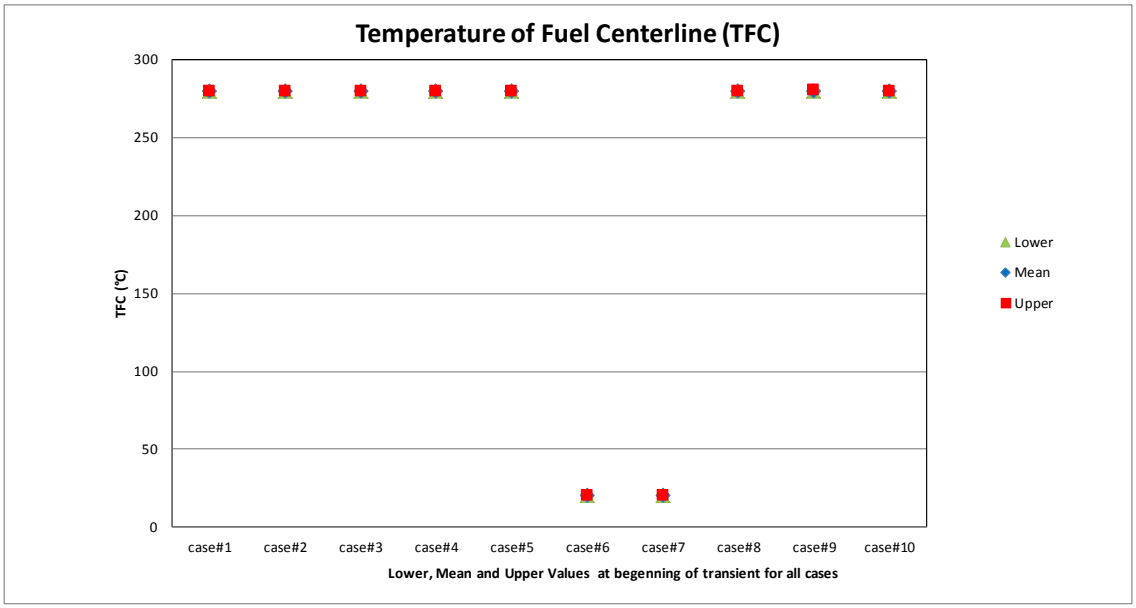

Figure 4.3: Temperature of Fuel Centreline at beginning of transient for all Cases

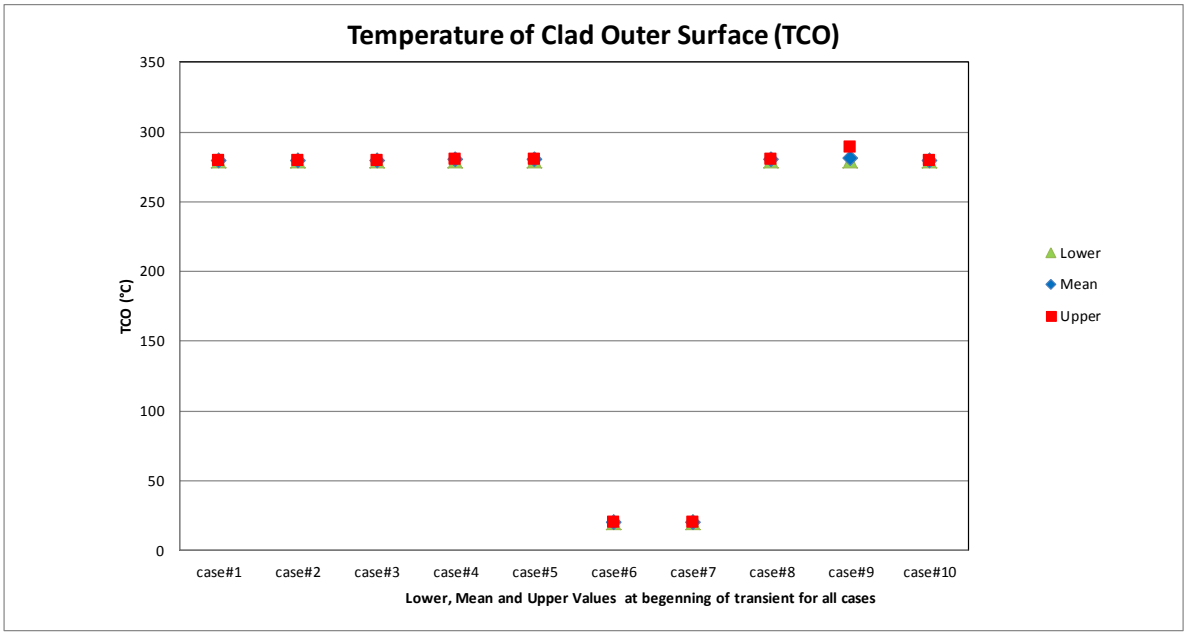

Figure 4.4: Temperature of Clad Outer Surface at beginning of transient for all Cases

4.2.2 *Analysis of overall transient behaviour*

Regarding the radial average enthalpy variations during the transient, the comparison of different simulations as a function of time are shown in Figure 4.5, Figure 4.6, Figure 4.7, and Figure 4.8 for Cases 4, 5, 6, and 7 respectively.

The agreement is very good for Case No. 4 (PWR Case without DNB occurrence) during the whole transient; slight differences appear during cooling phase for Case No. 5 (PWR Case with DNB occurrence). For Case No. 6 (BWR Case without DNB occurrence), large differences appear during the cooling phase (with unexpected high values at the end of the transient), and for Case No. 7 (BWR Case with DNB occurrence) the agreement is very poor.

These discrepancies are the direct result of the poor agreement regarding the clad outer temperature (see below).

The same conclusions can of course be drawn about the comparison of fuel centreline temperature variations as a function of time (see Figure 4.9, Figure 4.10, Figure 4.11, and Figure 4.12).

In terms of maximum values for fuel enthalpy and centreline temperature, the agreement is much better (see Figure 4.13 and Figure 4.14) for all Cases. The maximum difference over all calculations between the lower and upper values is respectively 60°C for the fuel centreline temperature and 7 cal/g for the fuel enthalpy.

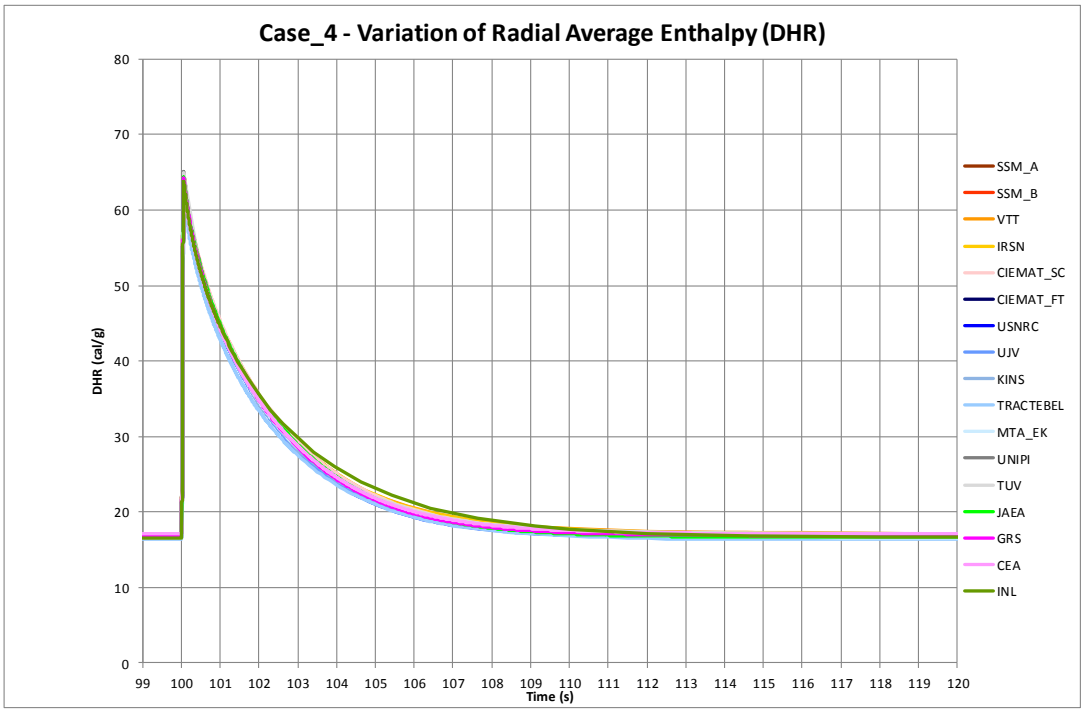

Figure 4.5: Case No. 4 – Variation of Radial Average Enthalpy

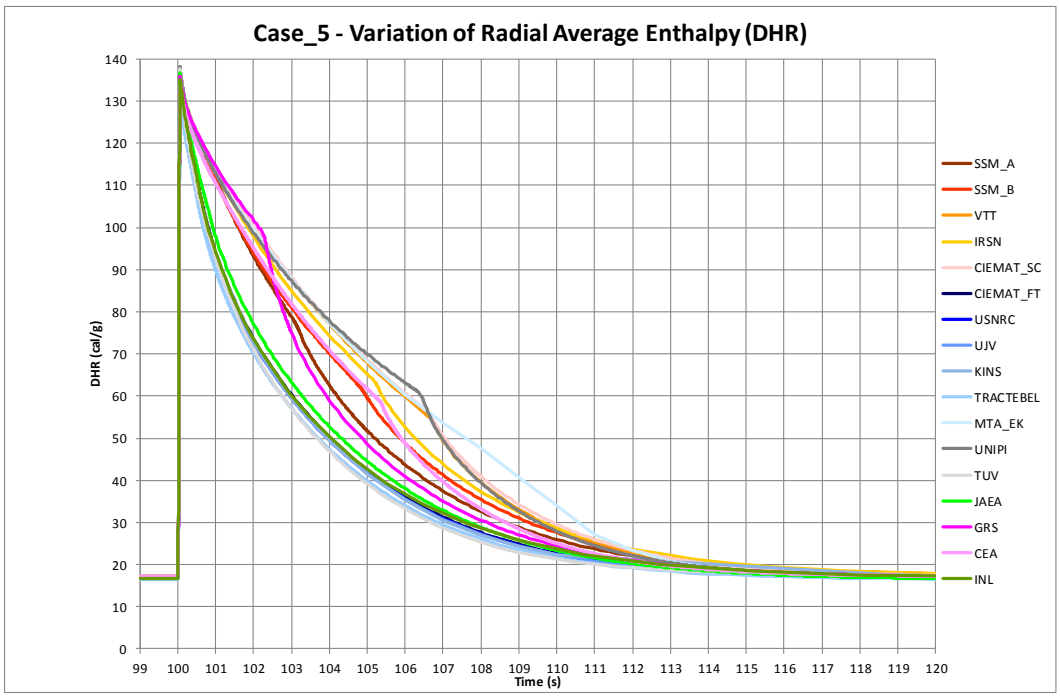

Figure 4.6: Case No. 5 – Variation of Radial Average Enthalpy

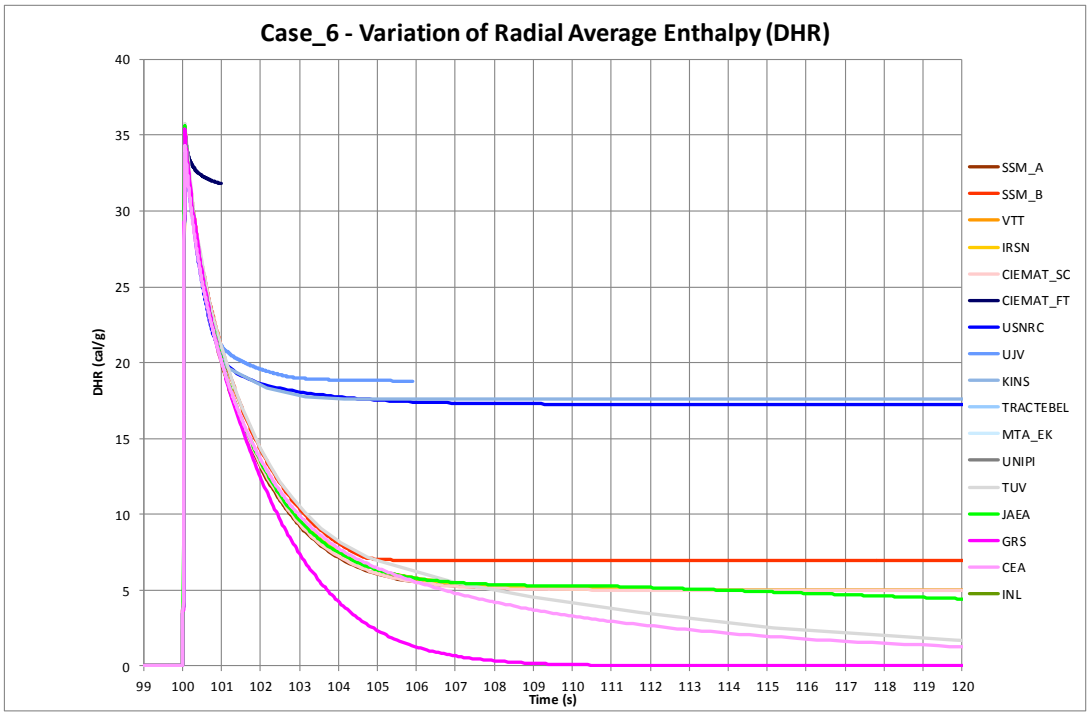

Figure 4.7: Case No. 6 – Variation of Radial Average Enthalpy

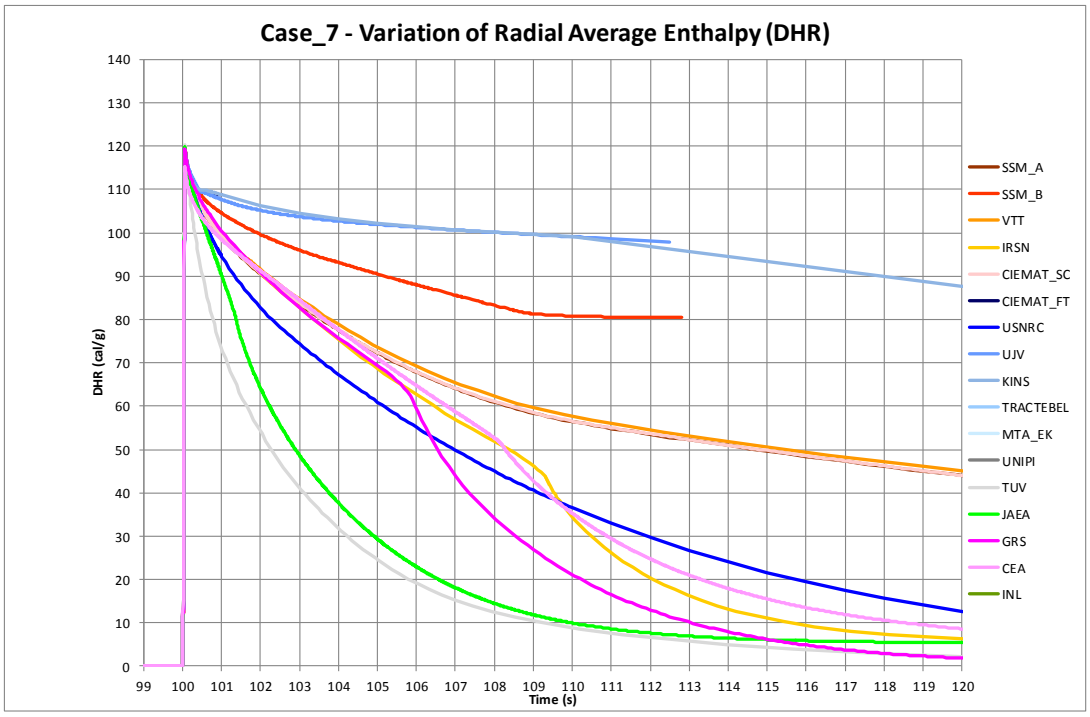

Figure 4.8: Case No. 7 – Variation of Radial Average Enthalpy

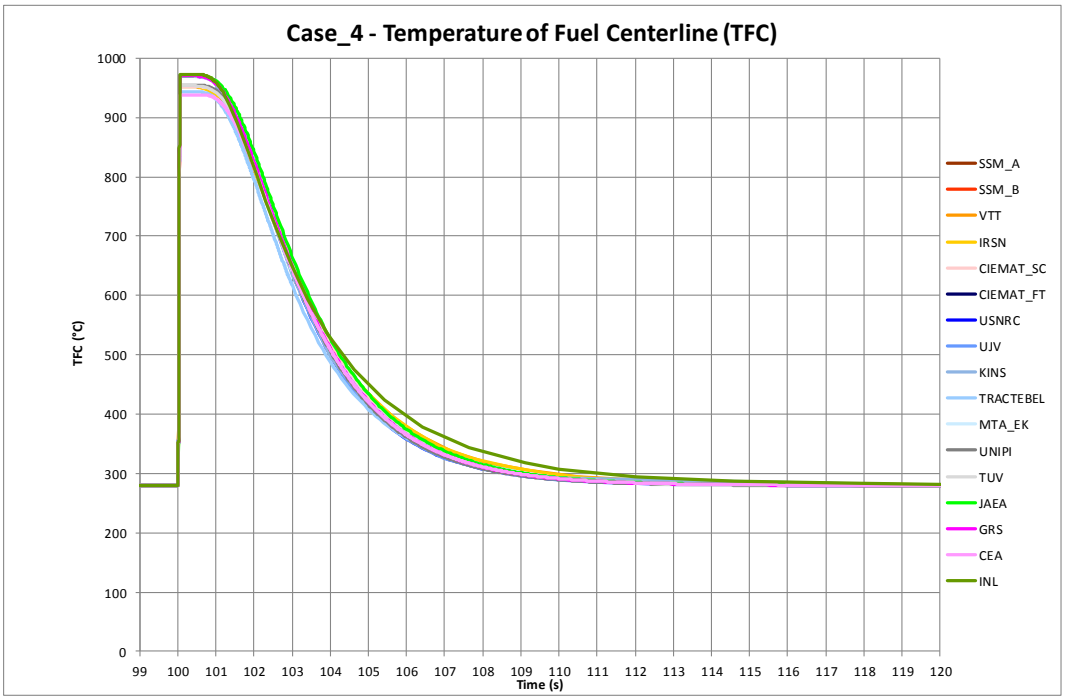

Figure 4.9: Case No. 4 – Temperature of Fuel Centreline

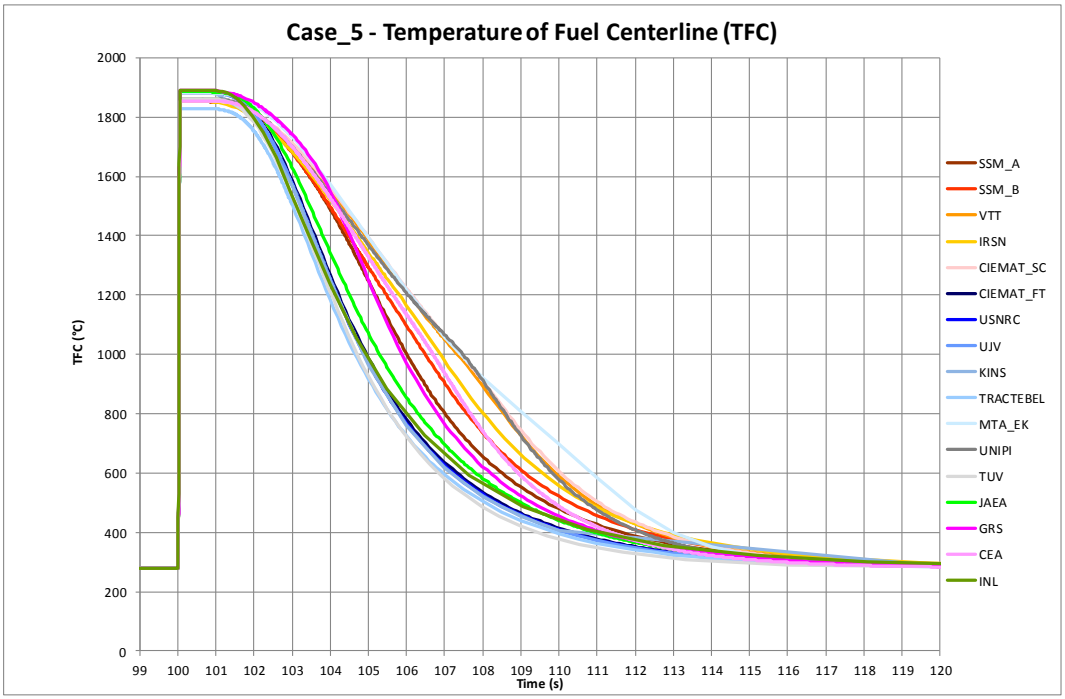

Figure 4.10: Case No. 5 – Temperature of Fuel Centreline

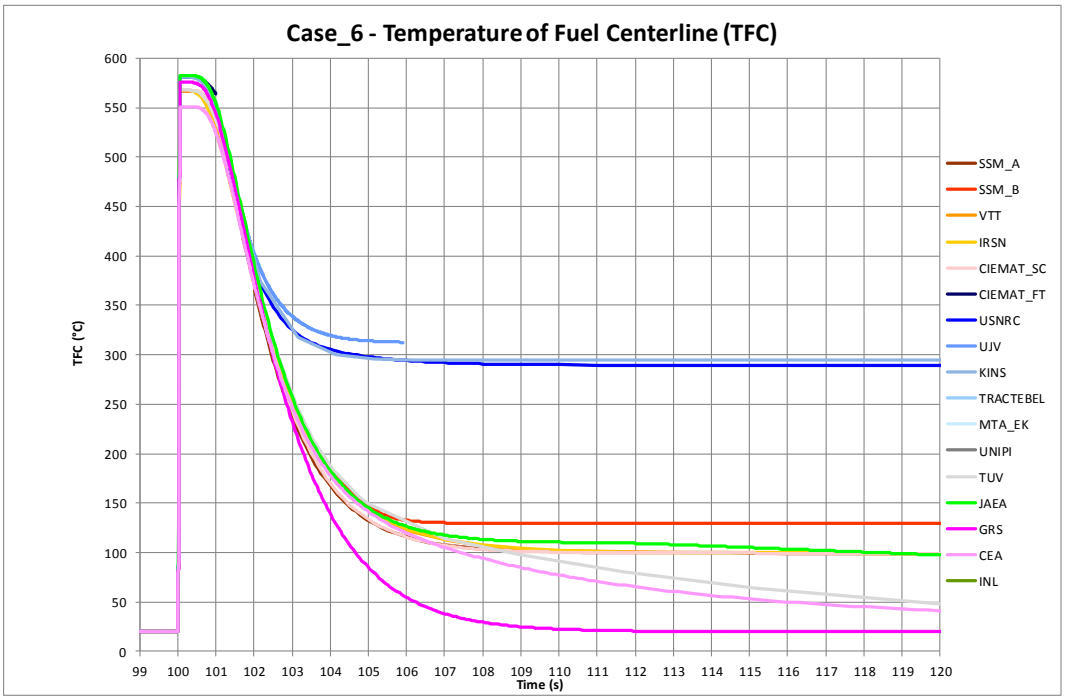

Figure 4.11: Case No. 6 – Temperature of Fuel Centreline

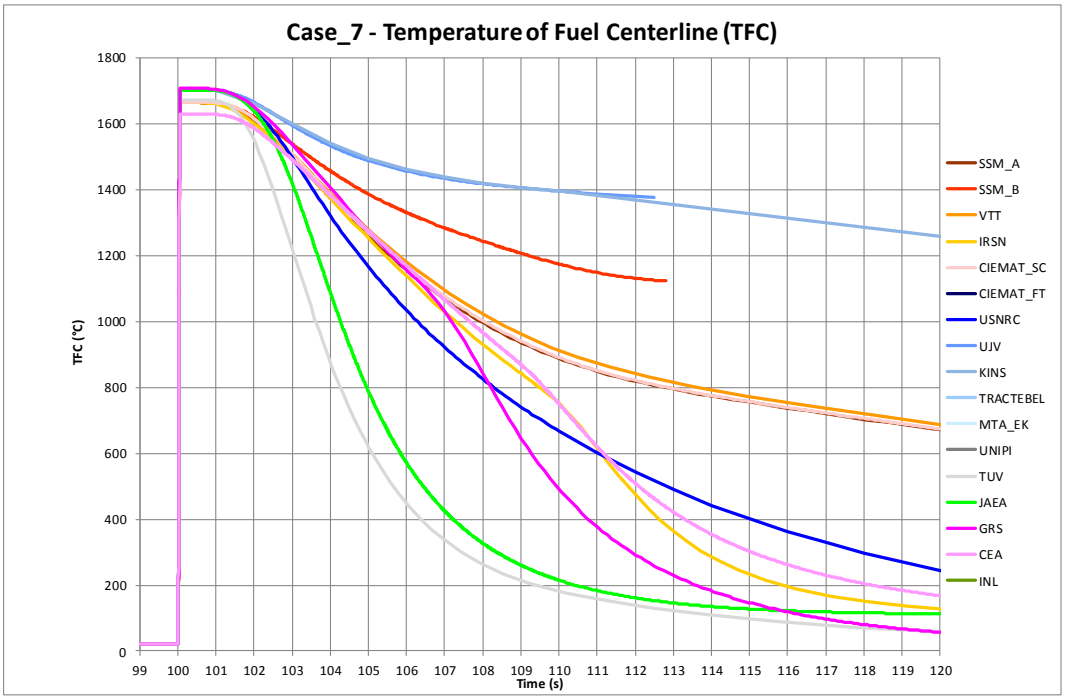

Figure 4.12: Case No. 7 – Temperature of Fuel Centreline

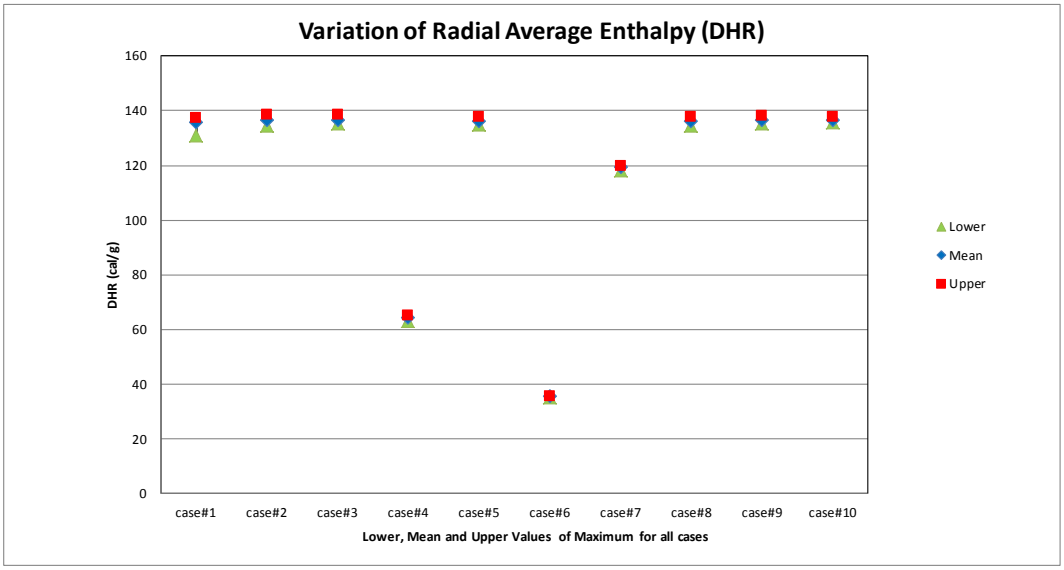

Figure 4.13: Variation of Radial Average Enthalpy – Values of Maximum for all Cases

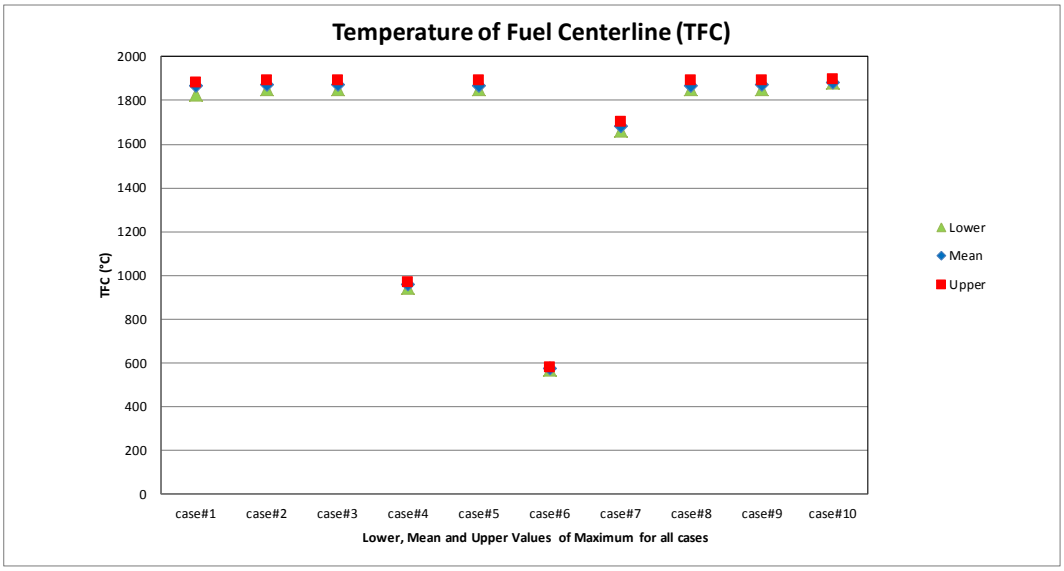

Figure 4.14: Temperature of Fuel Centreline – Values of Maximum for all Cases

With regard to the cladding temperature predictions, the comparisons of the variation of the cladding outer temperature are shown in Figure 4.15, Figure 4.16, Figure 4.17, and Figure 4.18 for Cases 4, 5, 6, and 7 respectively.

For Case No. 4 (PWR Case without DNB occurrence) the agreement is very good while it is not so good for Case No. 5 (PWR Case with DNB occurrence). In Case No. 5, almost all calculations show DNB occurrence, followed by a post-DNB phase with very high clad temperatures that ends with a quenching phase. If the physical trend is very similar for all calculations, the maximum temperature reached by the

clad varies from 491°C to 977°C, and boiling duration [1] ranges from 0.3 s to 7.6 s (Figure 4.19 and Figure 4.20).

Regarding Cases 6 and 7 (BWR Cases), the agreement is very poor. For Case No. 7 (BWR Case with DNB occurrence) it should also be noted that some simulations failed to reach the end of transient because an unphysical boiling duration (up to 100 s) and very high clad temperatures are predicted.

In terms of maximum values for clad temperature and boiling duration, the lower, upper and mean value (extracted from all simulations) are presented in Figure 4.19 and Figure 4.20 for all Cases. The scatters are very important for Cases where coolant boiling occurs. In the worst Case, the maximum clad temperature ranges from 669°C to 1311°C while the boiling duration ranges from almost 0 s to 28 s. This last value can reach almost 100 s if one takes into account simulations that failed.

As it is shown in Chapter 0, boiling under RIA conditions is known to be significantly different from boiling under steady state conditions. Some codes assume that the steady state correlations are applicable to RIA conditions while other codes use specific fast transient correlations (for critical heat flux, heat exchange in film boiling, rewetting conditions ...). In addition, as boiling in RIA conditions have not been extensively studied until now, specific fast transient correlations have still to be developed and validated for BWR and PWR conditions.

In conclusion, the agreement between all simulations for cladding temperature is rather good for Cases with no boiling crisis, and very poor when two-phase flow conditions are met. Simulations with codes having specific fast transient correlations seem to provide more credible results, but those codes still have to be validated in real reactor conditions.

Finally, the poor agreement obtained for some Cases on clad temperature can partially explain the discrepancies concerning the fuel temperature, clad hoop strain, and fuel/clad elongation observed in those Cases (see paragraph 4.3).

1. Boiling duration is the difference between the quenching time and DNB time

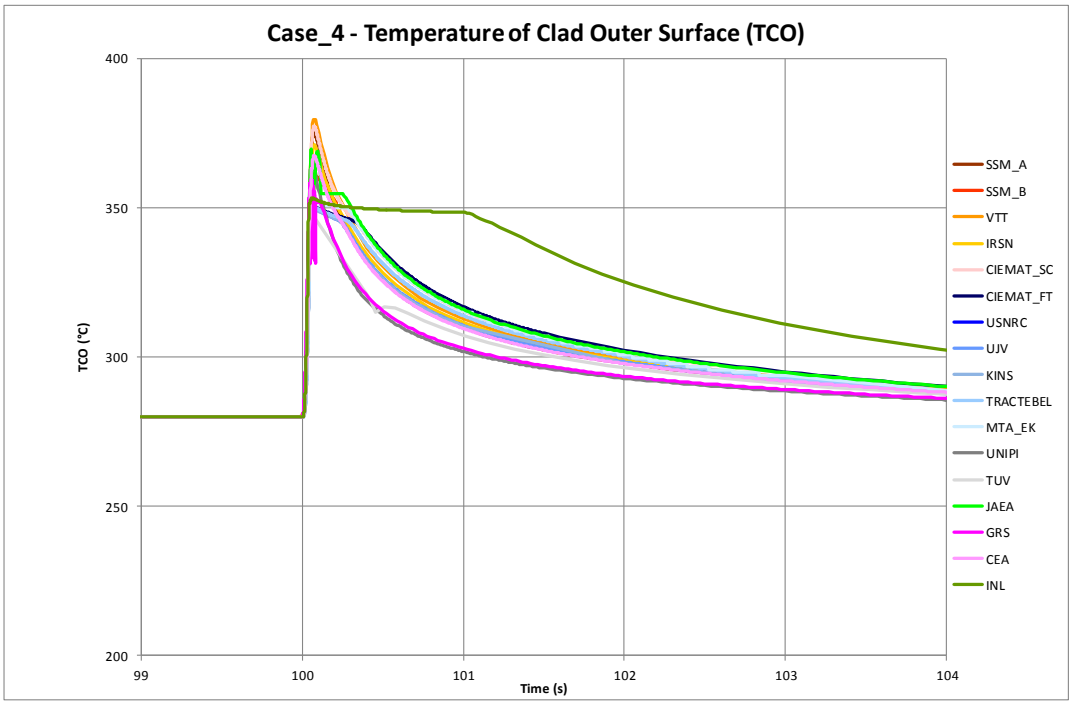

Figure 4.15: Case No. 4 – Temperature of Clad Outer Surface

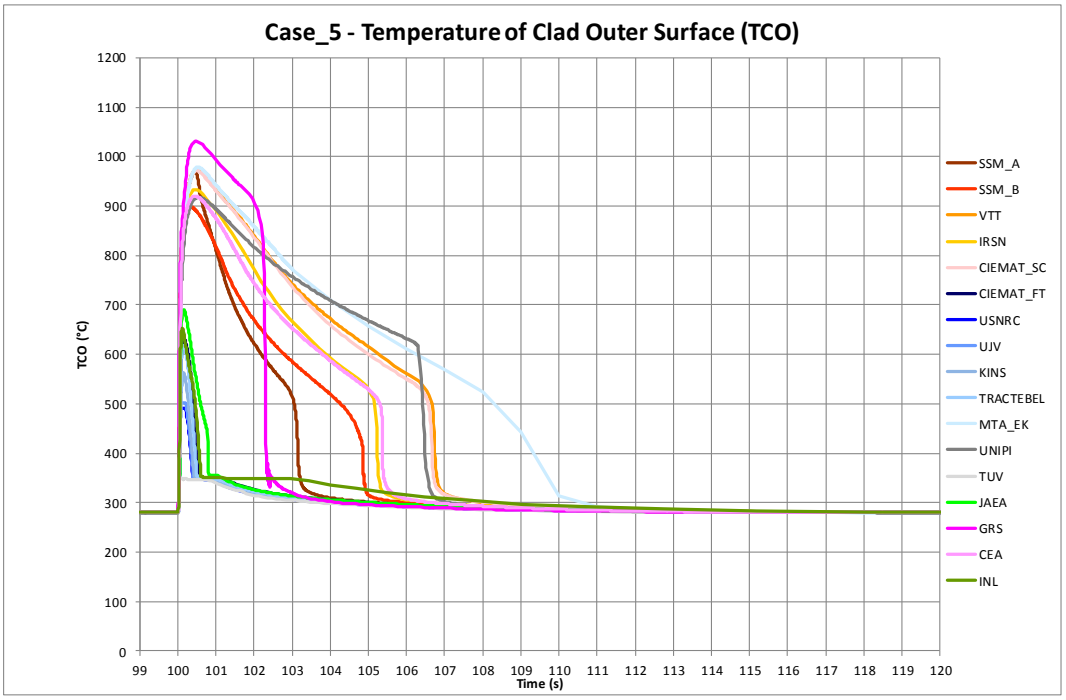

Figure 4.16: Case No. 5 – Temperature of Clad Outer Surface

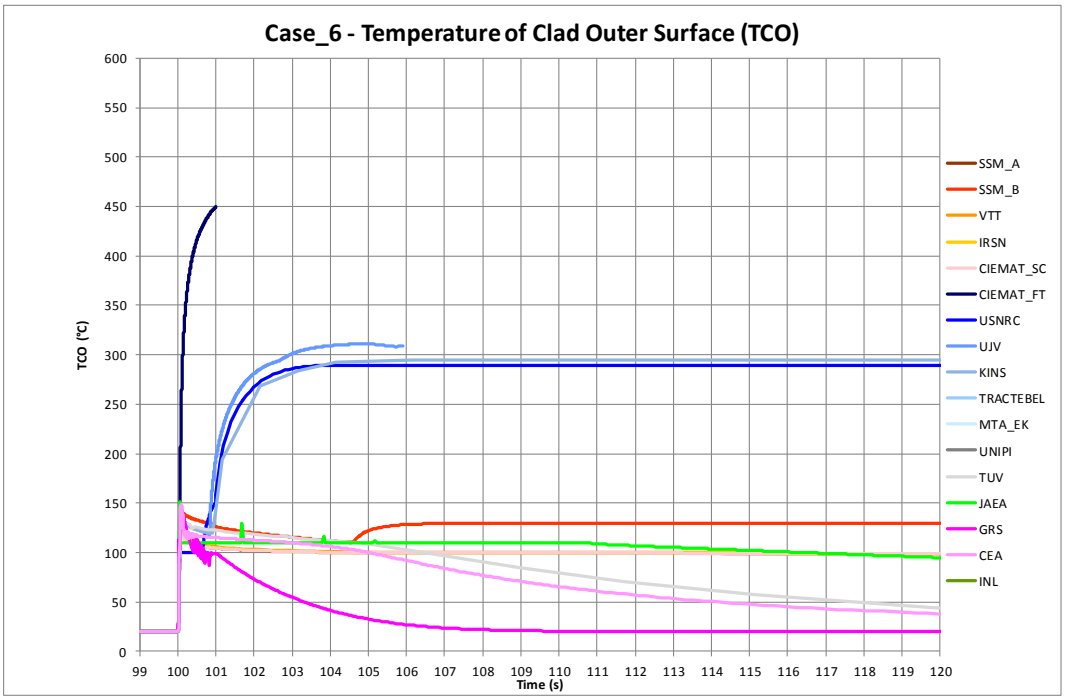

Figure 4.17: Case No. 6 – Temperature of Clad Outer Surface

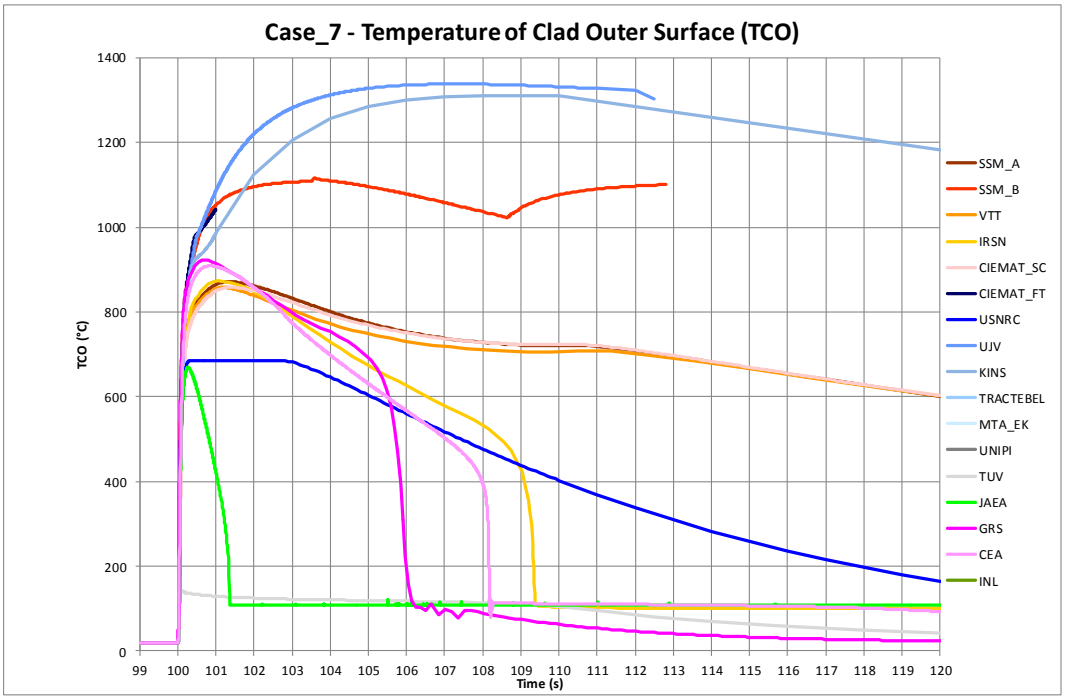

Figure 4.18: Case No. 7 – Temperature of Clad Outer Surface

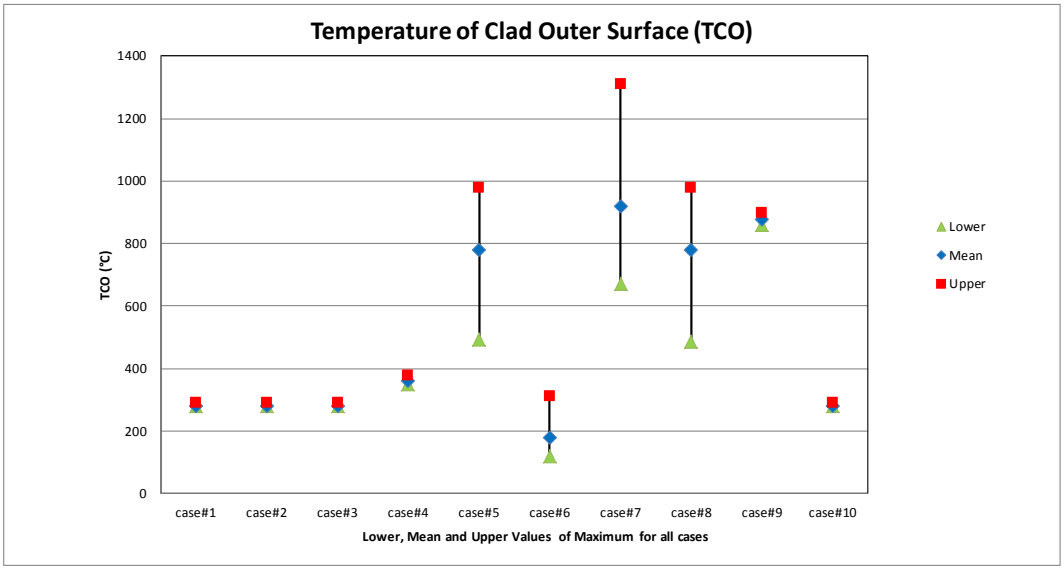

Figure 4.19: Temperature of Clad Outer Surface – Values of Maximum for all Cases

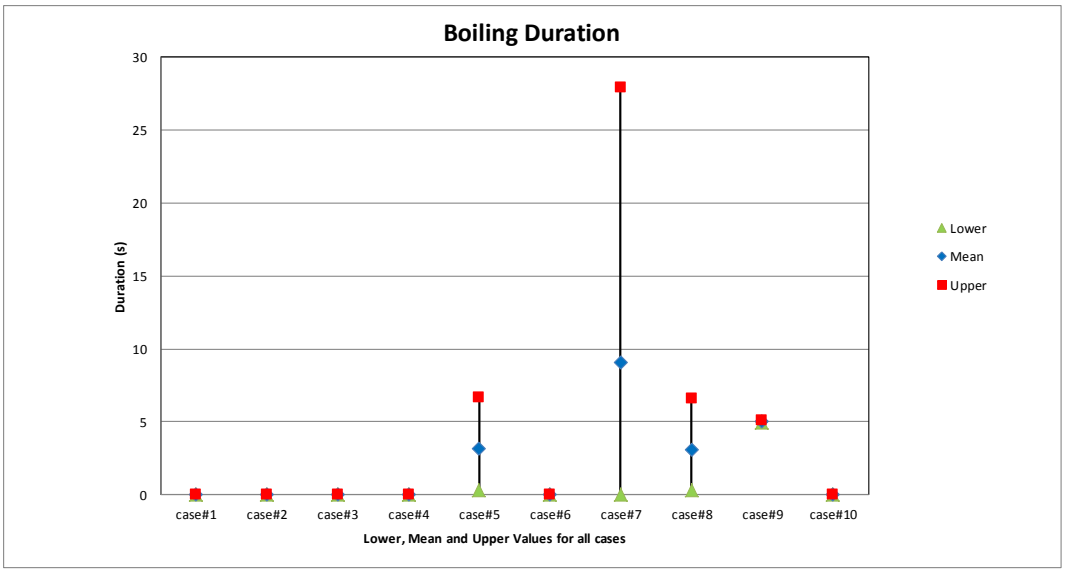

Figure 4.20: Boiling Duration – Values for all Cases

4.2.3 *Analysis of heat-up phase*

In addition to the analysis of overall thermal behaviour, it is interesting to look at the results during the heat-up phase of the transient, where power is injected in the fuel leading to fuel temperature increase and fuel expansion (This phase is between 100.00 s and 100.06 s).

As for the overall behaviour, the agreement regarding fuel centreline temperature is very good for all Cases and all simulation (see Figure 4.21 for Case No. 2 and Figure 4.22 for overall synthesis).

Figure 4.23 and Figure 4.24 show the fuel outer surface temperature evolutions for Cases 1 and 2 (with imposed fixed coolant temperature with or without an initial gap). One can remark that although the evolution trends are almost the same for all calculations, there are some discrepancies up to 105°C between the lower and upper values at the end of heat-up phase. This fact clearly shows that the modelling of fuel-to-clad heat transfer is not the same for different codes (in the two Cases the clad outer temperature is imposed). The phenomenon is observed for all Cases (see synthesis on Figure 4.25).

With regards to clad outer temperature, scatter in the values computed is limited compared to the one of the overall simulation (see Figure 4.26 for Case No. 7 and compare Figure 4.27 with Figure 4.19 for synthesis). This is because the boiling regime has not yet been fully reached at the end of the heat phase and thus the maximum clad temperature has not been reached.

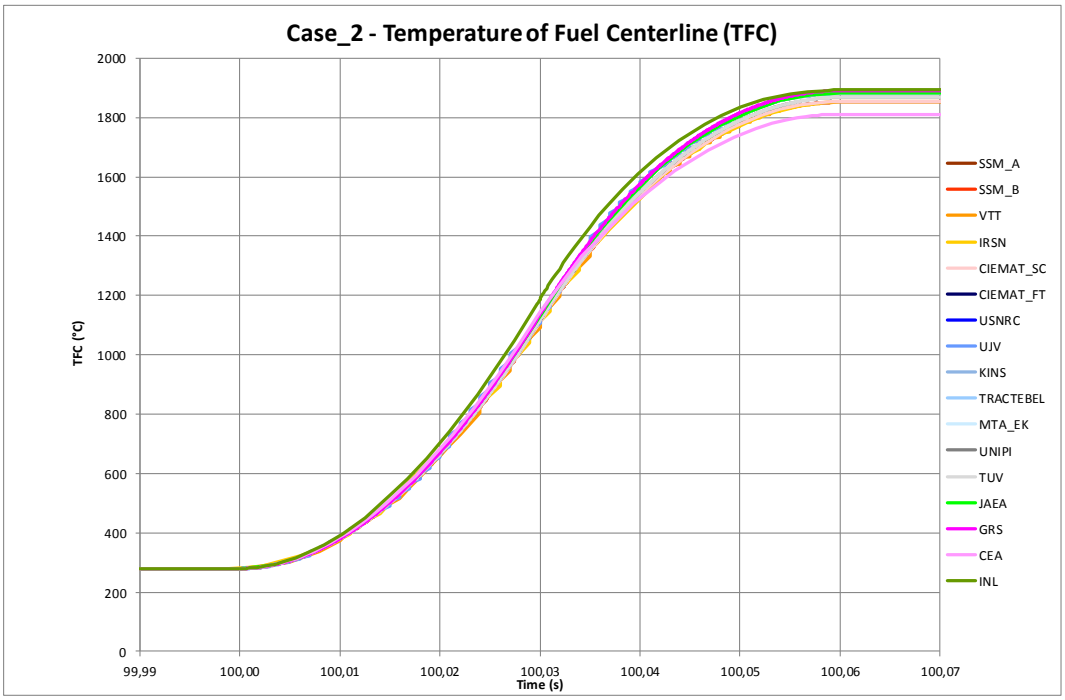

Figure 4.21: Case No. 2 – Temperature of Fuel Centreline (Heat-up Phase)

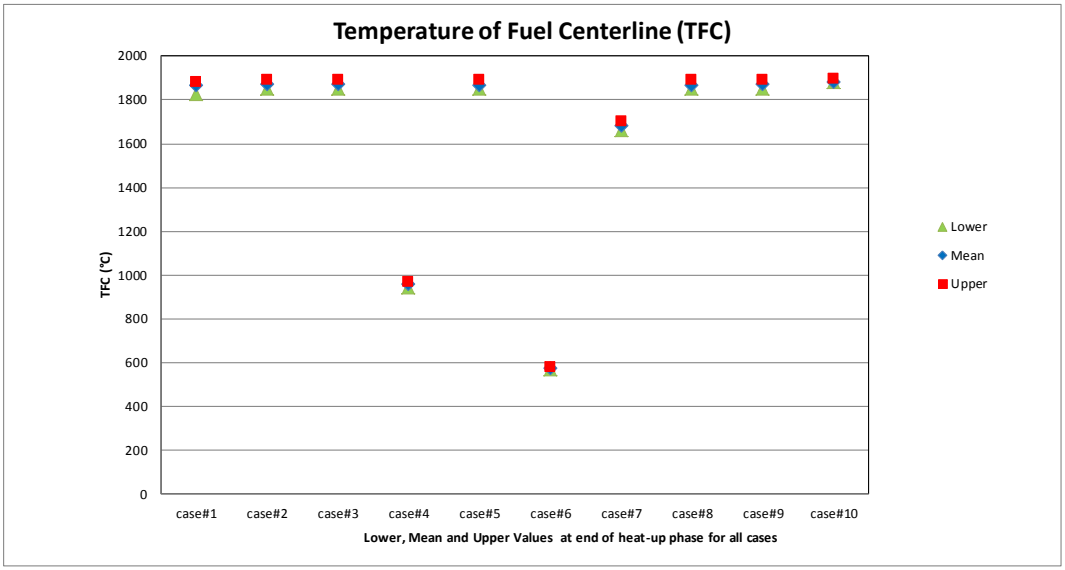

Figure 4.22: Temperature of Fuel Centreline – Values at end of Heat-up Phase for all Cases (Heat-up Phase)

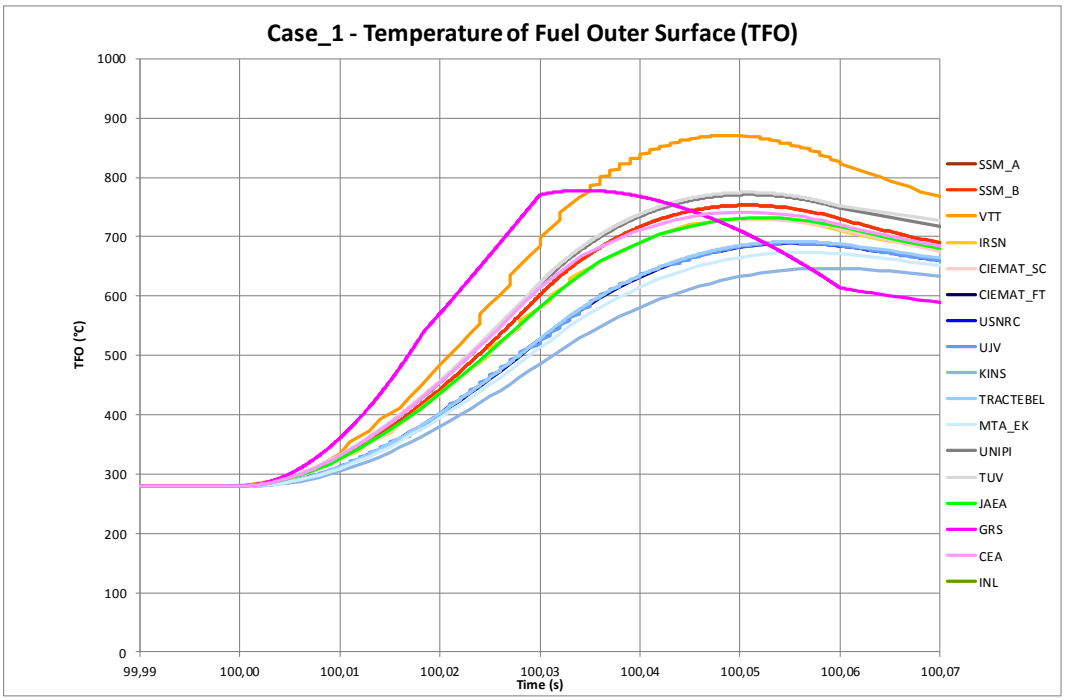

Figure 4.23: Case No. 1 – Temperature of Fuel Outer Surface (Heat-up Phase)

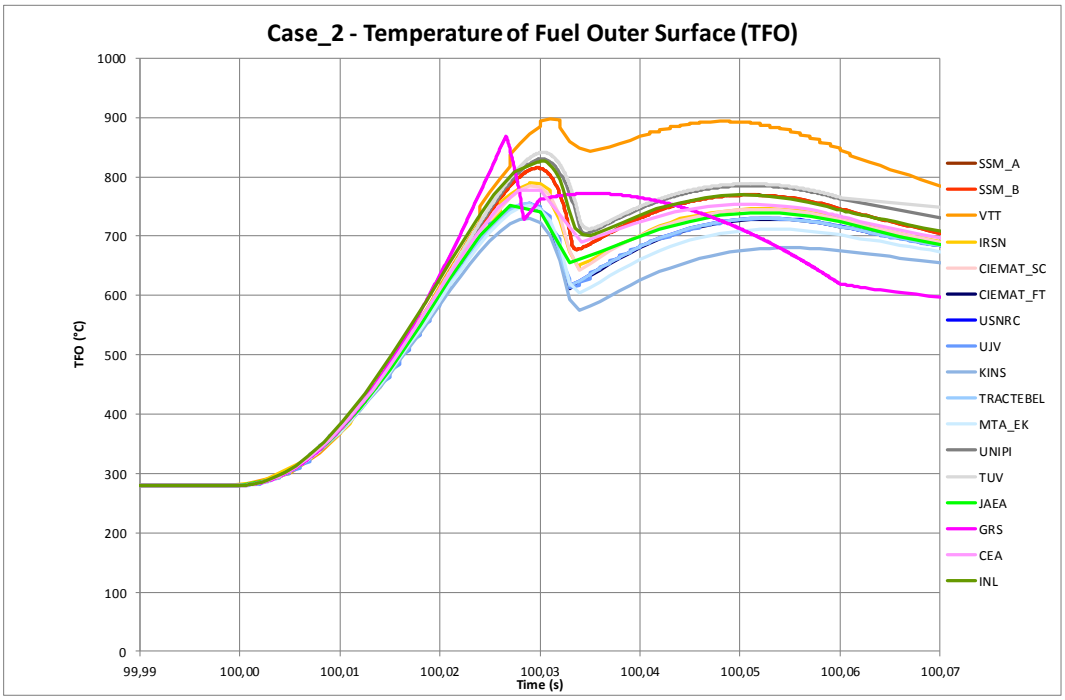

Figure 4.24: Case No. 2- Temperature of Fuel Outer Surface (Heat-up Phase)

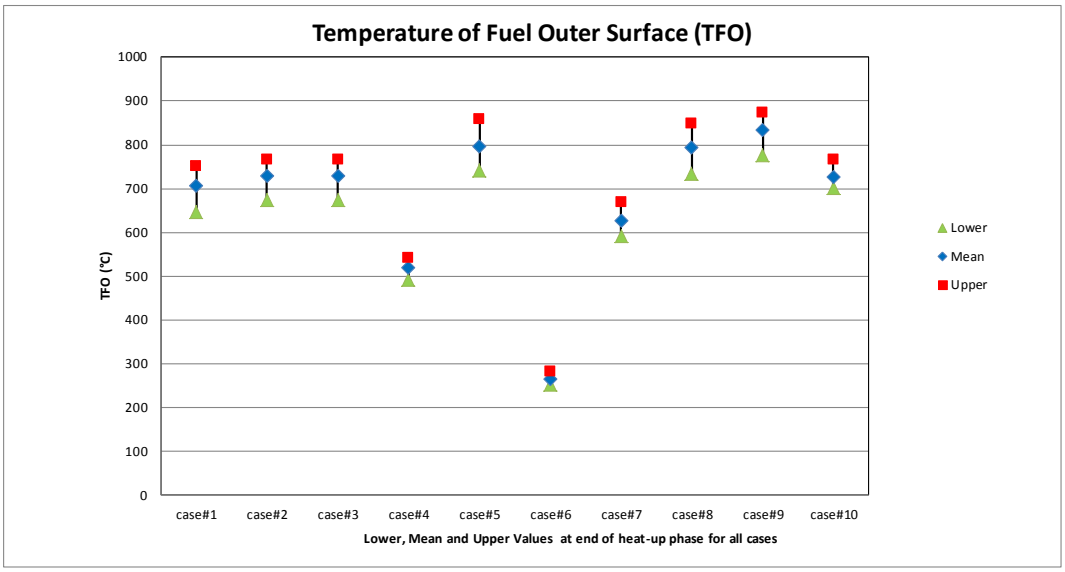

Figure 4.25: Temperature of Fuel Outer Surface – Values at end of Heat-up Phase for all Cases

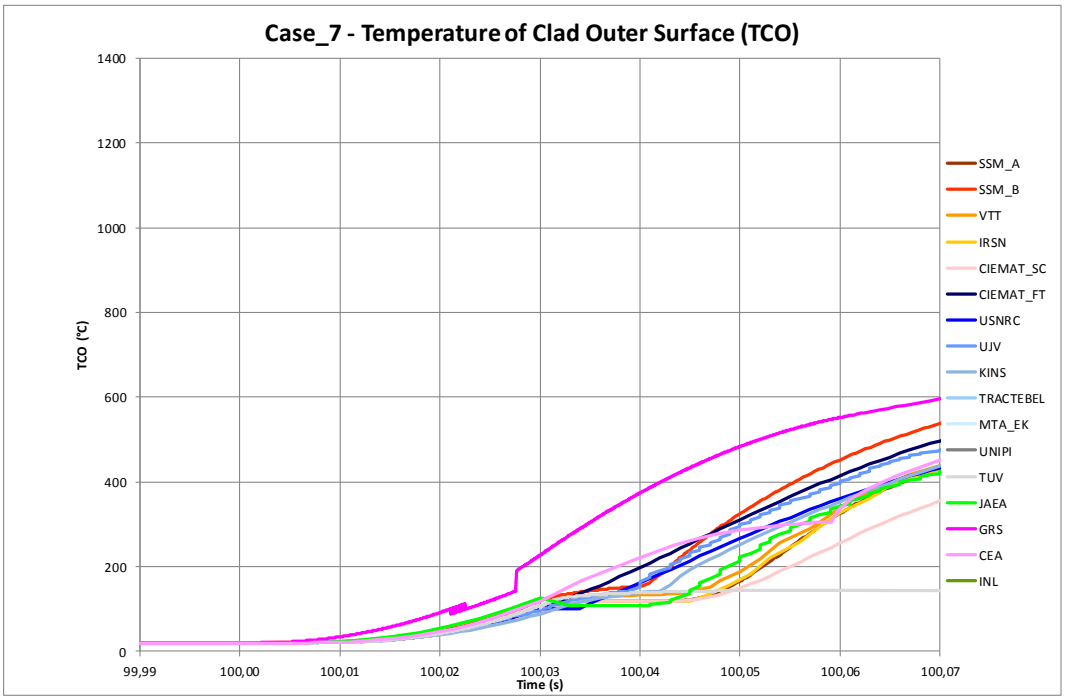

Figure 4.26: Case No. 7 – Temperature of Clad Outer Surface (Heat-up Phase)

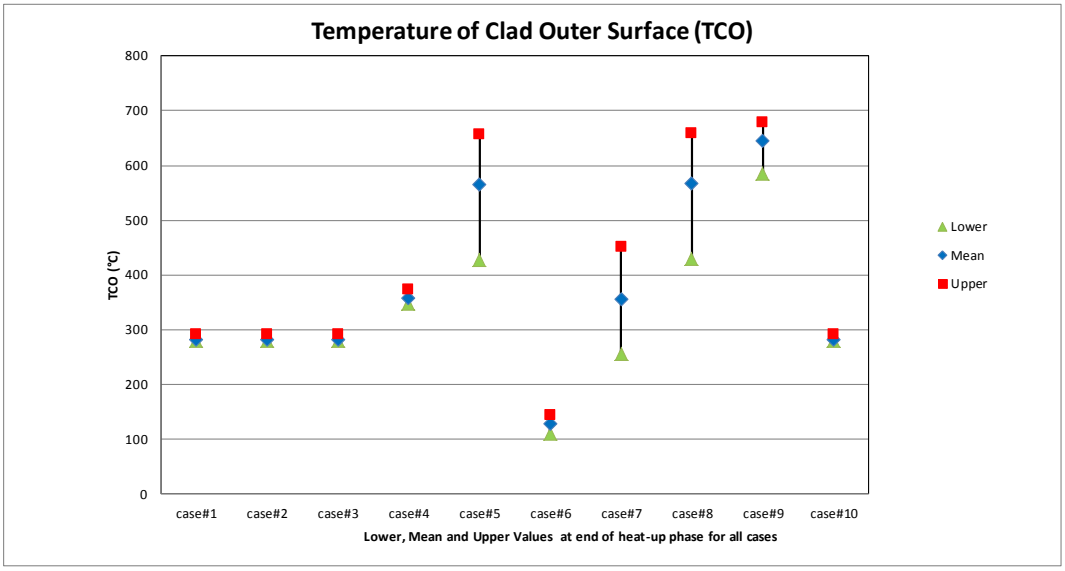

Figure 4.27: Temperature of Clad Outer Surface – Values at end of Heat-up Phase for all Cases

4.3 Mechanical behaviour

The mechanical behaviour was evaluated by comparing several parameters: the clad total axial elongation, the clad total hoop strain, the clad hoop stress, the fuel total axial elongation, the fuel outer radius, and the gap width. These parameters were compared at the beginning of the transient (end of stabilization phase of simulations), during the whole transient, and during the heat-up phase of the transient. Gap opening or closing times (depending on the Case) were also compared.

4.3.1 *Analysis of initial state*

As for thermal parameters, the initial state of the rod regarding mechanical parameters was carefully checked.

Figure 4.28, Figure 4.29, and Figure 4.30 summarize the state of the rod for all Cases at the beginning of the transient. Regarding clad total hoop strain, although differences can be observed, the difference between lower and upper values is relatively small and seems to be acceptable. The same observation is true for fuel outer radius (see Figure 4.29). However, one can remark on that figure, that the thermal expansion for the fuel is different in the different codes (this could have an impact during the transient).

Finally with regards to clad hoop stress, the differences between all simulations are relatively low. Most of the codes predict positive clad hoop stress when no initial gap between fuel and clad is assumed and all codes predict negative clad hoop stress when an initial gap is imposed (Case No. 2, Case No. 3 and Case No. 10).

Compared to the results of the RIA benchmark Phase I, as expected, the use of simplified Cases with fresh fuel leads to less scatter for mechanical parameters at the beginning of transient.

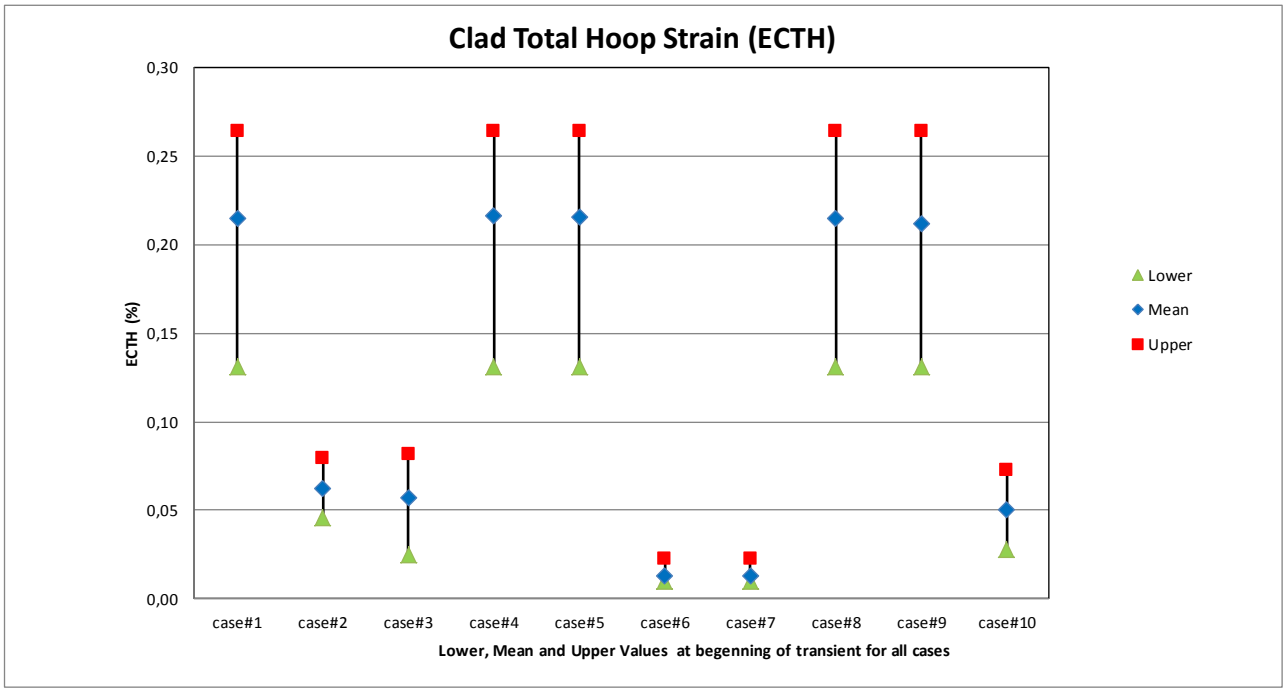

Figure 4.28: Clad Total Hoop Strain at beginning of transient for all Cases

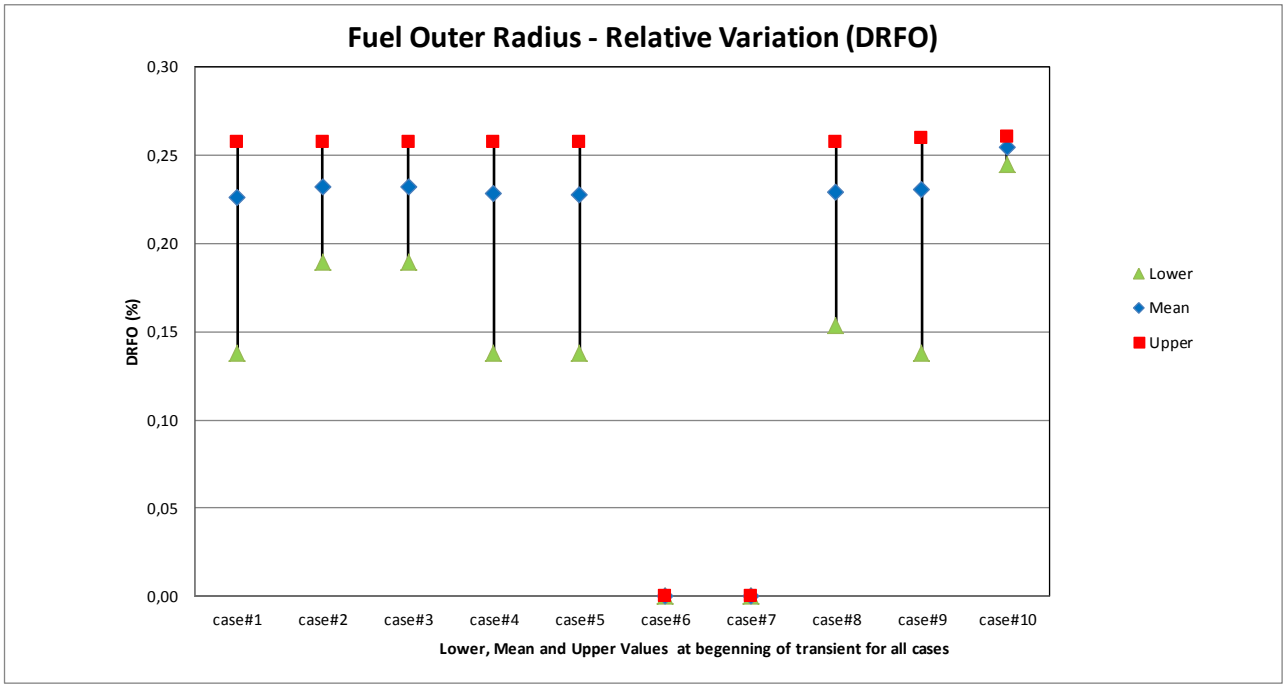

Figure 4.29: Fuel Outer Radius – relative variation at beginning of transient for all Cases

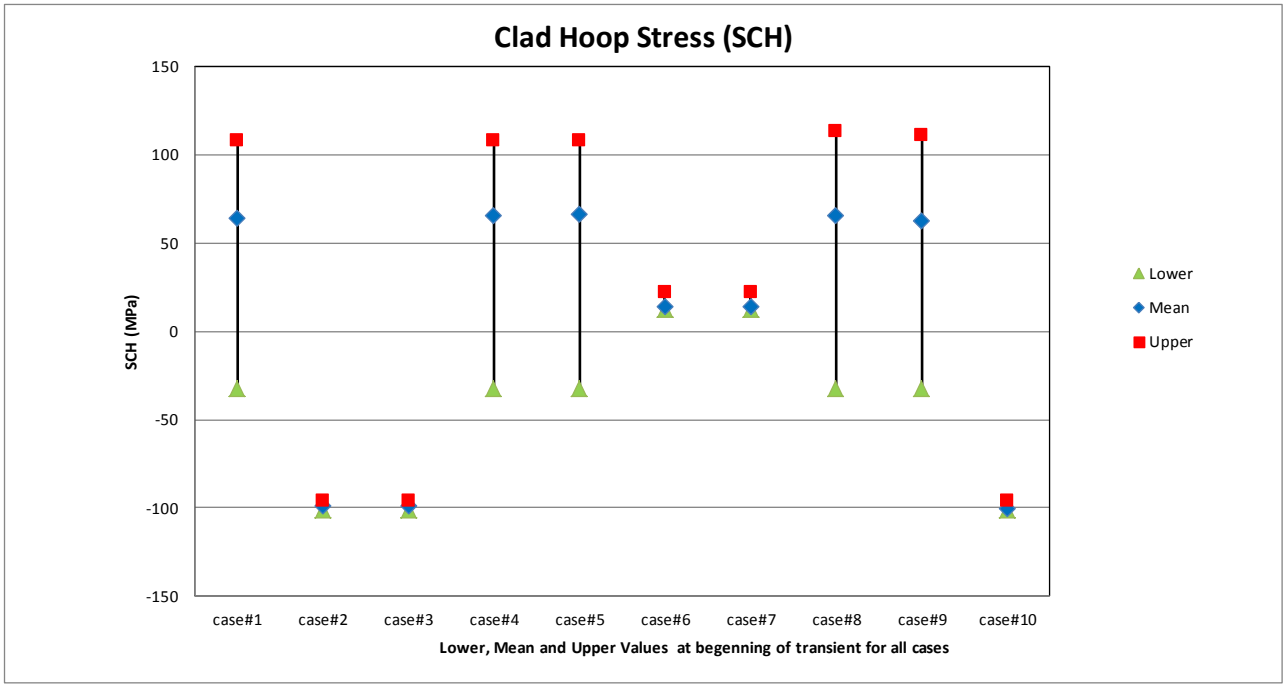

Figure 4.30: Clad Total Stress at beginning of transient for all Cases

4.3.2 *Analysis of overall transient behaviour*

Examples of clad total hoop strain evolution are given in Figure 4.31 and Figure 4.32 for Case No. 1 and Case No. 5 (similar cases with and without thermal conditions imposed).

The behaviour for these two Cases is qualitatively similar in all simulations from the different codes: a maximum value is reached during the beginning of the transient when the gap is closed and a residual hoop strain is reached after the gap opening. The long term behaviour displays some differences because the gap opening time changes a lot among the benchmarked codes (see Figure 4.34).

it seems that the scatter regarding the trend of the long term behaviour is more important for Case No. 5 (compared to Case No. 1): in this Case, as the thermal behaviour of the clad is not imposed, larger clad temperature differences (see paragraph 4.2.2) lead to different clad mechanical behaviours.

Except for Case No. 7 (with outlying results for some codes), the difference between lower and upper values for the maximal clad hoop strain is between 20 and 75% (of the mean value), which is less compared to the RIA benchmark Phase I exercise (see Figure 4.33).

One can also note that in all Cases the loading of the cladding is only PCMI, because the value of the inner rod pressure is always below the coolant pressure, even for Case No. 8 with the higher initial rod pressure(see Figure 4.36). Thus a part of discrepancies observed on clad hoop strain estimations can be explained by differences regarding fuel radius evaluations. The difference between lower and upper values for the maximal fuel radius relative variation is between 10 and 60% (see Figure 4.35).

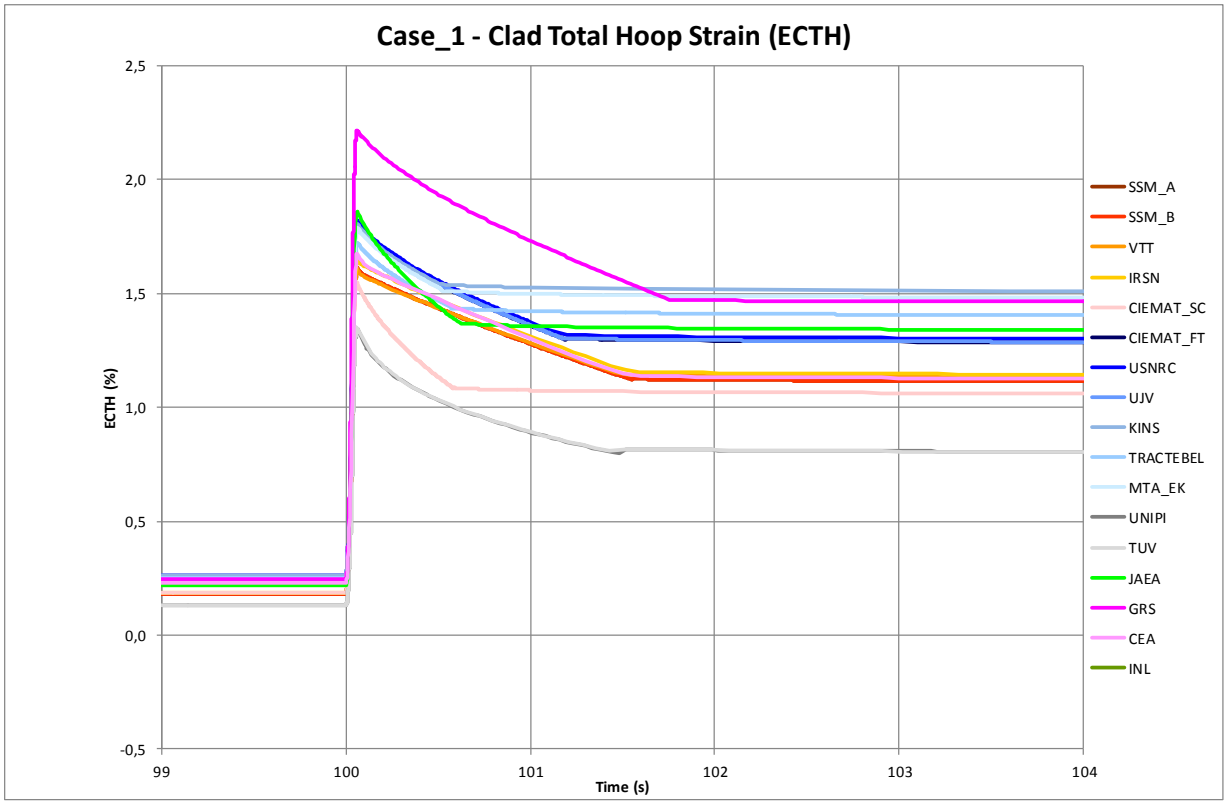

Figure 4.31: Case No. 1 – Clad Total Hoop Strain

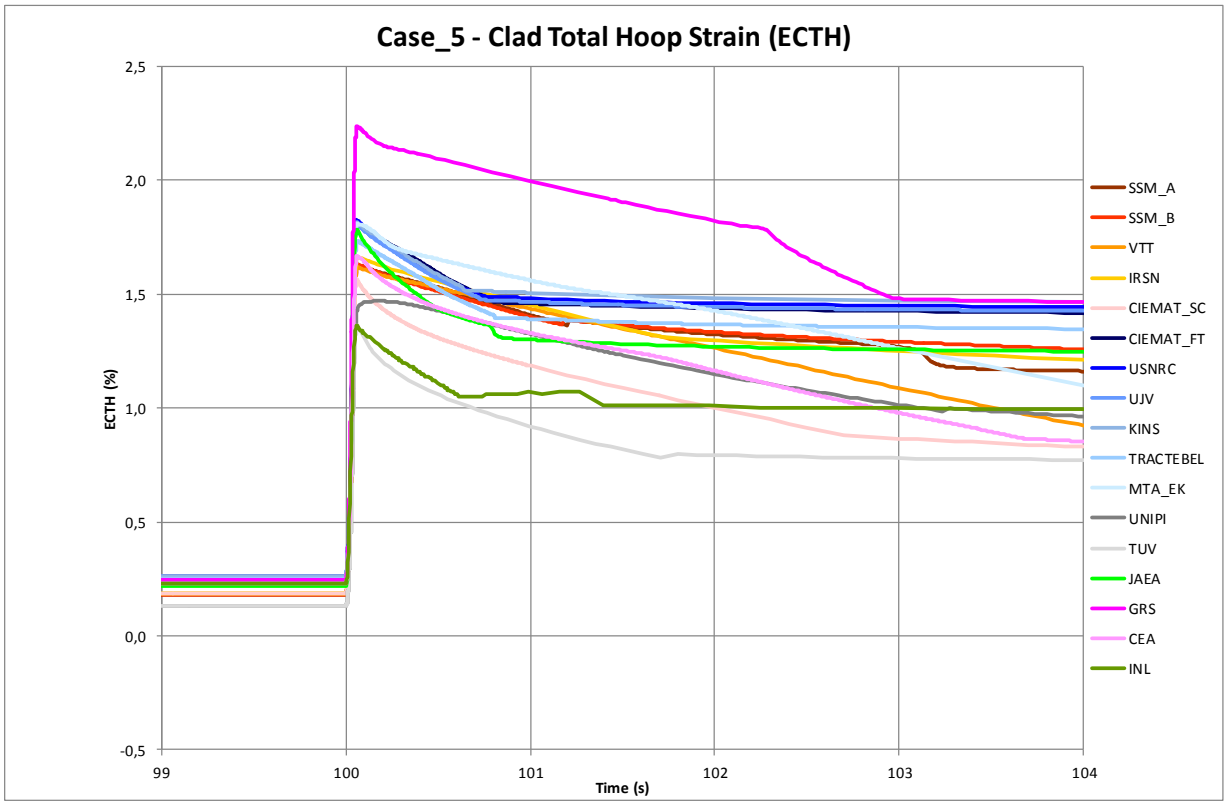

Figure 4.32: Case No. 5 – Clad Total Hoop Strain

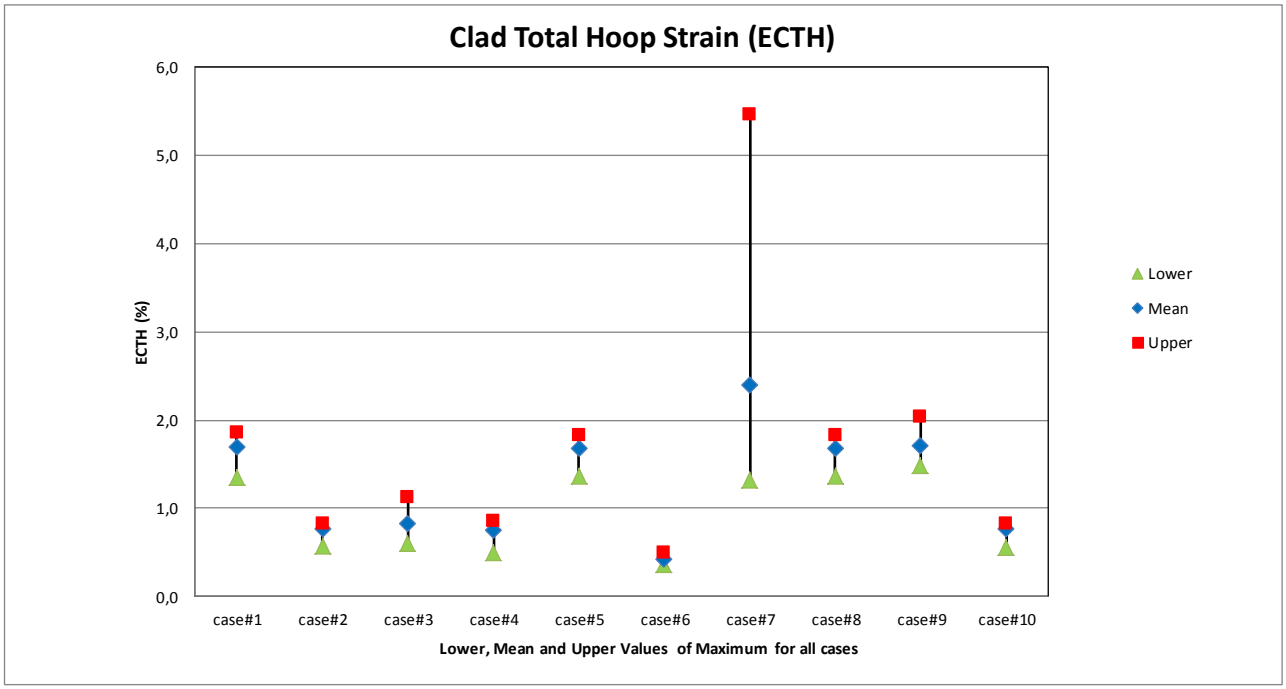

Figure 4.33: Clad Total Hoop Strain – Values of Maximum for all Cases

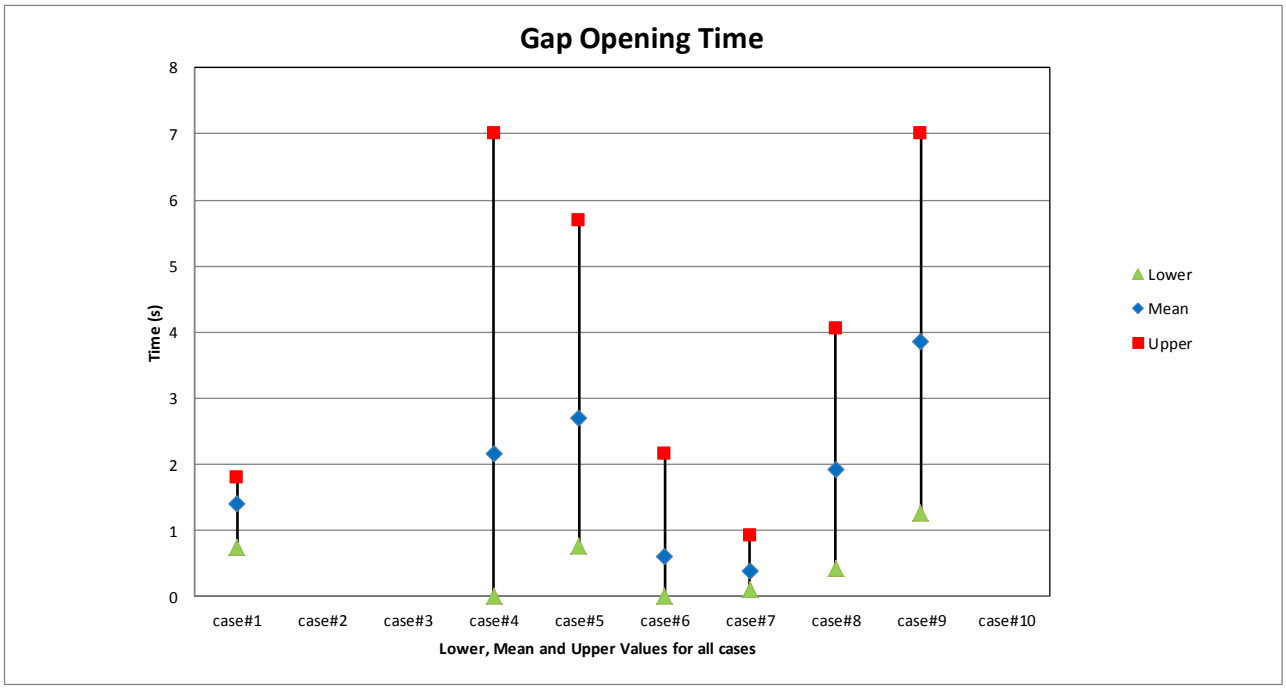

Figure 4.34: Gap Opening Time for all Cases

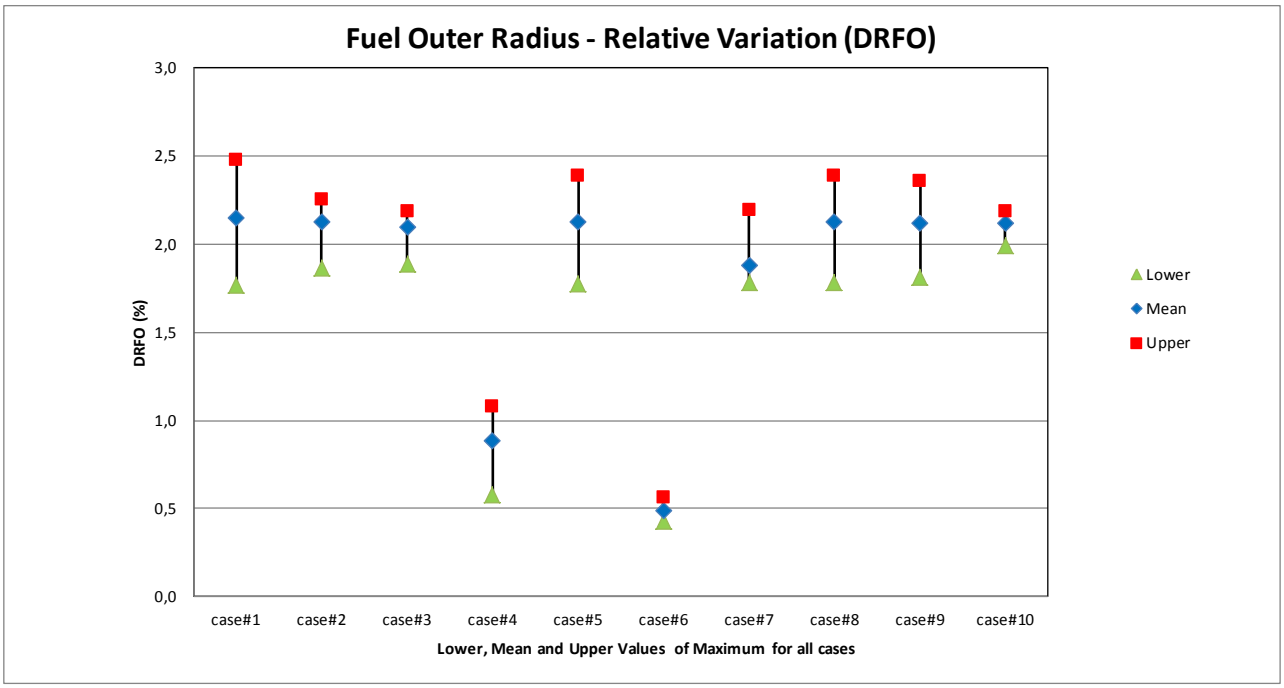

Figure 4.35: Fuel outer Radius – Values of Maximum of relative variation for all Cases

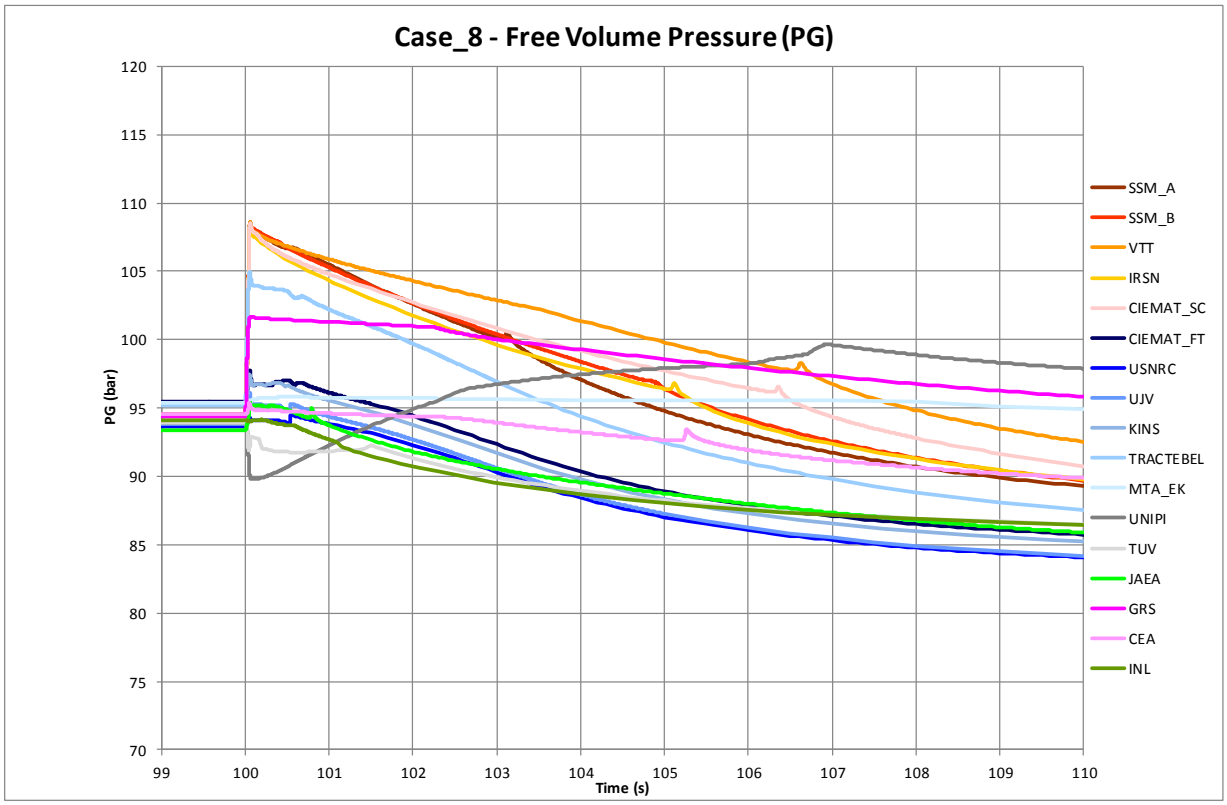

Figure 4.36: Case No. 8 – Free Volume Pressure

The fuel total elongations for Cases 1 and 5, as well as synthesis of the maximum values for all Cases and all simulations are given in Figure 4.37, Figure 4.38, and Figure 4.39. The fuel elongation evolutions are very similar for all Cases because the main contributing factor is the thermal expansion driven by fuel temperature evolutions, which are very similar in all simulations (see 4.2.2). The difference between lower and upper values for the maximal fuel elongation estimation is between 15% and 75% (of the mean value).

For Cases where no slipping between the fuel and the clad is assumed (when the gap is closed), the clad elongation follows the fuel one when the gap is closed, and the maximum value for clad elongation and fuel elongation are relatively similar. Lower values for clad elongation are observed for Case No. 2, Case No. 3 and Case No. 10 where an initial gap is assumed.

As a consequence, the difference between lower and upper values for the maximal clad total elongation is between 20 and 75% (of the mean value) except for Case No. 7 (see Figure 4.42).

However, the long term behaviour is not the same for all simulations (see Figure 4.40 for Case No. 1 and Figure 4.41 for Case No. 5) because the permanent elongation reached is strongly linked to the gap opening time.

Figure 4.43, Figure 4.44, and Figure 4.445 show the gap width evolution for Case No. 1, Case No. 5, and Case No. 3 respectively: the gap opening time is clearly very different between all simulations.

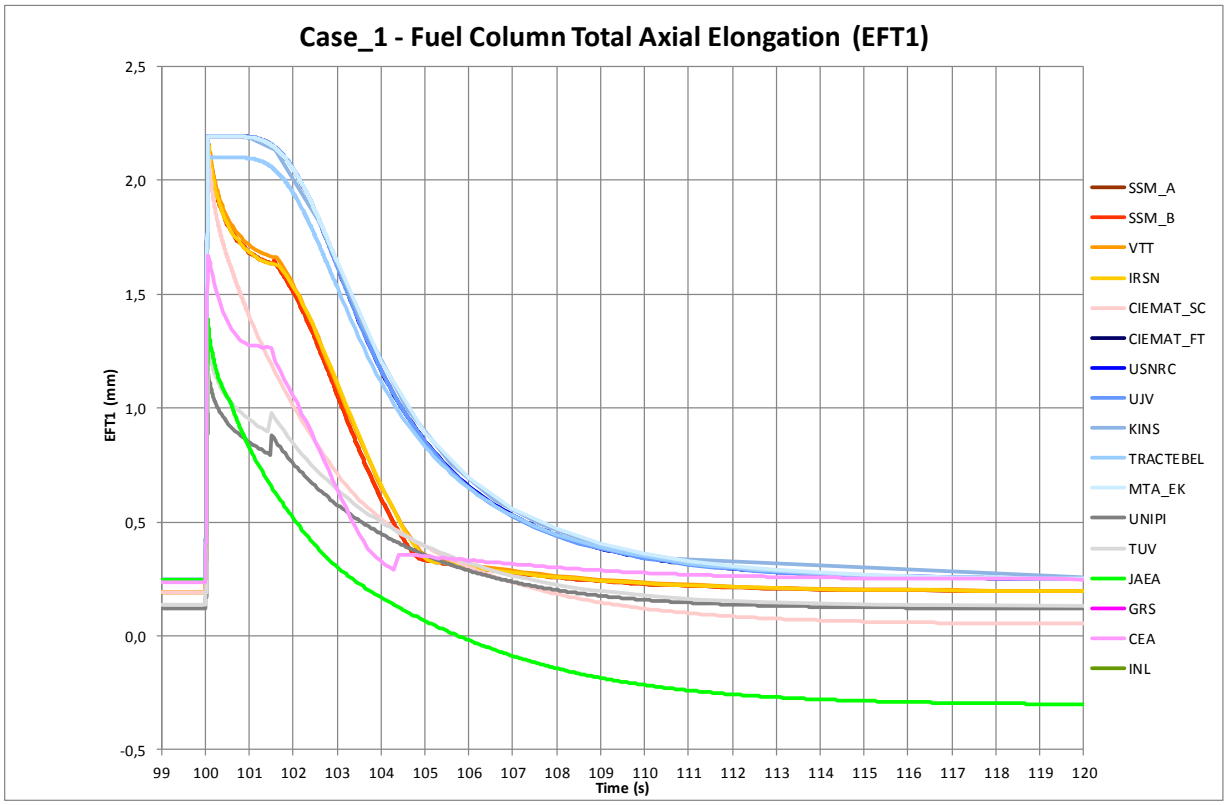

Figure 4.37: Case No. 1 – Fuel Total Axial Elongation

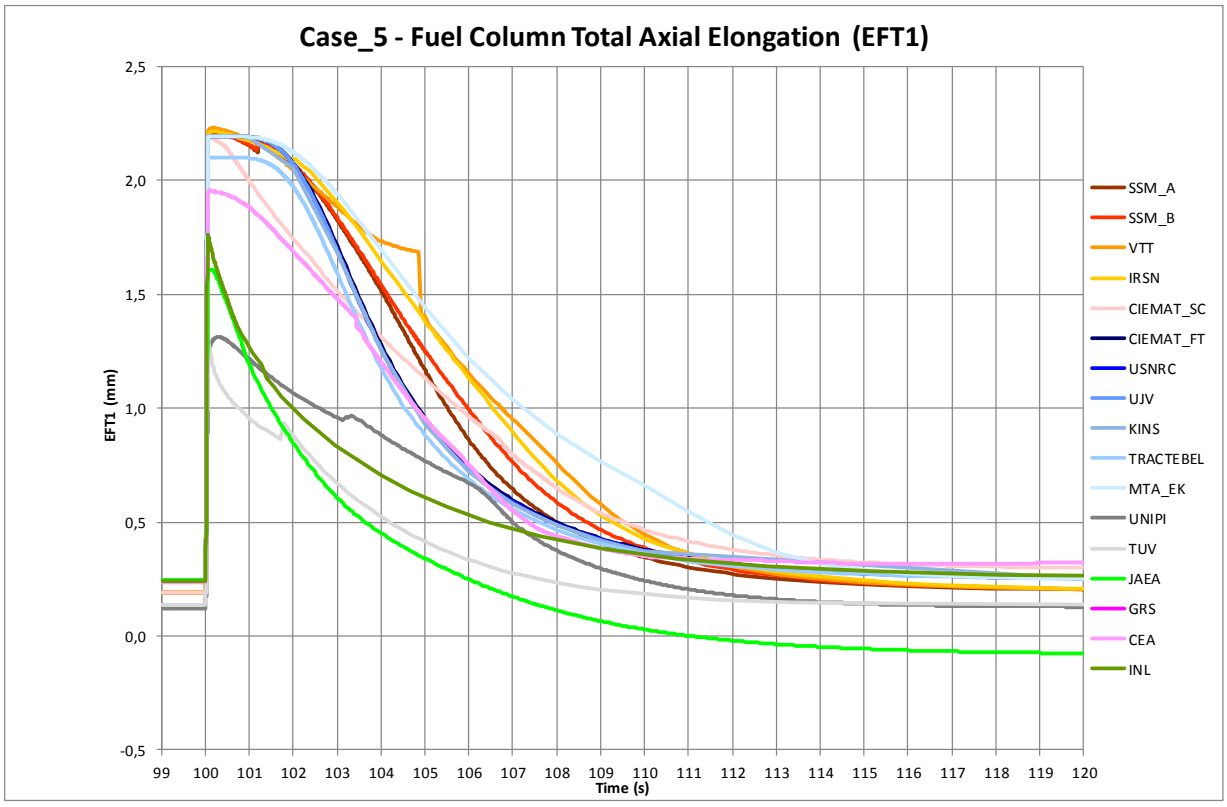

Figure 4.38: Case No. 5 – Fuel Total Axial Elongation

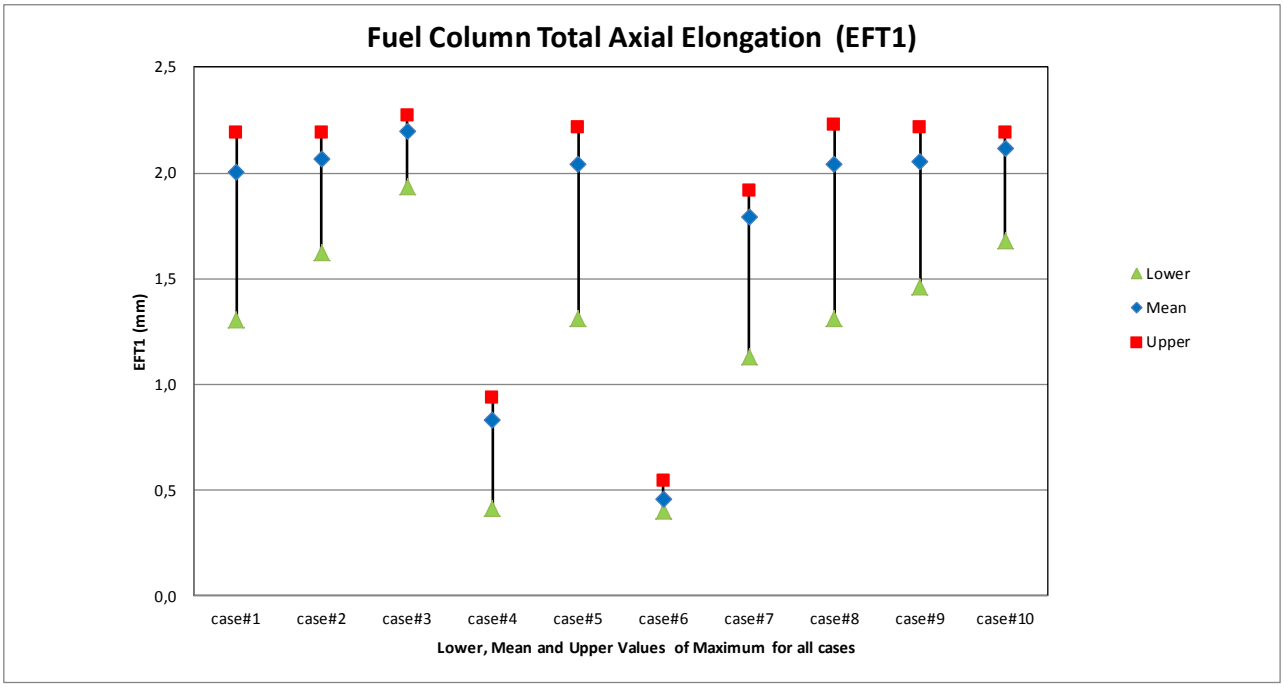

Figure 4.39: Fuel Total Axial Elongation – Values of Maximum for all Cases

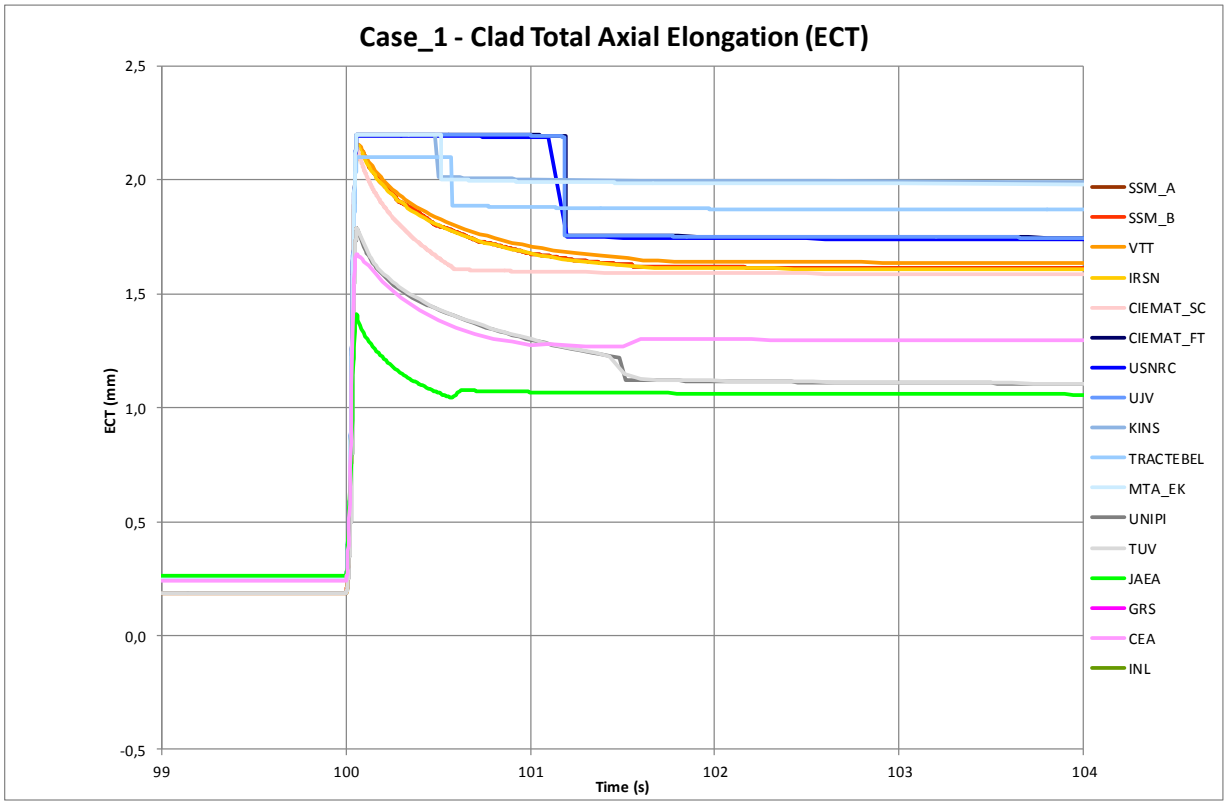

Figure 4.40: Case No. 1 – Clad Total Axial Elongation

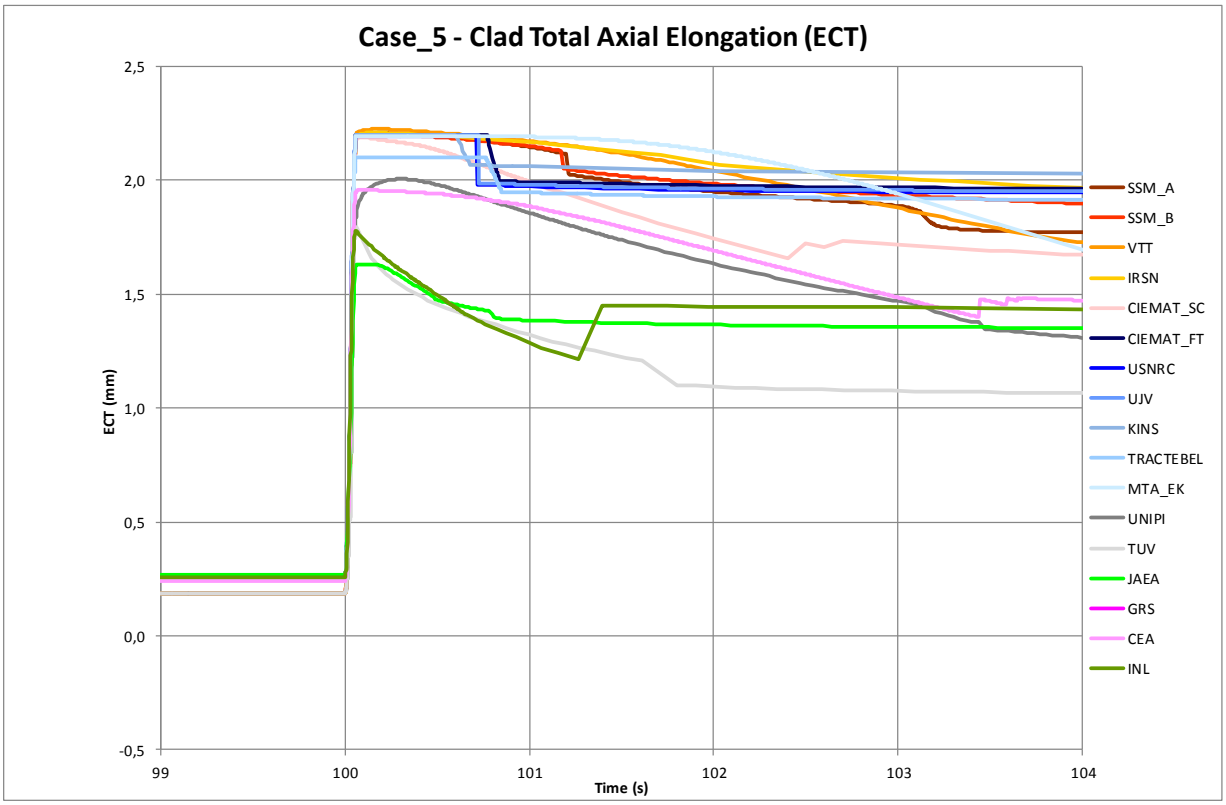

Figure 4.41: Case No. 5 – Clad Total Axial Elongation

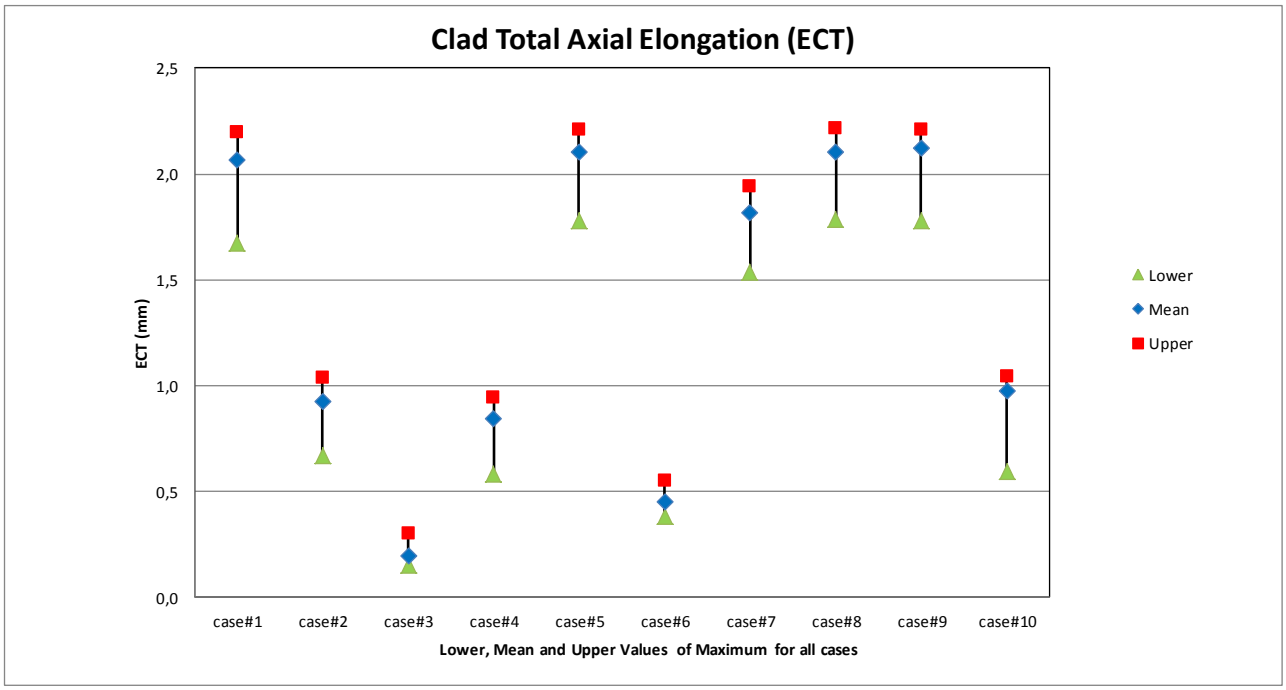

Figure 4.42: Clad Total Axial Elongation – Values of Maximum for all Cases

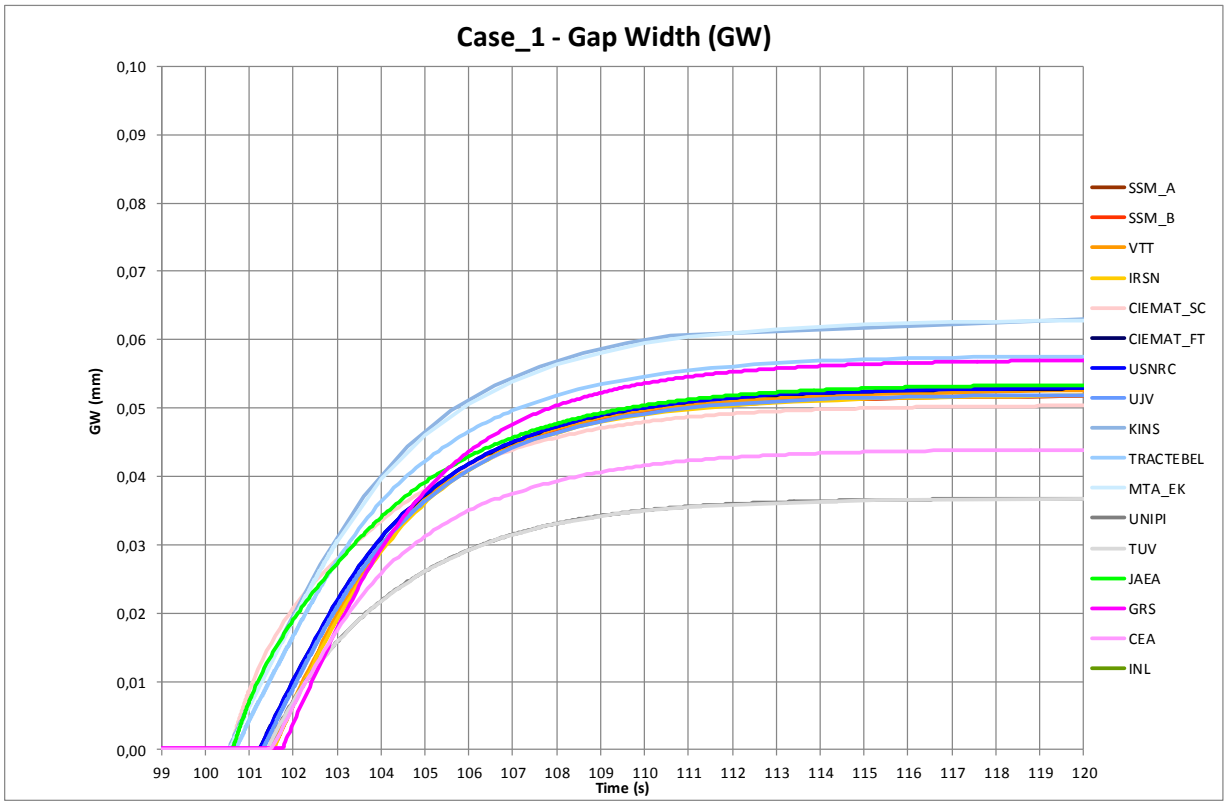

Figure 4.43: Case No. 1 – Gap Width

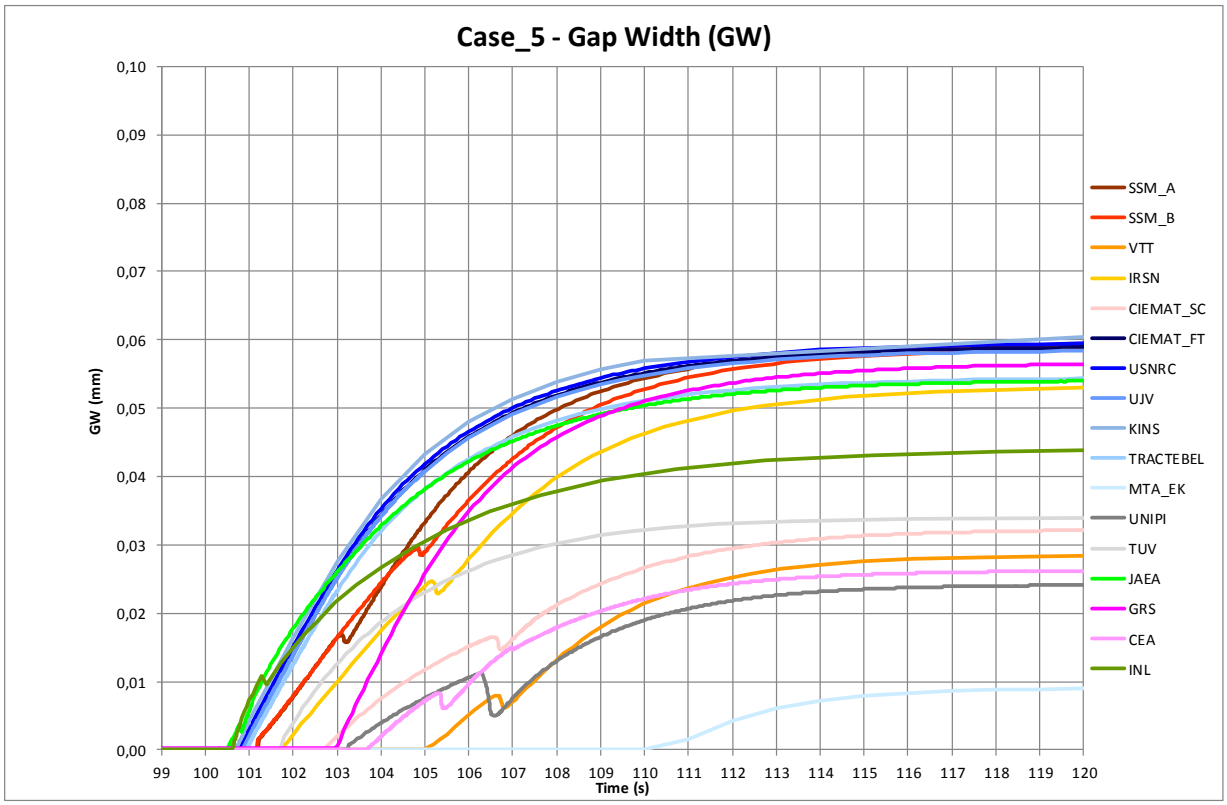

Figure 4.44: Case No. 5 – Gap Width

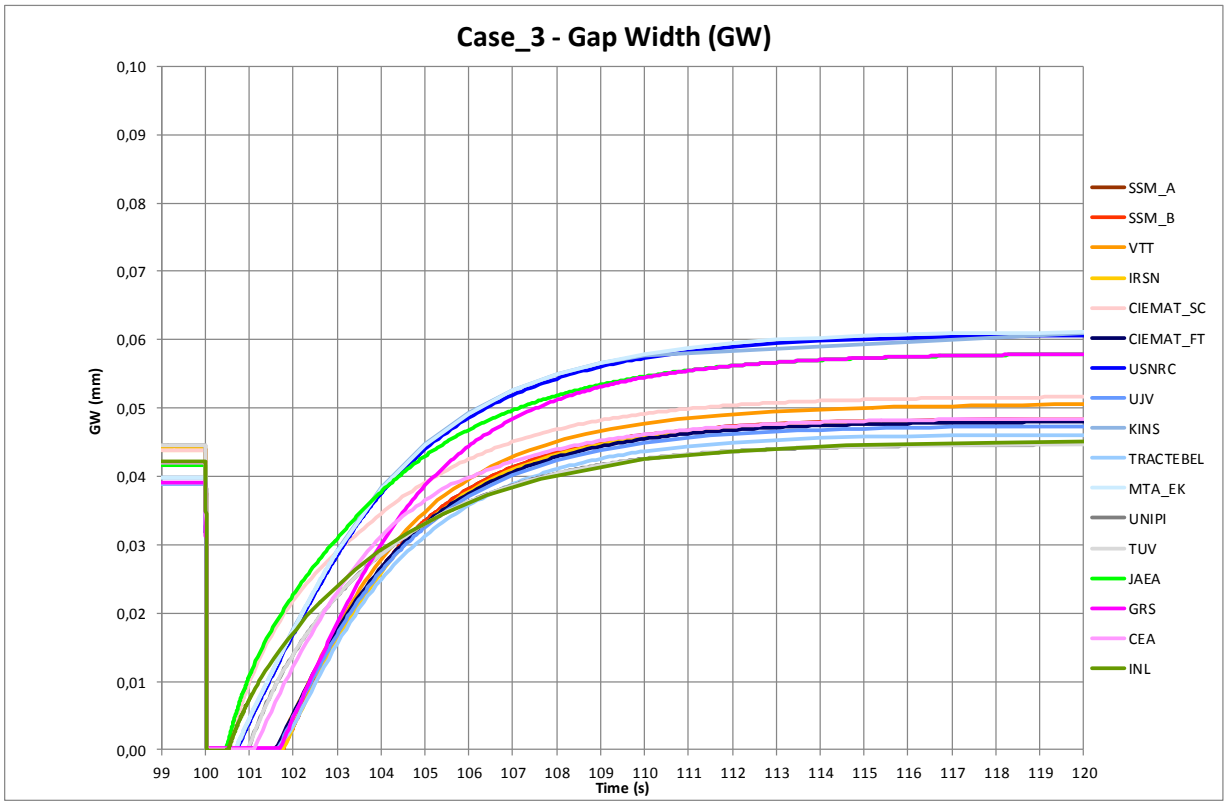

Figure 4.445: Case No. 3 – Gap Width

Finally, Figure 4.47 and Figure 4.48 show clad hoop stress evolutions for Case No. 1 and Case No. 2 (same Cases with and without an initial gap). As for the clad strain estimations, the behaviour is qualitatively similar in all simulations. But as can be seen in Figure 4.46, the difference between lower and upper values of the maximum clad hoop stress is very large up to about 170% (of the mean value). The long-term behaviour is also strongly influenced by gap opening time.

Those large differences can only be explained by very different modelling choices and different associated properties (like yield stress) in the codes for fuel and clad mechanical modules.

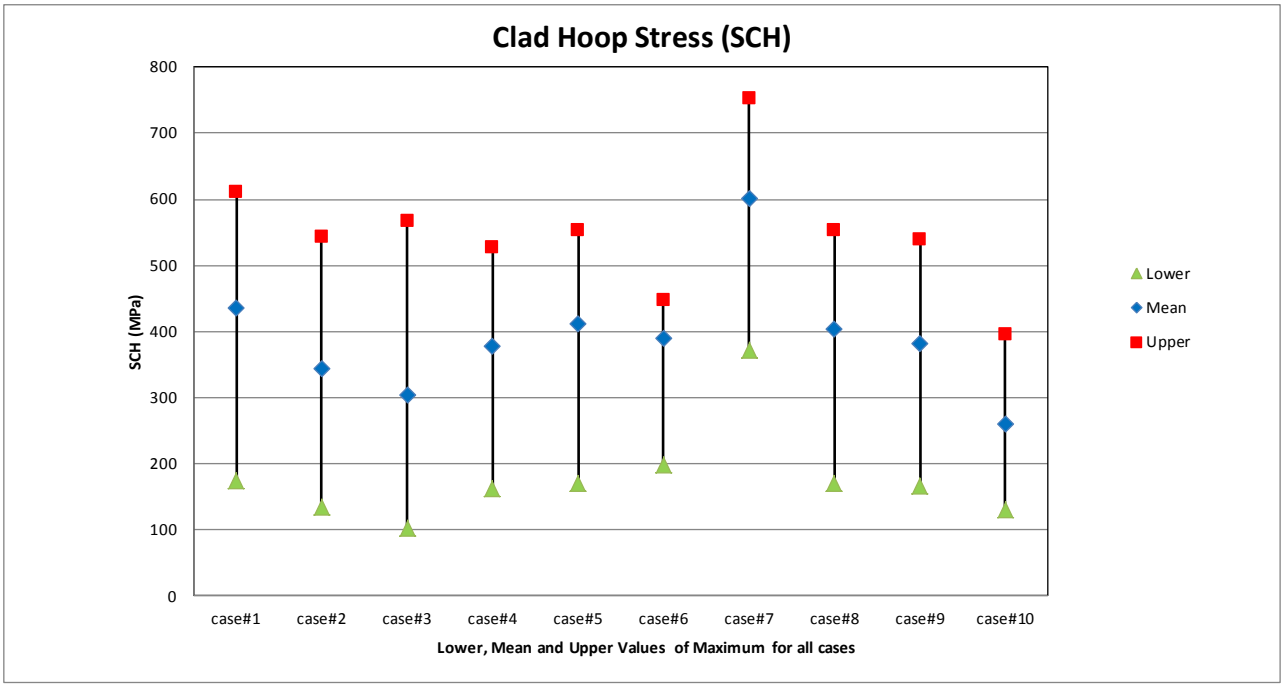

Figure 4.46: Clad Hoop Stress – Values of Maximum for all Cases

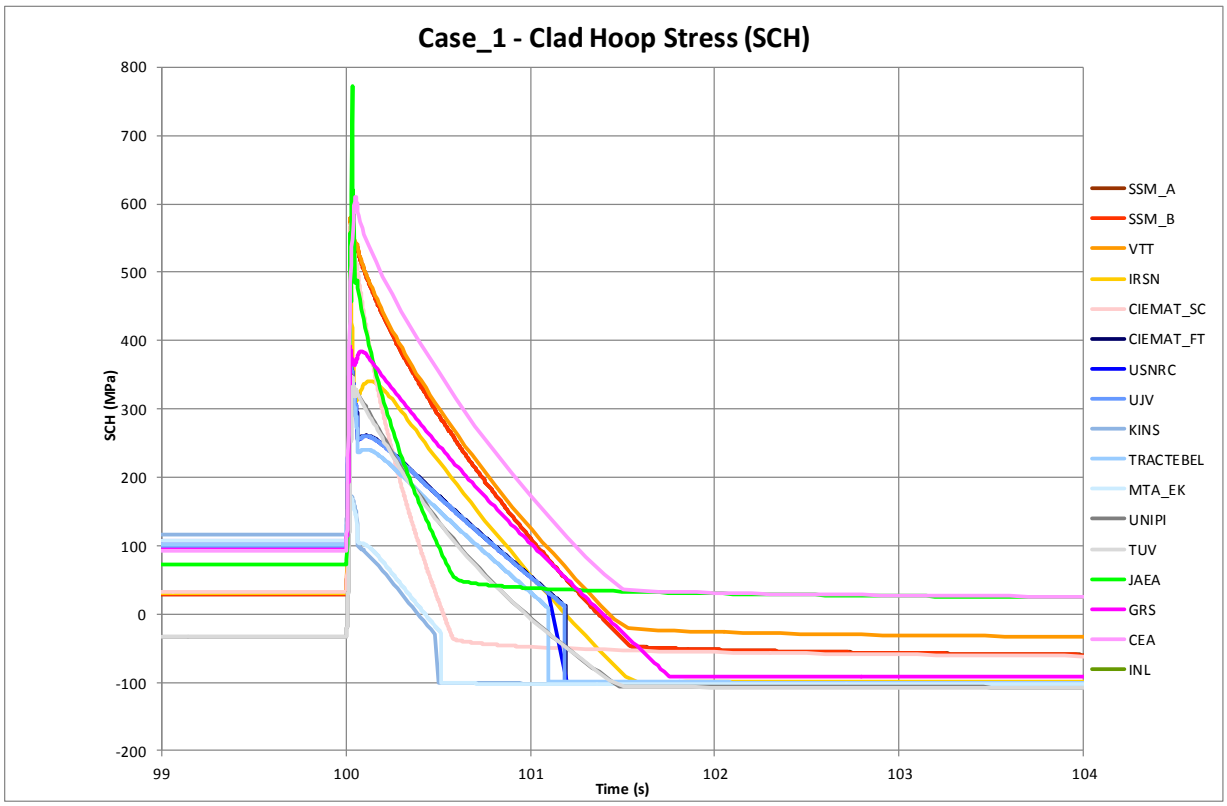

Figure 4.47: Case No. 1 – Clad Hoop Stress

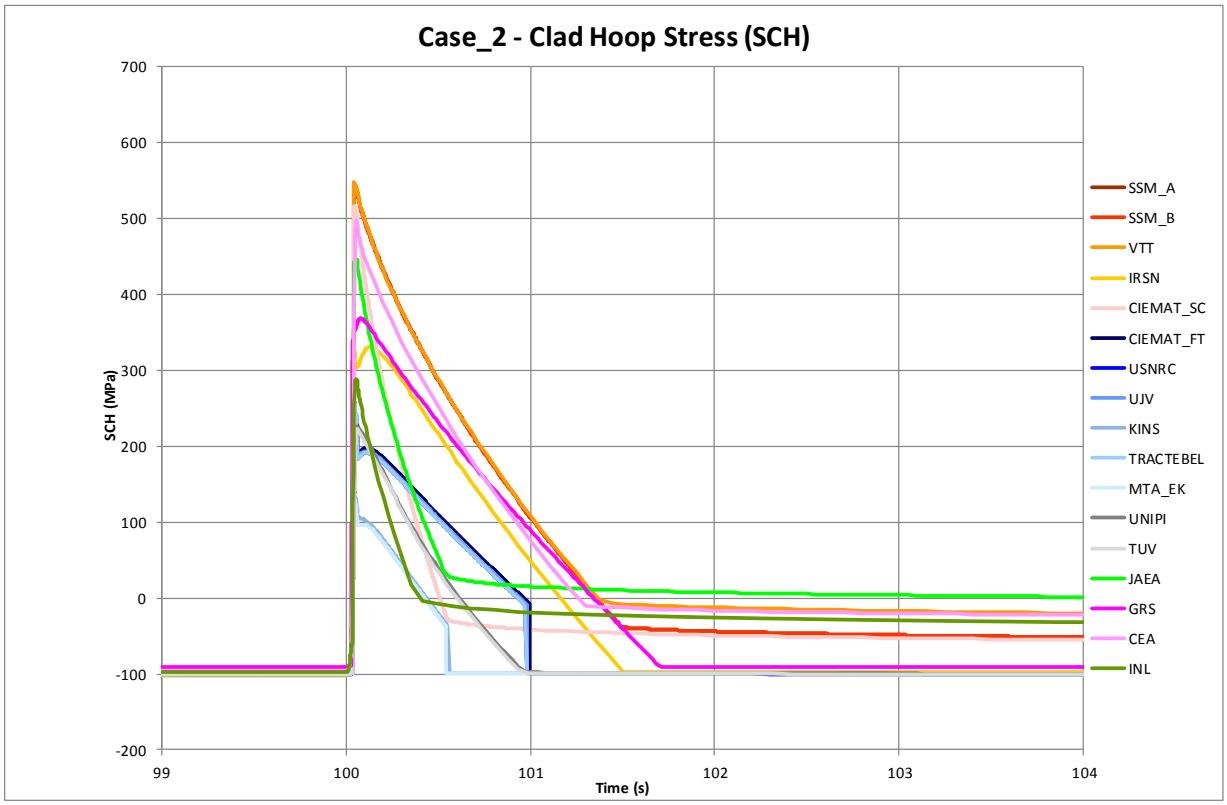

Figure 4.48: Case No. 2 – Clad Hoop Stress

4.3.3 *Analysis of heat-up phase*

As was done for the thermal parameters, evolutions of mechanical variables were analysed during the heat-up phase.

Figure 4.49, Figure 4.51, Figure 4-53, and Figure 4-55 show the evolution of clad hoop strain, clad total elongation, fuel total elongation and clad hoop stress for some Cases. All mentioned quantities behave similarly (among each other) during the heat-up phase, in contrary to the long term.

During the heap-up phase, all parameters reach a maximum value. The scatter regarding this maximum is between 25 and 65% for clad hoop strain, between 20 and 50% for clad total elongation, between 15 and 65% fuel total elongation and between 50 and 290% for clad hoop stress.

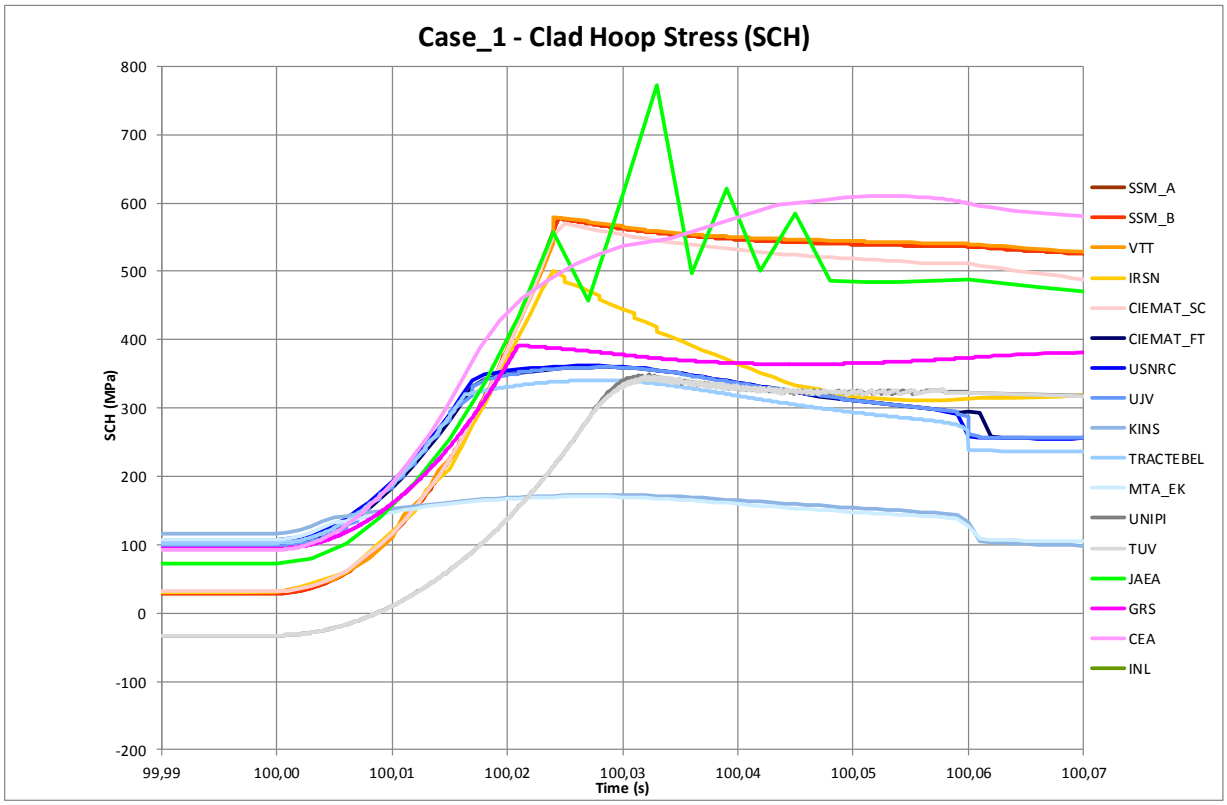

Figure 4.49: Case No. 1 – Clad Total Hoop Strain (Heat-up Phase)

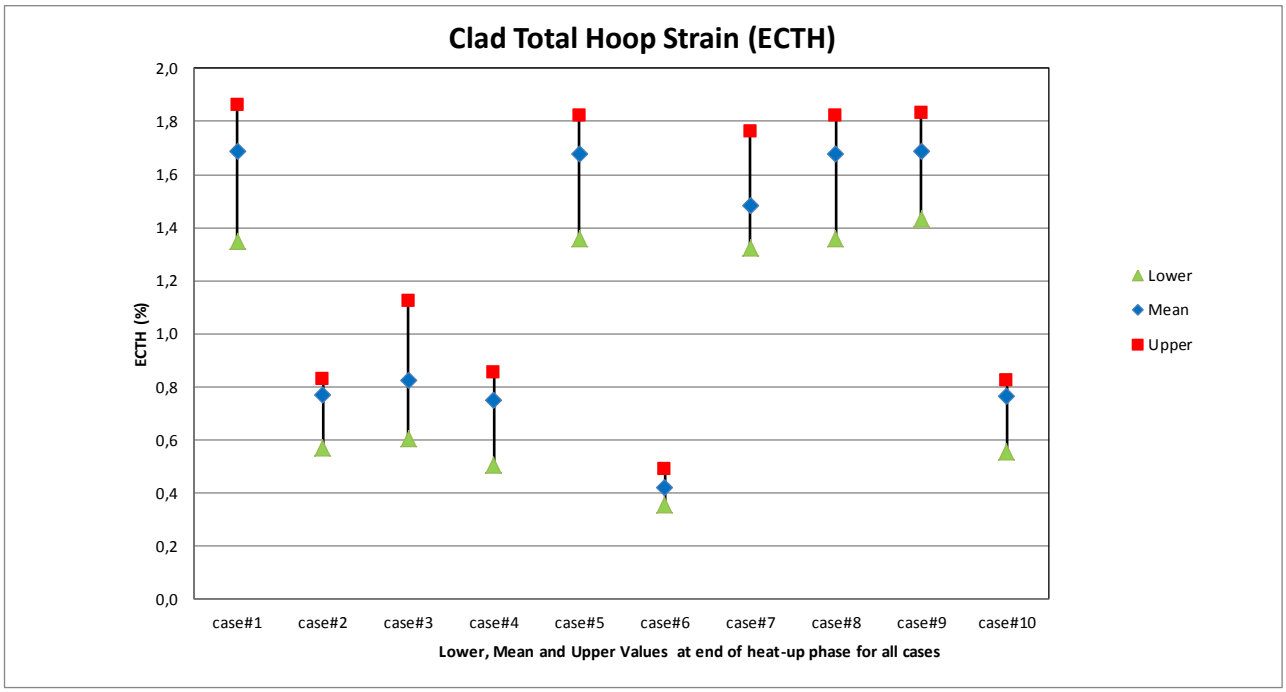

Figure 4.50: Clad Total Hoop Strain – Values at end of Heat-up Phase for all Cases

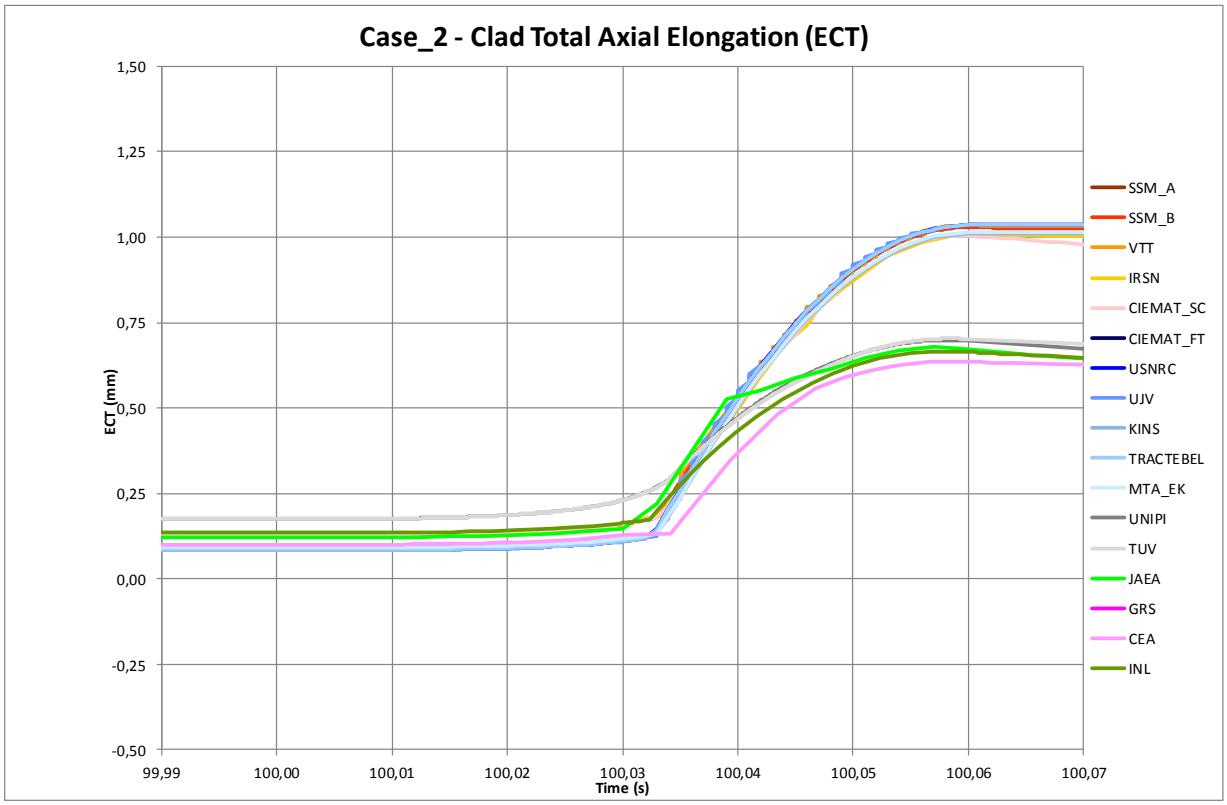

Figure 4.51: Case No. 2 – Clad Total Axial Elongation (Heat-up Phase)

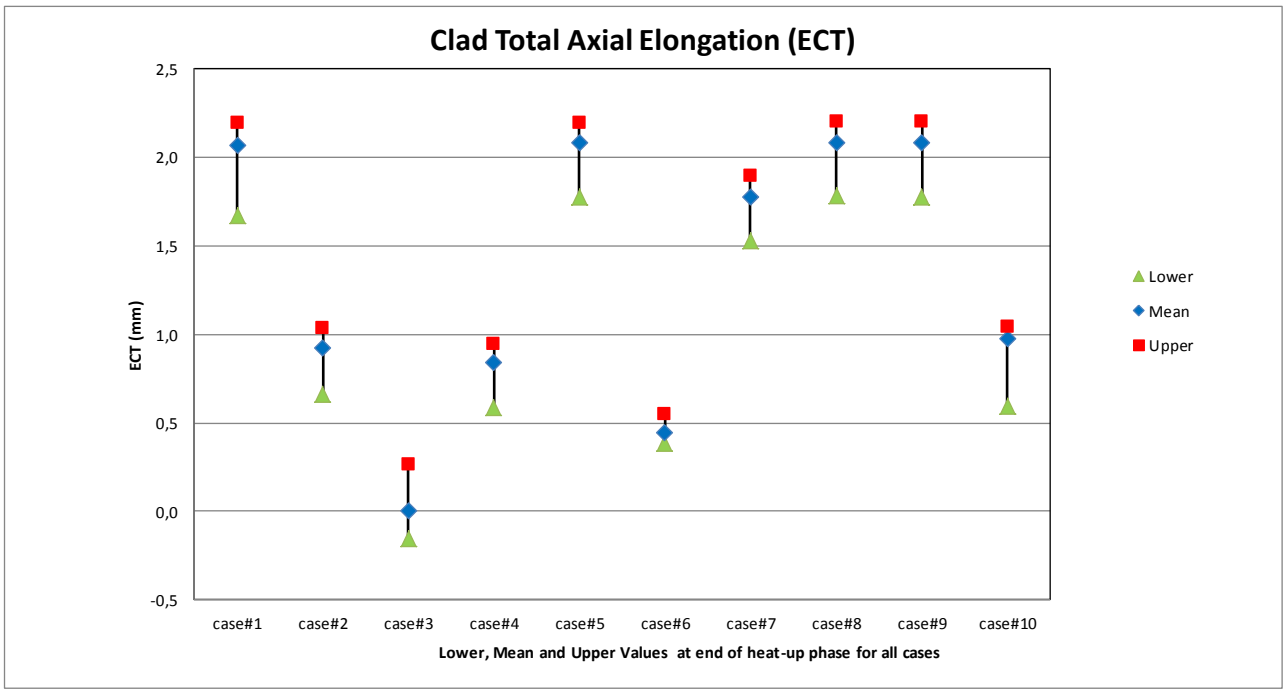

Figure 4.52: Clad Total Axial Elongation – Values at end of Heat-up Phase for all Cases

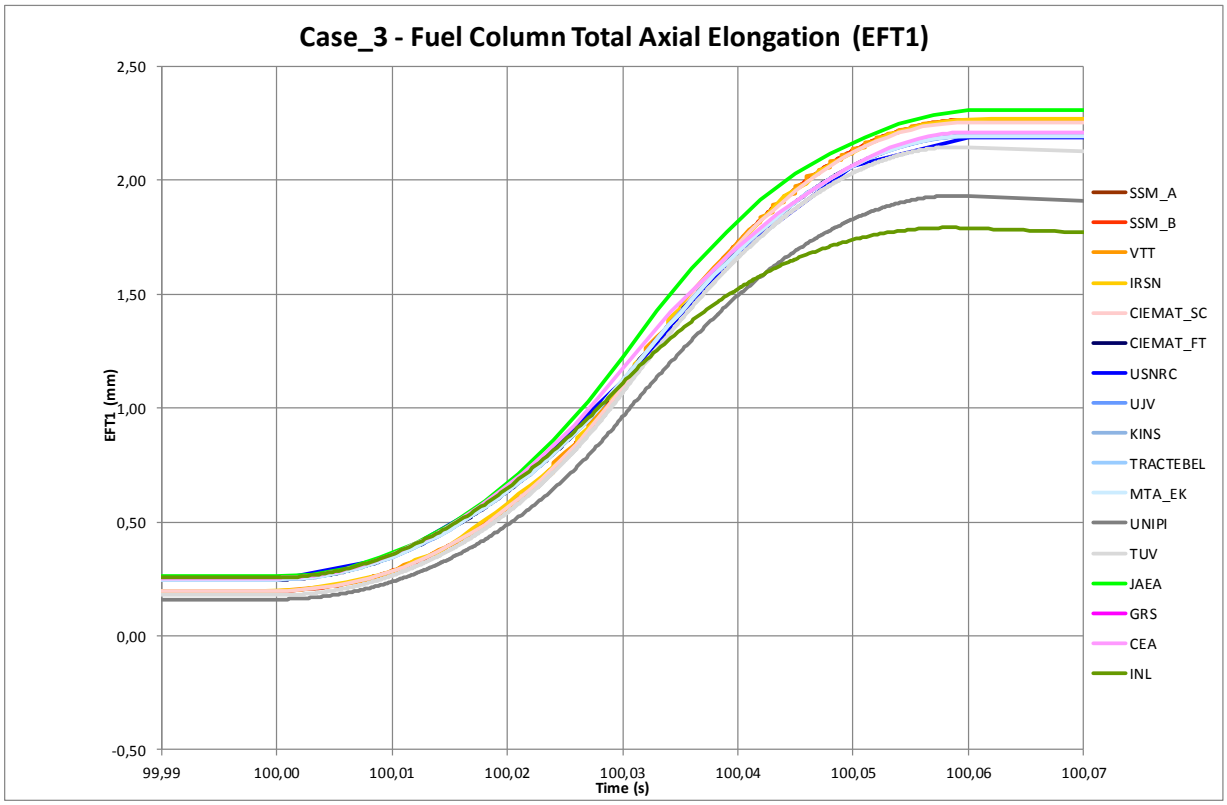

Figure 4-53: Case No. 3 – Fuel Total Axial Elongation (Heat-up Phase)

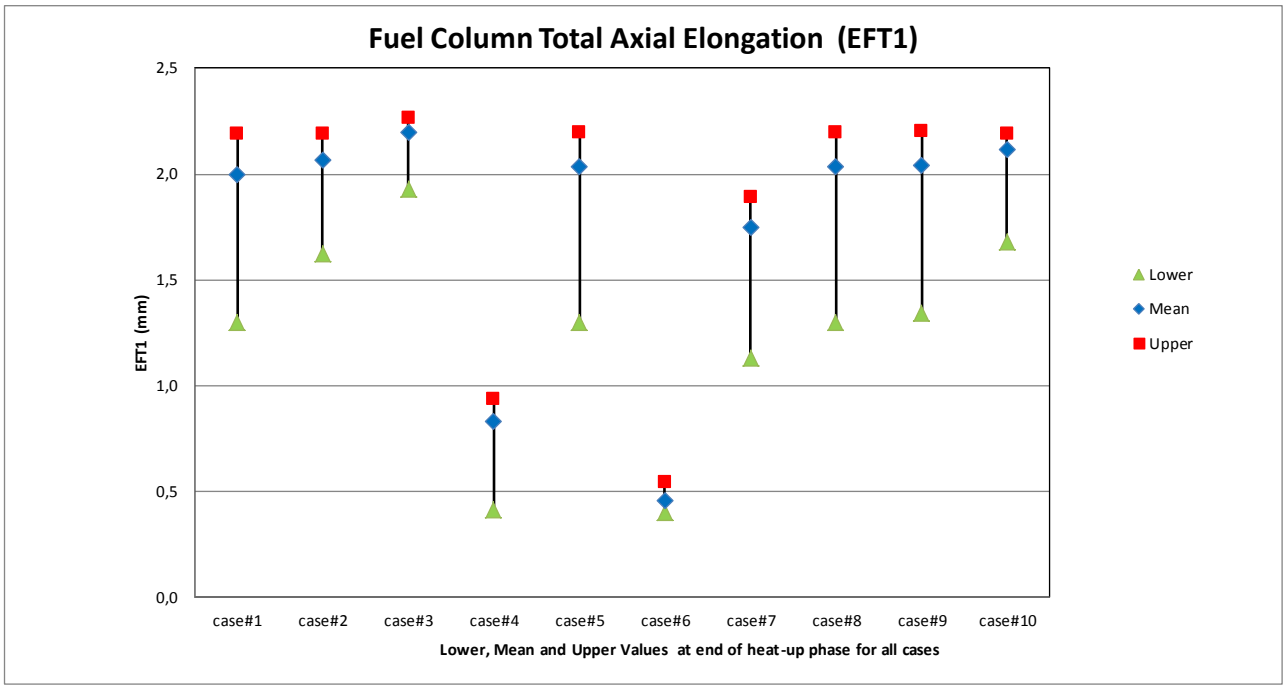

Figure 4-54: Fuel Total Elongation – Values at end of Heat-up Phase for all Cases

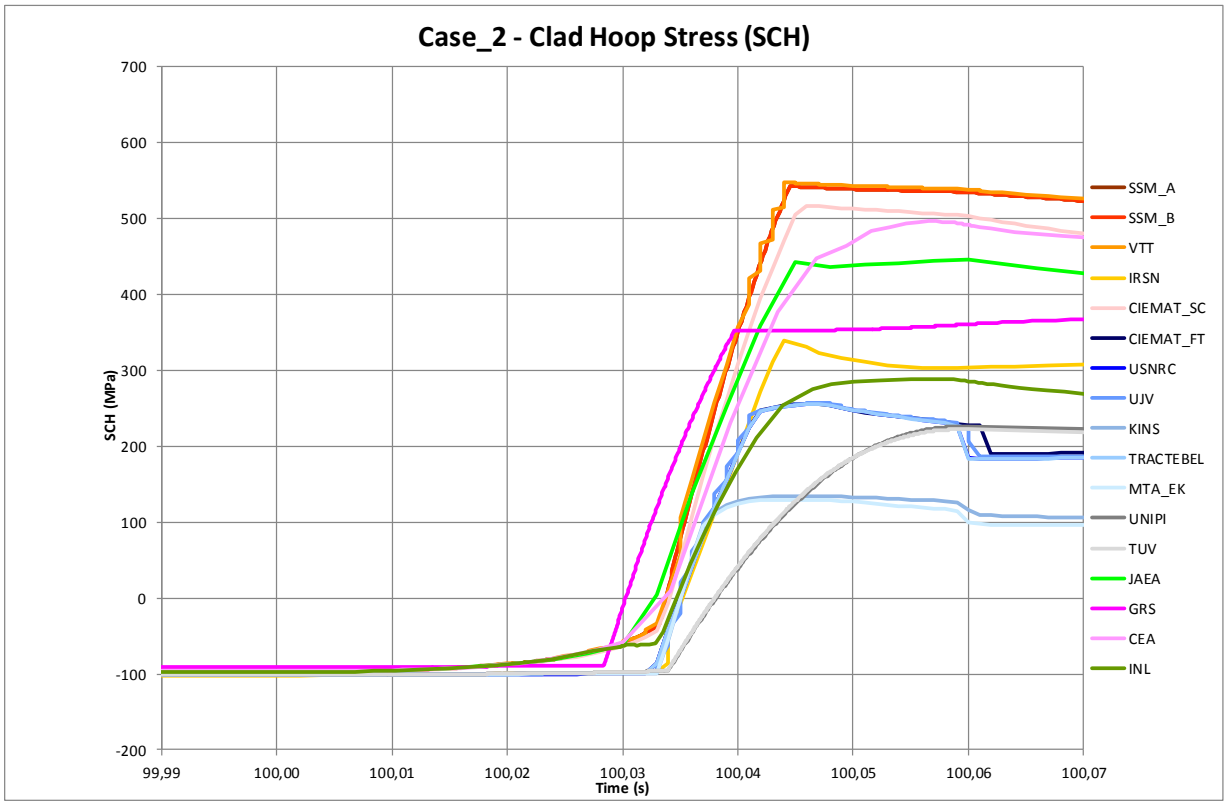

Figure 4-55: Case No. 2 – Clad Hoop Stress (Heat-up Phase)

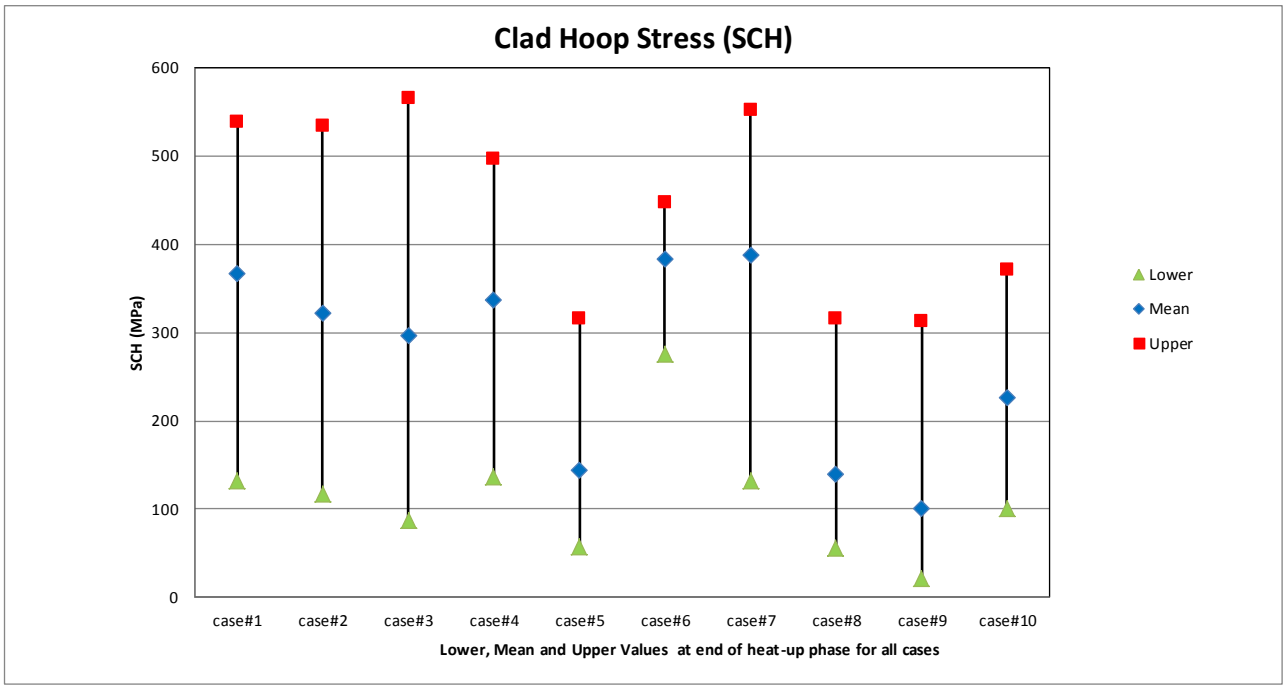

Figure 4-56: Clad Hoop Stress – Values at end of Heat-up Phase for all Cases

4.3.4 *Influence of clad temperature*

A special Case (Case No. 9) was chosen to study the influence of clad temperature on the mechanical behaviour of the rod. In that Case the coolant bulk temperature and the clad to coolant heat transfer coefficient were imposed to simulate a boiling crisis (similar to the one observed in SCANAIR calculation of Case No. 5) and the same power transient as in Case No. 5 was imposed.

The clad hoop strain evolutions for Case No. 5 and Case No. 9 are shown in Figure 4.57 and Figure 4.58. The scatter between all estimations is very similar: the differences on clad temperature prediction cannot fully explain the differences on mechanical parameters.

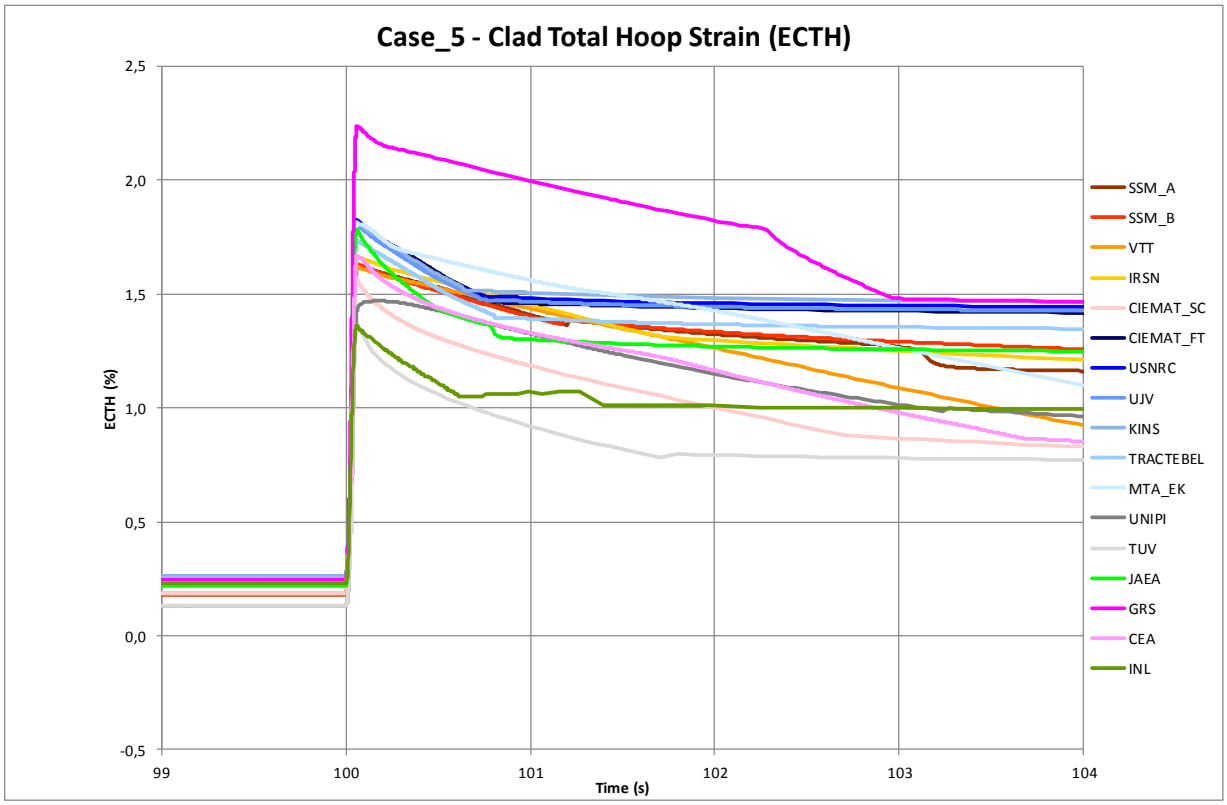

Figure 4.57: Case No. 5 – Clad Total Hoop Strain

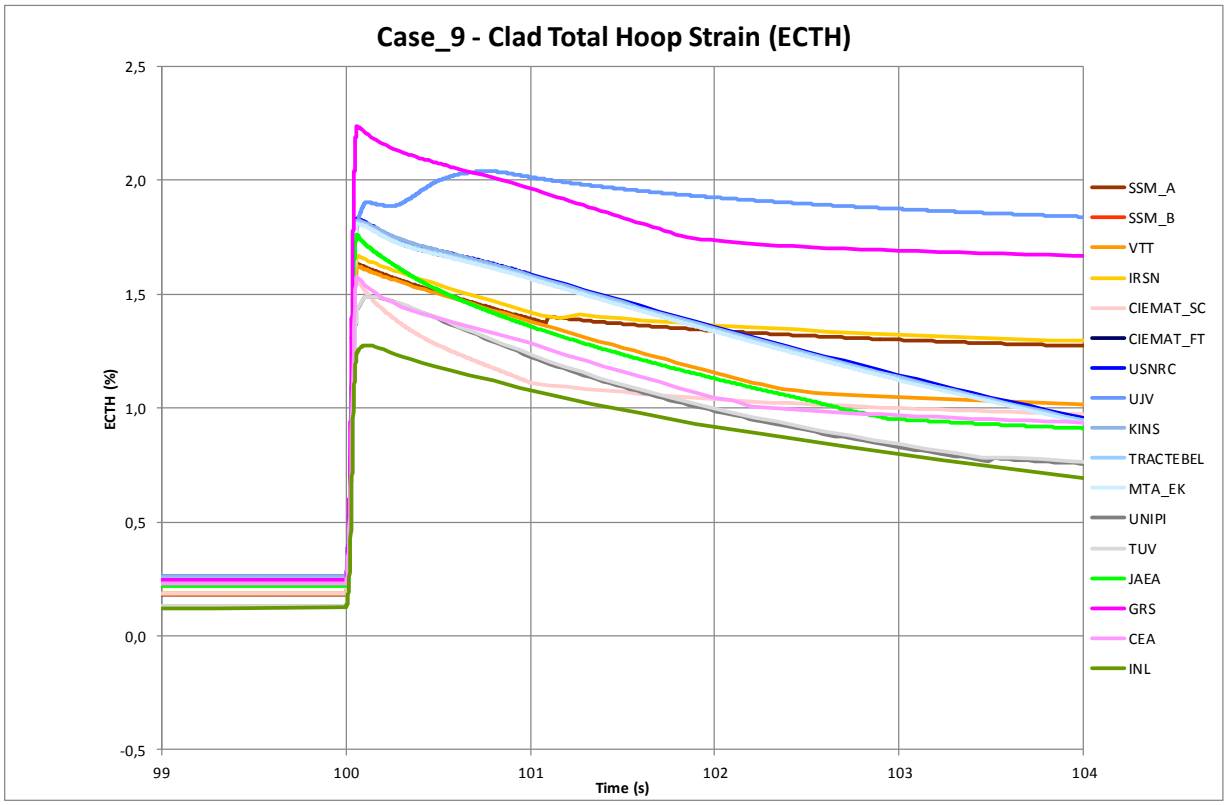

Figure 4.58: Case No. 9 – Clad Total Hoop Strain

4.3.5 *Influence of clad/fuel modelling*

The last Case (Case No. 10) was built to study the influence of clad/fuel modelling: modellers were requested to try to impose clad/fuel thermal and thermal-mechanical properties and models as close as possible to those of FRAPTRAN.

Figure 4.59, Figure 4.60, Figure 4.61, Figure 4.62, and Figure 4.63 show the clad hoop strain, clad total elongation, fuel total elongation, and clad hoop stress (for the transient and for the heat-up phase).

First of all, it is worth to note that it was rather difficult for some contributors to either perform this simulation or to follow the specifications because sometimes large code re-programming was necessary.

Nevertheless, two SCANAIR calculations give results very close to the FRAPTRAN ones for clad hoop strain, fuel total elongation, and clad total elongation. Concerning the clad hoop stress, one SCANAIR calculation is very close to FRAPTRAN during the beginning of the heat-up phase. But, after gap opening, which occurs earlier in FRAPTRAN, the agreement is poorer. This result shows once more that the gap opening has a great impact on the clad mechanical behaviour.

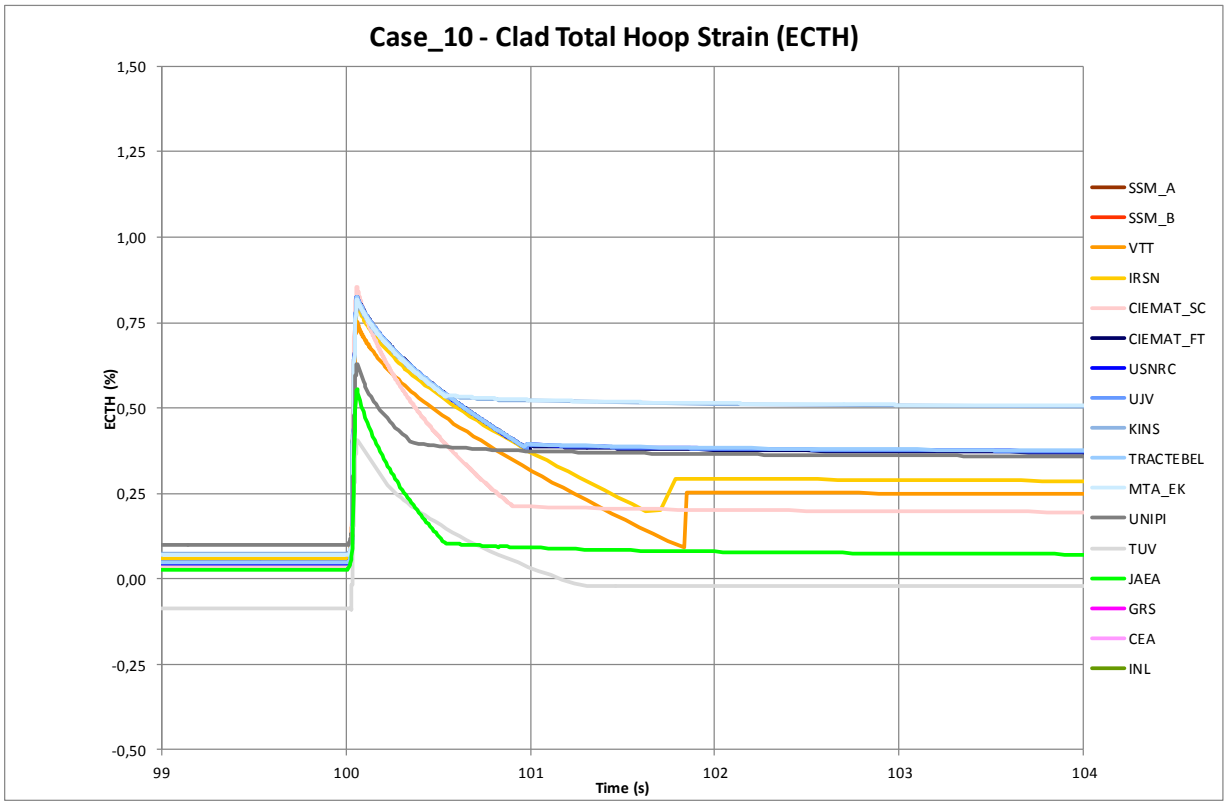

Figure 4.59: Case No. 10 – Clad Total Hoop Strain

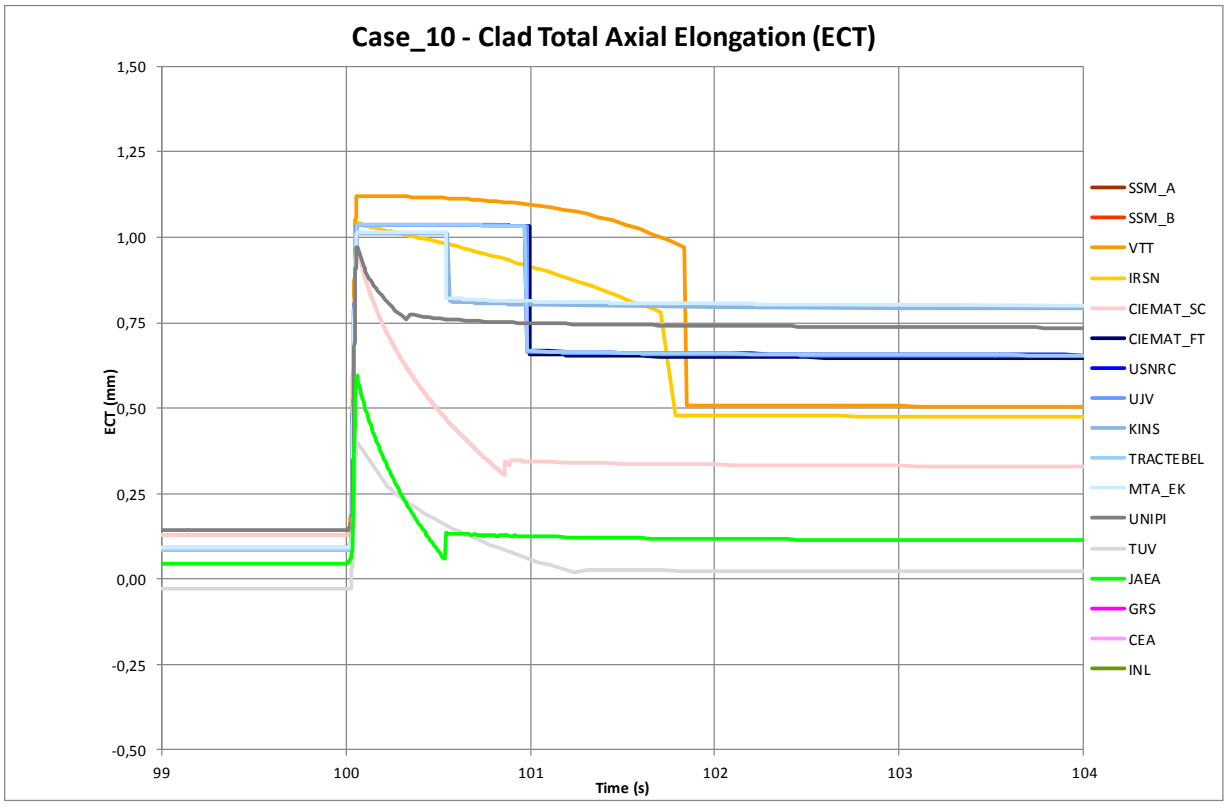

Figure 4.60: Case No. 10 – Clad Total Elongation

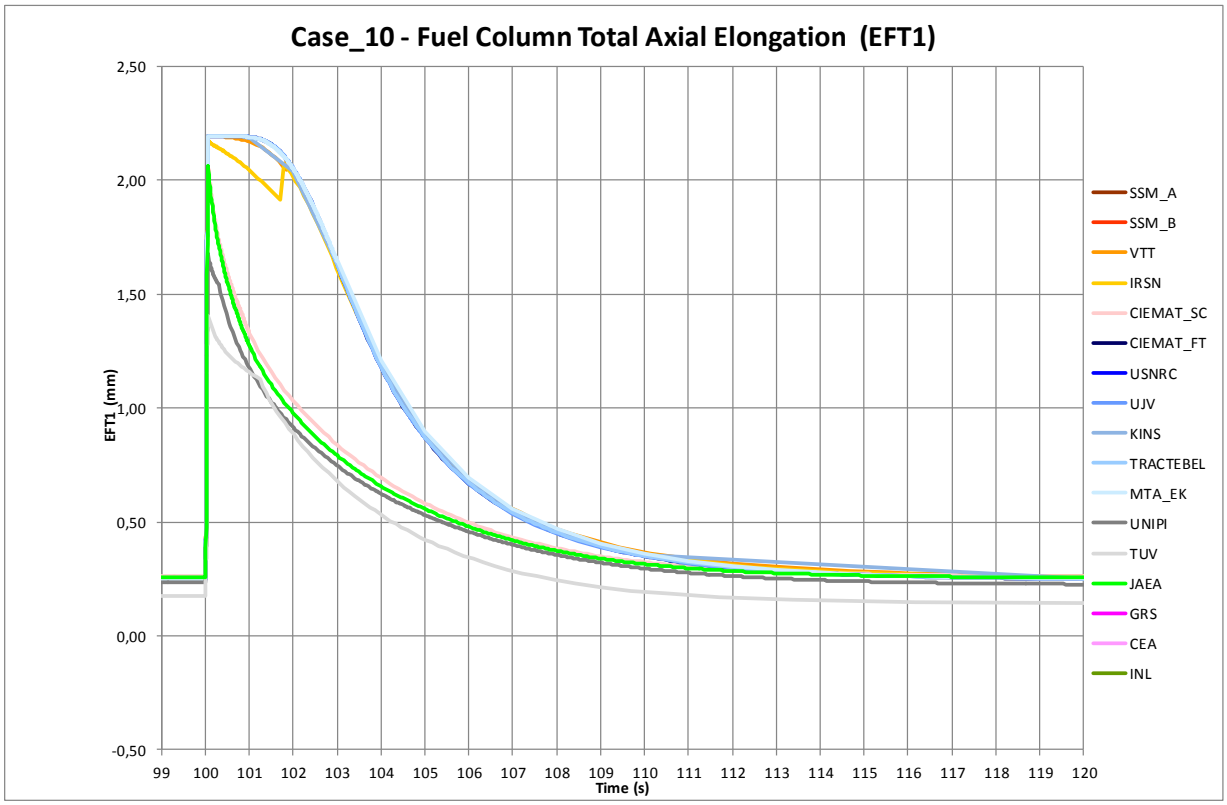

Figure 4.61: Case No. 10 – Fuel Total Elongation

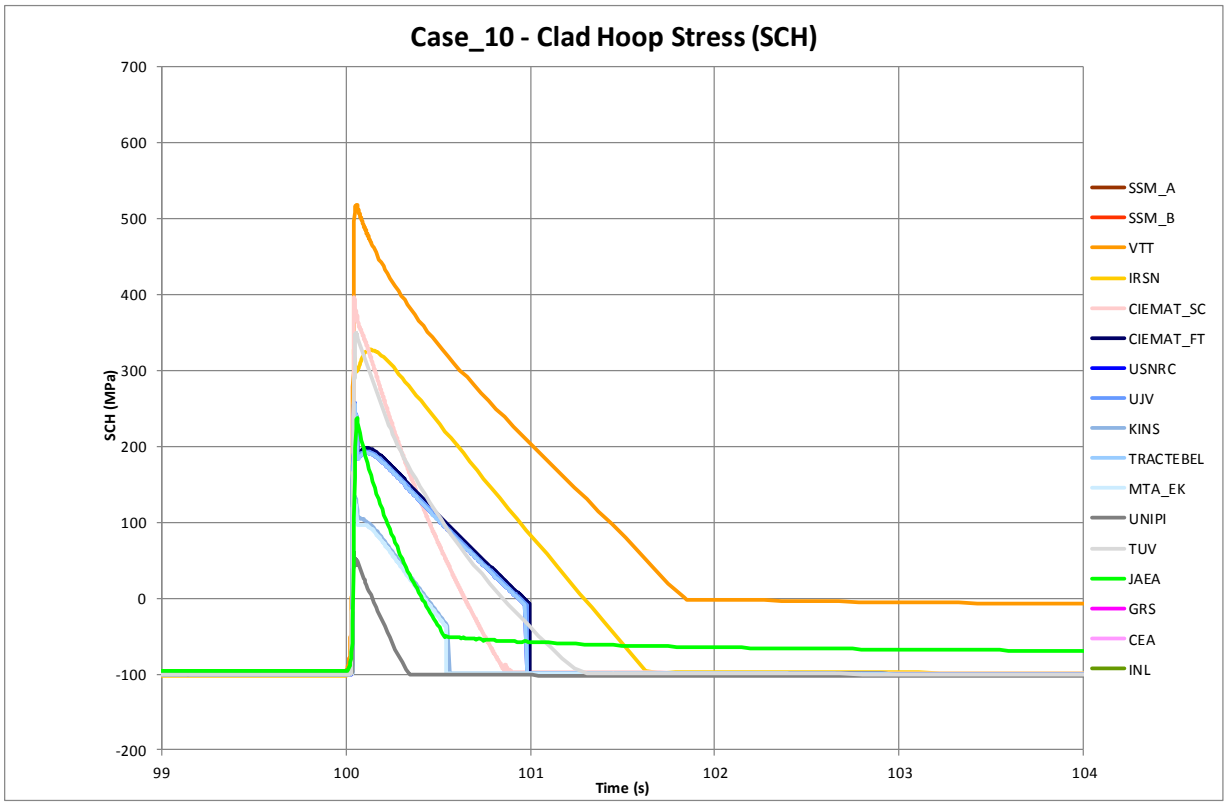

Figure 4.62: Case No. 10 – Clad Total Hoop Stress

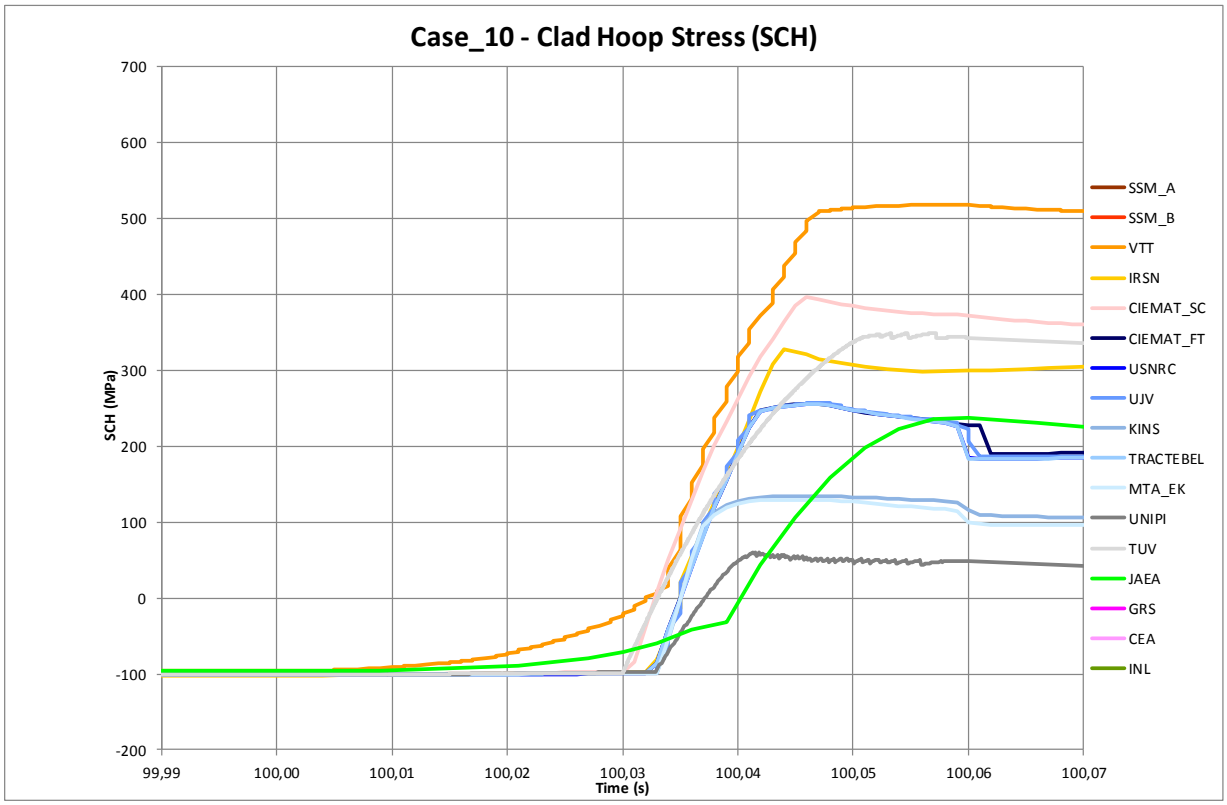

Figure 4.63: Case No. 10 – Clad Total Hoop Stress (Heat-up Phase)

5. RIA THERMAL HYDRAULICS – STATE-OF-THE-ART REVIEW

5.1 Introduction

Whenever risk of a rod's failure other than by PCMI during a RIA has to be estimated, the clad temperature, and therefore the clad-to-coolant heat transfer, is an issue. There is experimental evidence that reactivity-induced power transients can lead to sharp and complex variations of clad temperature. Boiling can be triggered that leads to a possible transition of heat transfer regimes with large variations of the heat transfer toward coolant during the transient. The analysis of the in-pile and out-of-pile experimental database dedicated to RIA with boiling shows that the heat transfer coefficient in the RIA-related conditions has very different values with respect to classical values and is sensitive to the power pulse width. It is very difficult to perform accurate measurements in those conditions. Moreover, there are few studies and a lack of understanding concerning transient boiling even in simpler configurations. Analysis of this database is still ongoing and all RIA dedicated boiling heat transfer models have a large part of empiricism. It follows that the heat transfer coefficient values deduced from the database cannot be directly applied to any real plant RIA transient; uncertainties have to be considered.

Thermal hydraulics in the RIA context concerns the model for the clad to coolant heat transfer that includes a model for the coolant flow. The Chapter 0 of this document provides a description of the models in several fuel rods codes. Thermal hydraulics is a matter of interest for the clad thermomechanical behaviour as far as the late phase (the so-called post-DNB phase) is concerned. Statistical analysis of the numerical simulation of this phase with a set of RIA fuel rod codes has been considered in the CSNI benchmark's exercise. It shows that the scattering is large in the prediction of temperature transients. Modelling improvements are still required to validate these codes in the post-DNB phase, and, among others, for the clad to coolant heat transfer, e.g. [52]. This low performance of the codes is a logical consequence of the hereinabove statement concerning transient boiling models reliability.

This statement has already been expressed in a previous state-of-the-art report [2]. The goal of the present analysis is to go beyond this statement by performing a more detailed analysis of the specificities of boiling heat transfer during a RIA. Similarities and peculiarities between classical and RIA related boiling heat transfer will be outlined. Most recent interpretations of experimental database and models will be used to improve and update the current understanding review. This synthesis provides elements of analysis of the scattering and of the level of confidence for numerical simulations of rod behaviour during a RIA as well as some orientations for future R&D programmes.

This review is organized as follows. In a first part, main peculiarities of the heat transfer toward coolant during a RIA will be determined. Then a selected summary of the present understanding of the boiling regimes is proposed. It focuses on the regimes of interest during a typical RIA and it includes a review of the corresponding available studies about transient boiling. Finally, the main tendencies of the experimental database are analysed thanks to this understanding and RIA dedicated heat transfer models are reviewed. It allows concluding on the remaining issues and on the possible origins of the uncertainties.

5.2 High clad temperature transients during a RIA

5.2.1 *Quantities of interest*

Whenever the heat of the power pulse cannot be efficiently released toward the coolant, clad temperature can reach high levels. According to the temperature levels and time length of this transient, cladding properties could be affected. Potential large deformation or different potential failure modes have then to be considered (large deformation and burst induced by a decrease of its strength, embrittlement induced by oxidation, or even melting).

To quantify the associated risk, one has to estimate the peak cladding temperature, the length of the high temperature phase or a more integral quantity, e.g., the time-at-temperature defined by van Houten [11] in a similar context. Those quantities depend on the model of the heat transfer toward the coolant.

5.2.2 *A high temperature phase that appears for large enthalpy insertion*

Let us consider the variation of a parameter of a typical RIA power transient, e.g. the maximal radial average fuel enthalpy, all other conditions equal. Above a threshold in this parameter, peak cladding temperature deviates from its initial value (that is the coolant temperature) by hundreds of degrees K and begins to be correlated with further increase of the parameter, see Figure 5.1. This sharp increase of clad temperature, far above the fluid saturation temperature, is a clear indication that no more liquid, but rather vapour, is in contact with the clad and that heat transfer toward coolant has been highly deteriorated. This sharp transition between heat transfer efficient and deficient regimes is classically referred as a boiling crisis or a departure from nucleate boiling. This phenomenon, which could lead to burnout of the heating materials for steady power conditions, corresponds actually to the onset of the so-called film boiling heat transfer regime. A vapour layer covers the clad and generates a high thermal resistance layer between the rod and the bulk of the coolant. After the temperature peak, the heat transfer stays low for a large temperature range and the cooling is slow.

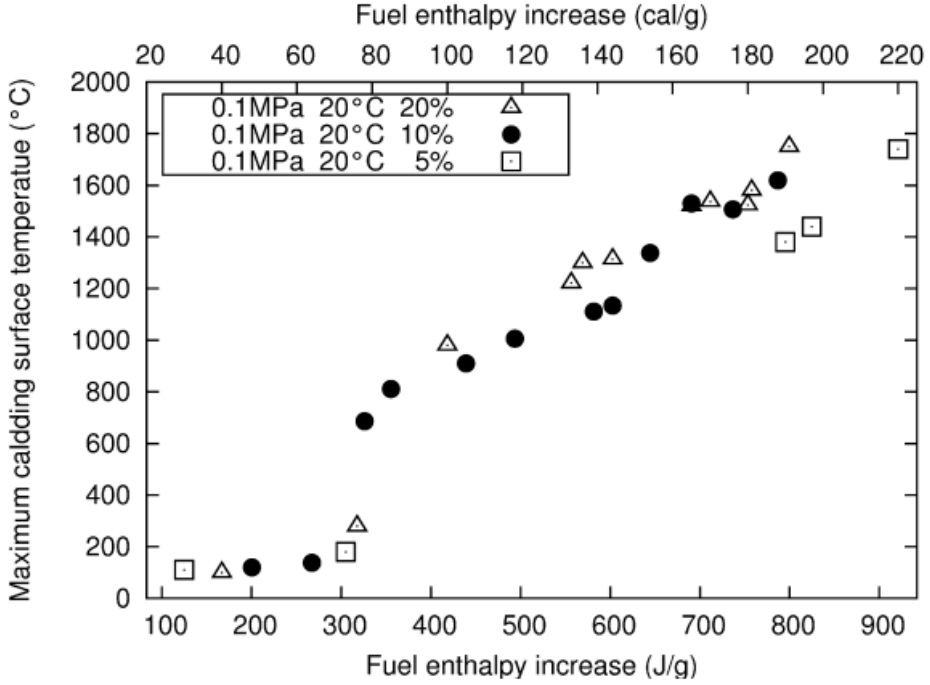

Figure 5.1: Maximum cladding surface temperature measurements for different fuel pellet enrichment, stagnant flow [3]

To provide some orders of magnitude, let us report, for example, about the thermocouple measurements of the cladding temperature history during a test performed in the NSRR facility that is illustrated in Figure 5.2. The temperature increases by several hundreds of degrees over approx. 1s and then decreases slowly during several tens of seconds till a sharp final decrease. From an inverse calculation of the heat transfer within the clad, and knowing the power pulse, it is then possible to deduce from this temperature measurement the time variation of the clad to coolant heat transfer, namely the wall heat flux Φ in W/m^2. The clad thermal path of a test can then be drawn on a wall heat flux vs wall temperature map. It is worth noting out that the transients features presented can vary substantially according to thermal-hydraulics or power pulse parameters and must not be considered as generic.

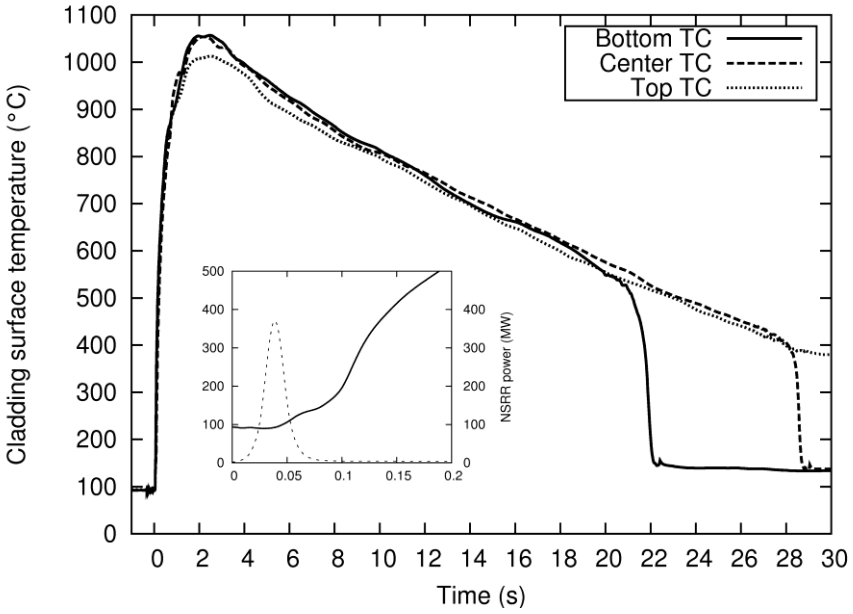

Figure 5.2: Cladding temperature evolution recorded on NSRR test 103-31-1 (0.1MPa, stagnant water at 90°C) and NSRR power (dashed line centre plot) [3]

Let us consider the path as reproduced schematically in Figure 5.3. It clearly shows a curve with several portions, corresponding to different heat transfer regimes, with a hysteresis. It is therefore really similar to the boiling curve or Nukiyama curve that allows describing the boiling heat transfer regimes of a given system (non-boiling, nucleate boiling, transition boiling, and film boiling). Boiling over a cylindrical rod with or without convective flow is a classical heat transfer configuration for which several models can be used to estimate the heat transfer coefficient in steady state cases. Plotting such models (the steady state dotted curve on Figure 5.3) and RIA-related experimental data on the same map shows a huge difference: heat fluxes and temperature ranges of each regime have significant variations in the power transient case with respect to the steady state cases described in the literature. It can be shown that those variations somewhat scale with the power pulse characteristics such that its width or the subsequent increase rate of the cladding temperature. As an illustrative example, Figure 5.4 shows the peak of wall to fluid heat flux, denoted CHF on the curve, as a function of the maximum linear heat rate for several pulse and clad conditions.

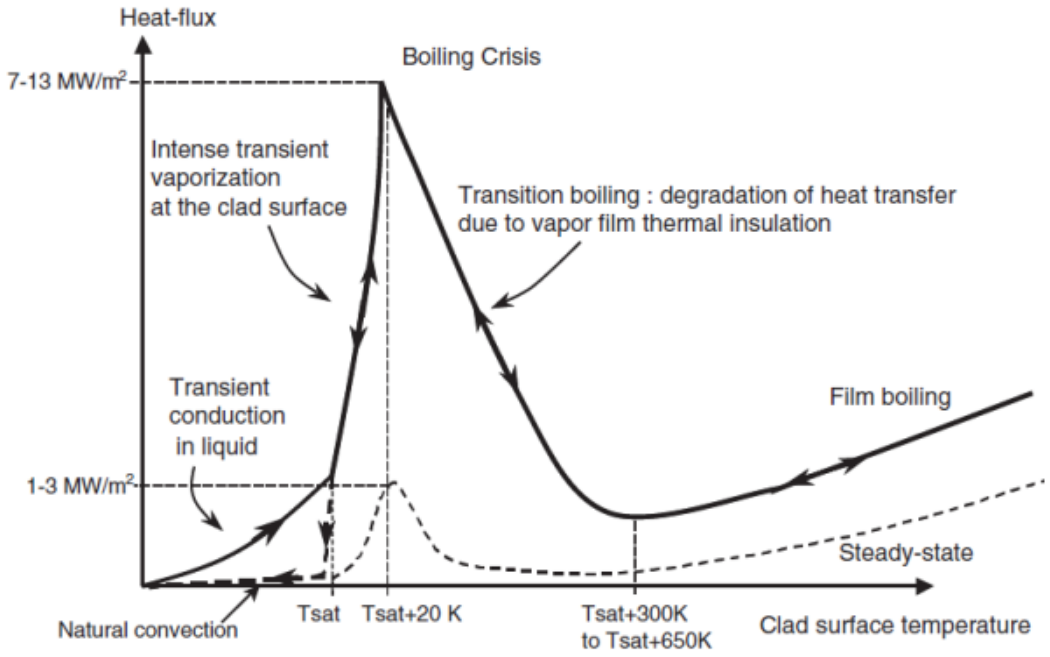

Figure 5.3: Schematic view of the experimental boiling curve in the NSRR tests, [4]

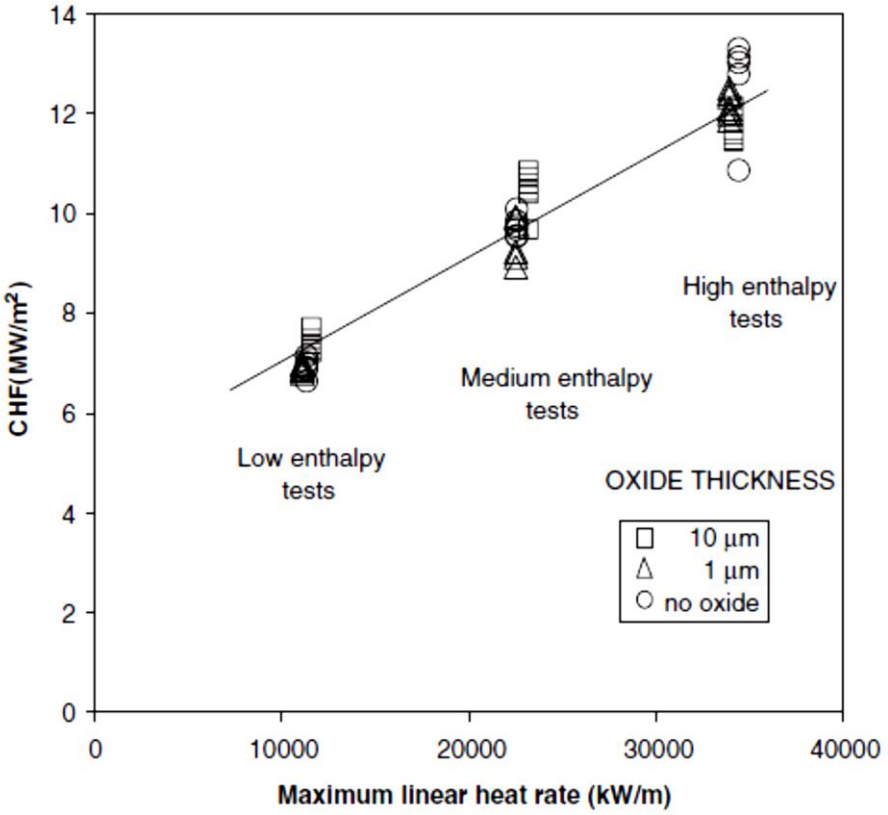

Figure 5.4: Variation of the CHF versus the maximum linear heat rate in the NSRR Surface Effect Tests, [4]

5.2.3 *Main difficulties to model the heat transfer coefficient*

A possible adaptation of classical models

The convective boiling heat transfer is known to depend on the main thermal hydraulic parameters: wall temperature, thermodynamic quality of the fluid[2], pressure and flow rate. The pressure mainly determines the coolant thermodynamics properties for liquid and vapour phases. Classical models all rely on relations between those parameters to express heat transfer coefficient and are valid for a given range of parameters. On the one hand, using the relations inherited from the thermal hydraulics study, e.g. of other nuclear applications, involving steady state convective boiling over fuel rods (e.g. LOCA or DNB related studies) without any modifications will not allow matching the RIA related experimental database. On the other hand, the RIA-related heat transfer models, e.g. [4], [5] or [6], rely on some adaptations thanks to empirical fitting of those latter classical models. Several remarks concerning their limitation have to be outlined; all are related to the rather complex phenomena involved in this heat transfer process.

A limited set of data to be deduced from experimental tests

The set of data obtained for RIA transients using sodium as the coolant could not be helpful mainly because sodium has very different thermodynamics properties as compared with water (boiling temperature and Prandtl number more especially).

The data considered come from the NSRR and PATRICIA programmes. Among the hundreds of tests performed on the NSRR facility, and especially those that simulate a power excursion in a RIA, some provide temperature measurements of clad temperature, [6]. They cover a large range of different thermal hydraulics conditions, from stagnant to flowing water, at different water temperature and for 3 different pressure levels (ambient, 7MPa or 13-16MPa). Nuclear fuel rods types, irradiation, oxidation thickness of the clad are also varied.

Such boiling heat transfer transient has been reproduced with similar geometry and water as the coolant but different materials and heating mode in the PATRICIA experimental program. This thermal-hydraulics loop reproduced a large set of thermal hydraulics conditions to cool a cylindrical rod whose transient heating was controlled by Joule effect, e.g. [5].

Experimental study of heat transfer during a RIA-type power transient, and more especially for high pressure, high temperature and high flow rate of interest for the nuclear reactor applications, is very difficult to perform together with a high level of instrumentation and accuracy of the data. The quantity of main interest is the wall temperature of the clad on the liquid side. Temperature measurements using thermocouples on the clad wall can locally perturb flow and heat transfer. Moreover, to deduce the wall to fluid heat transfer, inverse heat calculations have to be performed that leads to rather high inaccuracies for such rapid transients (wall temperature increase rate can reach several thousands of degrees K per second). Uncertainties have been studied for both PATRICIA and NSRR experimental programmes, [4], [5]. They are relatively large and necessarily affect the precision of the models derived. Nevertheless, despite those uncertainties, heat transfer can be evaluated and variations according to main parameters can be analysed.

The amount of experimental data used to perform these models adaptation is rather small and does not cover the whole range of thermal hydraulics parameters and/or power transient of interest for RIA related studies. Even for out-of-pile studies, like PATRICIA, the power levels required leads to complex experimental devices and the risk of burnout, and it is very hard to get high temperature data.

2. The thermodynamic quality is the difference between the fluid enthalpy and the liquid enthalpy at saturation, scaled by the latent heat of vaporization. Subcooled liquid has therefore negative quality, and the value for two-phase fluid at thermodynamic equilibrium ranges between 0 and 1.

A limited understanding of the way transient heating affects boiling

The main reason of the adaptation of the models is the established statement that there exists an impact of the power transient on the heat transfer coefficient. As shown in Figure 5.5, the discrepancy between the heat transfer predicted by a model for the film-boiling phase, [14], and NSRR data is large and fitting parameter can be as large as a factor 8, e.g.[6], hindering the natural dependency of the models upon other parameters. But the choice for the adjustment parameters cannot be based upon physical arguments, simply because too little is known about transient boiling. In addition, as pointed out by Udagawa et al. [6], the irradiation effect that could act on the clad wettability leads to an additional empirical factor that does not rely on a model. Therefore, the range of validity of the RIA-related heat transfer model is reduced and the extrapolation above its bounds leads to a large uncertainty.

A sensitivity of the results to the models

Bessiron [5] has shown that the targeted results say the peak cladding temperature or the film boiling duration, are rather sensitive to some of those models, mainly the models that initiate the film boiling (departure from nucleate boiling) and the film boiling heat transfer at high wall temperatures.

The hereinabove analysis of the limitation of the RIA-related boiling heat transfer models clearly motivates the need for additional experimental studies as well as for further improvement of transient boiling understanding to improve their reliability.

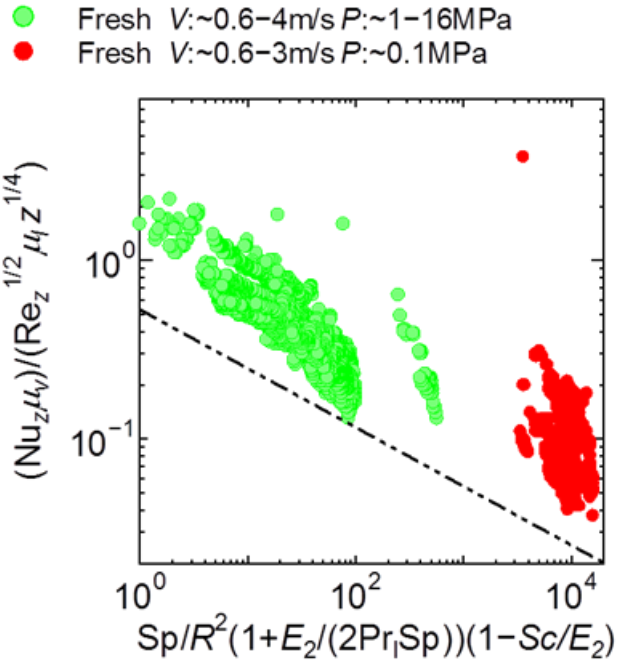

Figure 5.5: Comparison of inverse-heat-conduction calculation results with correlation by Shiotsu for forced flow condition, [6]

5.2.4 *Partial conclusion*

As a partial conclusion, the boiling heat transfer during a typical RIA power transient differs significantly from the corresponding steady state case even though the different heat transfer regimes are similar. The dedicated experimental data obtained so far have been used to determine some empirical modifications of classical models. Since only a few codes include such modifications, a large scattering is observed in the estimation of cladding temperature as soon as the power pulse does activate film boiling heat transfer (see Chapter 0).

The experimental database available to determine RIA-related heat transfer model is restricted to a small set of thermal hydraulics conditions that cannot cover the whole range of interest. Those conditions are not compatible with a high degree of precision in the experimental measurements. The use of empirical factors to modify the classical models can help to fit the experimental data but extrapolation out of the range of available data leads to uncertainty. Since the results appears to be sensitive to rather small variations of those models, this leads naturally to a low predictive level of cladding temperature transient for the nuclear fuel rod codes for the high temperature phase of a RIA.

This clearly indicates that further improvement could come from a deeper understanding of the variation of boiling heat transfer with transient power and subsequent analysis of the available data.

5.3 Boiling flows of interest for RIA-related heat transfer

Convective heat transfer in a given heater and flow geometry is known to depend on a set of parameters that can be reduced to the Reynolds and Prandtl numbers. Basic and classical relations, like the Dittus-Boelter correlation for turbulent flows, provide accurate estimation for steady cases. As soon as boiling occurs, the large set of possible flow configurations as well as the large variations of fluid properties on a reduced temperature scale (around the saturation temperature) leads to a complex variation of the heat transfer coefficient. Reviews of boiling heat transfer are numerous, e.g. [7] and [8], and the present section, intended for non-specialists of thermal hydraulics, will attempt to outline what is peculiar to RIA-related boiling and how the transient effect on the wall to fluid heat transfer could be understood.

5.3.1 *The onset of boiling*

When a wall is heated and its temperature goes beyond saturation temperature, the most common mode to initiate boiling is called heterogeneous nucleation. It corresponds to the growth of bubble nuclei entrapped in small defects of the wall. Models, e.g. [21], can explain the relation between geometry of cavities due to wall surface roughness, fluid thermodynamics properties and the wall temperature at the onset of boiling. For water, it leads to a few degrees above the saturation temperature. Transient heating can modify the onset of boiling temperature and be the dominant factor of its deviation from the saturation temperature, as shown by Sakurai et al. [20] among others. This can be explained by the deviation between steady state and transient boundary layers above a heated wall: onset of boiling conditions that corresponds to a possible bubble growth within the fluid nearby the wall can be obtained for different wall temperatures. It has been experimentally studied and modelled for transient convective boiling of refrigerant, [10]. Nevertheless, no model is available to determine the criteria for the onset of boiling over a rod in the subcooled convective case of interest.

5.3.2 *Nucleate boiling*

Efficiency of the boiling heat transfer is mainly related to the spatial arrangement of the liquid-vapour interface at which latent heat can be either absorbed or released and its distance from the heat source. The most efficient boiling regime is the nucleate boiling regime for which the wall mainly wetted has a low temperature whereas intense vaporization occurs at bubble foots. Those bubbles act as numerous and furtive latent heat conveyers and their dynamics as local mixing promoters. The typical process is therefore related to the “life cycle” of an individual bubble. Semi-empirical correlations can efficiently catch the

order of magnitude of the heat transfer but more mechanistic descriptions that clearly relate this bubble-scale process to the heat transfer coefficient are still not mature, [15]. Intense research and development activity exists, e.g. the development of numerical simulation, [16].

Transient heating can be understood to have an effect on the heat transfer process as soon as the associated time scale is small with respect to the bubble-scale process period. Very few research has been devoted to the study of transient nucleate boiling, e.g. [19] and for little different conditions. In transient heating experiments, the occurrence of nucleate boiling after its onset can lead to a stabilization of wall temperature as long as efficient heat transfer takes place. A so called temperature plateau is observed. It can be seen in the cladding temperature time evolution of Figure 5.2 (zoom of the centre plot between 0.07s and 0.1s).There is experimental evidence of this phenomenon in several experiments. Bessiron et al. [4] reported such plateau for high pressure boiling in the PATRICIA programme. In the NSRR programme, Sugiyama et al. [23] studied the impact of clad properties on the plateau level. In some transient cases, not even the time for a bubble cycle has passed before heat transfer deterioration and the nucleate boiling regime has not to be considered.

5.3.3 *Departure from Nucleate boiling*

Departure from nucleate boiling corresponds to the highest temperature or wall heat flux that can be sustained by the established steady nucleate boiling regime. Increasing either temperature or heat flux leads to the transition toward another boiling regime and to the vapour blanketing of the wall. The intrinsic or extrinsic nature of the limitation of the nucleate boiling regime is not clearly understood. Most of the time, empirical correlations, or look-up tables have to be used, and mainly provide a value for the corresponding critical heat flux, say CHF. It varies with pressure, flow rate, subcooling and heater geometry. Fundamental research is still going on to understand the phenomenon.

During a power transient leading to boiling, and according to the power pulse, the peak heat flux can either correspond to a transient peak in an efficient boiling regime before coming back toward steady nucleate boiling regime and quasi stable wall temperature, or to the beginning of a wall temperature sharp increase that indicates further transition toward film boiling. Around this peak, the intensity of the wall to fluid heat transfer can be very high and is not clearly correlated with the corresponding CHF values of the literature. As a function of the characteristic time scale of the power pulse, the peak heat flux deviates from the CHF that is recovered for large characteristic times. According to the pressure or the subcooling, the value of the peak heat flux can either decrease or increase when the characteristic time scale of the power pulse decreases, Sakurai [20], that proposed some interpretations of the tendencies.

Nevertheless, very little energy is transferred toward the coolant till peak heat flux due to the fugacity of this phase and the value of the peak heat flux is less determining for the clad temperature transient than the fact that transition toward film boiling occurs after that peak. It could be that the heat transfer intensity at the time for the peak is not the relevant parameter to determine further heat transfer deterioration. More than a model for the peak heat flux value, it is believed that a better understanding of the criterion for transition toward film boiling is required. This should rely on the study of the vapour formation process at the onset of boiling with high level power pulses.

5.3.4 *Film boiling*

Once the vapour film establishment conditions are satisfied, the key issue is how the heat transfer, that decreases, will unbalance the rod power, leading to the maximal temperature level and determining the film boiling phase duration.

In the film boiling regime where vapour is in contact with the heating wall, one can observe very different two-phase flow topologies and corresponding heat transfer processes: the liquid is either the bulk flow or a dispersed set of drops. There are therefore several film boiling sub-regimes as illustrated by the

different flow topologies that can be encountered above (and downstream) the quench front (QF) point on the scheme of Figure 5.6. Typical RIA-related thermal hydraulics conditions concern a low temperature coolant and therefore a large energy amount would be required to evaporate the coolant. This corresponds to a low negative value of the thermodynamic quality of the coolant flow, and the liquid is said to be sub-cooled. The corresponding film boiling regime corresponds to the so-called inverted annular film boiling (IAFB). Its experimental study requires large amounts of power, especially for water, therefore very little experimental data is available. As an illustrative example, in the Groeneveld look-up table, [13], that gathers all the available data of water film boiling, the lower limit in thermodynamic qualities is -0.2 whereas in the RIA context, either in NSRR or PATRICIA experiments, IAFB at thermodynamic qualities around -0.3 have been observed.

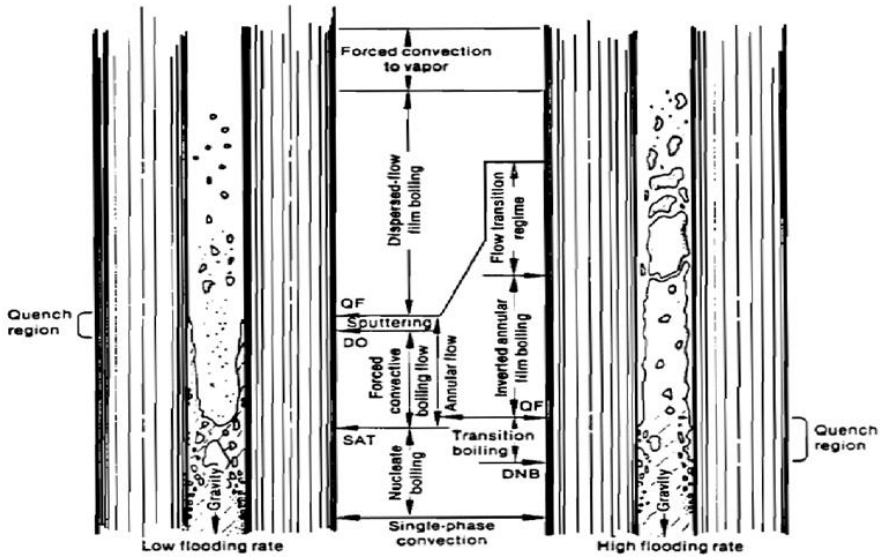

Figure 5.6: Scheme of the different flow boiling regimes for the cooling of hot rods thanks to a bottom-up liquid flooding rate [9].

In the IAFB regime, the heat transfer process from the wall toward the fluid is limited by the heat transfer resistance of the thin vapour film covering the wall. This rather simple flow topology allows modelling the heat and flow thanks to a two layer model. Some experiments using refrigerants have been used to model semi-empirically IAFB at low (negative) quality, [14], but additional empirical factors are still required to fit NSRR experimental data, [6]. It also reveals that the film thickness is an important issue. When film thickness, or void fraction, decreases, the heat transfer coefficient increases. This is not the case for any film boiling regime, and as an illustrative example, the inverse has to be considered for the dispersed flow film boiling regime (DFFB). Therefore, special care has to be taken when using film boiling correlations to estimate the heat transfer coefficient.

The time and space development of the vapour film can affect locally the heat transfer process at given macroscopic flow conditions, more especially close and/or just after the dryout location/time, e.g. [12]. This statement clearly indicates that during the establishment of the vapour film, the heat transfer coefficient can deviate from the corresponding steady state value. The experimental study of this low heat transfer regime at high temperature levels is difficult because of the associated risk of burnout of the wall. Except the data related to RIA, no experimental study involving water transient IAFB regime exist in the literature. Due to the difficulty to perform experiments and accurate measurements at high power, that is required to obtain this regime with water, experiments of transient heating leading to film boiling using refrigerants have been developed, by IRSN in collaboration with IMFT [17].

5.3.5 *Rewetting*

The end of the high temperature phase corresponds to a sharp transition toward efficient heat transfer regime, a quench that leads to a peak in the heat flux. The amount of heat released at the quench front can be very high, leading to a sharp decrease of the wall temperature toward a value close to saturation temperature and a stable nucleate boiling regime. Models for the minimum heat flux to sustain a vapour film between a hot wall and a bulk liquid flow that condensates the vapour exist in the literature. Some others correlate the quench occurrence to the wall temperature itself. There clearly exists an impact of history (speed of the quench front propagation) and of wettability on this process that limits the validity of the present models.

5.3.6 *Wettability of the fluid onto the wall and boiling*

The wall volumetric properties (heat diffusivity for example) have low influence on the boiling process that is mainly related to the vapour-liquid arrangement in the layer close to the wall. When liquid-vapour interface lies on the wall (the so-called triple line), like in the nucleate boiling regime, or to determine conditions for vapour film spreading or collapse, or when droplets impinge the wall, the wettability is a key parameter. Then, superficial chemical state, irradiation, surfactant, nano-particles or roughness of the wall are relevant parameters that could affect the boiling heat transfer. The wettability determines the relative affinity of the wall between the liquid and its vapour. It scales with the inverse of the surface tension of the fluid. High wettability promotes liquid contact and therefore heat transfer between the wall and the interface. In the RIA context, the results of Sugiyama et al. [23] of variations of the clad properties on boiling heat transfer at atmospheric pressure have been re-interpreted recently, [3] and [6]. For high pressure water, since surface tension is notably lower, the impact of surface properties on the boiling heat transfer should be lower and their determination require additional studies.

5.3.7 *Models for the boiling curve*

A set of expressions for the heat transfer coefficient, one for each regime, as well as criteria for regime transition is required to describe a whole “boiling curve” that can describe a boiling heat transfer process. The main thermal hydraulics parameters describing the heat transfer coefficient have known influence on its value, e.g. [7] or [8]. For example, an increase of the flow rate increases the heat transfer efficiency of a given regime. The pressure acts on the thermodynamics properties of water and increase of pressure tends naturally to decrease the difference between liquid and vapour. But no clear tendency on the heat transfer coefficient can be defined since various phenomena drive the boiling process along the whole boiling curve. A decrease of the liquid temperature as well as an increase of the bulk flow rate tends to increase the heat transfer coefficient in steady regimes. Due to the possible succession of regimes, there exist hysteresis effect due to the possible bifurcation of the heat transfer from a regime to another: when transition toward film boiling regime, one can have for the same heat flux a very different wall temperature than in the nucleate boiling regime.

But one has to keep in mind that most of these tendencies can be either negligible or irrelevant when the power transient highly modifies the heat transfer coefficient. In addition to the hysteresis effect, present with the classical boiling curve, heating or cooling rate of the wall affects the heat transfer coefficient in a given regime, and somewhat different branches have to be considered in the corresponding part of the boiling curve. Therefore, to guide further modelling attempts, we will consider the observed variations of the heat transfer coefficient for very rapid transients and interpret them, being enlightened by the hereinabove understanding of the boiling process.

5.4 Analysis of the different phases of the RIA-related boiling heat transfer

In this section, we consider the results of the PATRICIA and NSSR experiments enlightened by the statements issued from the boiling flows review. Its content will mainly be based upon the experimental results analysed in the recent works of Udagawa et al. [6] and Georgenthum et al. [3].

5.4.1 *Till the peak heat flux*

During the first tenth of seconds of the transient, very high heat transfer takes place (see Figure 5.7). One can observe the onset of boiling, the peak heat flux and, eventually, the progressive deterioration of heat transfer coefficient. Nevertheless, the energy transfer only contributes to a few % of the total amount of inserted energy, even for very large values of the peak heat flux.

Peak heat flux variations

This peak heat flux, often denoted CHF due to its similar location on the boiling curve map, is known to scale linearly with the fuel enthalpy increase, e.g. [3]. For low transients, it tends toward steady state CHF, and we recover the Sakurai [20] experimental results on wires. CHF appears to be insensitive to either flow rate or sub-cooling variations. Actually, not only the peak heat flux, but rather the whole heat flux and temperature time evolution data are all superimposed during the first tenth of second for different flow rate or subcooling values (in the latter case, only from the boiling onset time). This is illustrated in Figure 5.7. For a given power pulse, internal radial heat transfer from the fuel toward the clad depends on the pellet-cladding gap width. Whenever the time scale for closing this gap is large enough, it may reduce significantly the heat transfer toward the clad and affect the boiling transient. This effect has been studied, e.g. [3] or [22]. It is taken into account in the present fuel codes and its impact on the clad temperature transient has to be considered at least from a sensitivity study.

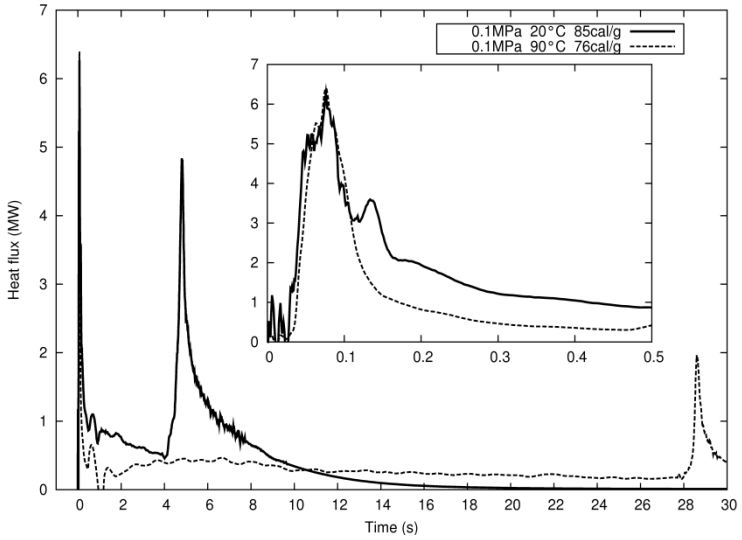

Figure 5.7: 253-3 (solid line) and 103-31-1 (dashed line) NSRR test cladding to coolant heat flux versus time, [3]

Models attempts

However, in models, peak heat flux plays a major role: if its value is fixed by a correlation, it is an absolute criterion for the transition toward film boiling. Use of classical correlations for CHF is not relevant and at least fully empirical modification fitted on relevant transient data are required. For ambient pressure conditions, Bessiron [5] proposed to rather model the boiling initiation phase, between onset and till peak heat flux, by a fixed wall temperature phase. The duration of this phase then models the transition toward

deteriorated heat flux regime. Actually, it allows recovering the experimentally observed temperature plateau.

The temperature level of the plateau corresponds to a few tens of degrees of wall superheat that is much higher than for classical nucleate boiling regimes. The length and level of the plateau is mainly affected by irradiation or oxidation of the clad that could affect wall surface properties. They are known to modify the wettability of the wall and the criterion for departure from nucleate boiling, [18].

For very rapid transient and when direct transition toward film boiling takes place, one can consider that not even a single bubble cycle occurs, e.g. [20]. In this context, the use of correlations for nucleate boiling regime heat transfer can provide high heat transfer coefficient value but is used out of the range of its validity. Some RIA-related models do not consider correlations but rather more simple analytical relations to connect convection to peak heat flux or basic phase change energy balance, e.g. [4] and [5]. To go beyond and to be able to accurately predict the heat transfer just after the onset of boiling, one should be able to better understand the vapour formation process along a wall under a power impulse.

Summary

During the first tenth of second of the transient, from the onset of boiling till the possible transition toward film boiling, the bulk flow (flow rate or liquid temperature) only slightly impacts the wall to fluid heat transfer. This is in large contrast with the heat transfer in the steady state nucleate boiling regime that is the similar part of the boiling curve. Pressure level, wettability of the wall, and power pulse characteristics are highly correlated with the peak heat flux. This rather short phase does not play any significant contribution for the energy transfer toward the coolant even though heat flux can be extremely high. Therefore, without any further understanding, it is required to consider the peak heat flux model as a criterion of possible transition toward film boiling of low reliability.

5.4.2 *Transition toward film boiling and peak cladding temperature*

Let us consider that transition toward film boiling occurs. The next tenths of second correspond to a large temperature increase till the peak cladding temperature. This peak cladding temperature is then very well correlated to the enthalpy increase of the fuel. This is logical since only a rather small part of the fuel energy has been released toward the coolant before the heat transfer decreases. Nevertheless, even if it is film boiling, wall temperature can be large and the heat flux is still large till the peak cladding temperature (around $10^6 W/m^2$). The temperature peak can occur after 1s. The vapour film has time to establish and the heat flux has time to be affected by bulk flow rate and temperature. This will affect the amount of energy released toward the coolant at the peak temperature time, and therefore the peak temperature itself. Therefore, as outlined by Georgenthum et al. or Udagawa et al., the peak cladding temperature decreases when flow rate increases or when bulk temperature decreases, as illustrated in Figure 5.8. If one considers subcooled IAFB, the models consider that the condensation at the vapour liquid interface is of major influence on the vapour film thickness and then on the wall to fluid heat transfer itself. This condensation rate scales with Reynolds number and thermodynamic quality of the bulk flow that is consistent with the previous results.

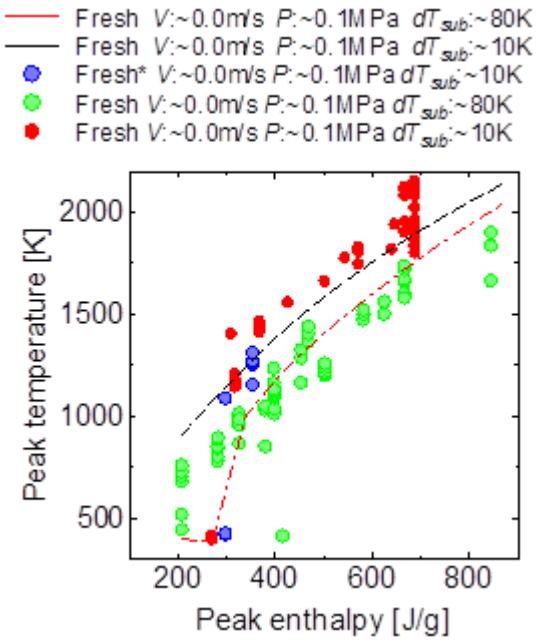

Figure 5.8: Peak temperatures at fuel rod surface for test Cases with fresh fuels conducted under the conditions of stagnant coolant, atmospheric coolant pressure, and varied coolant subcoolings. Legends with an asterisk like "Fresh*" denotes the result of the 2nd, 3rd, or the latter pulse irradiation in an iterative pulse-irradiation experiment in which a series of pulse-irradiations had been conducted on an identical test fuel rod, [6]

Peak cladding temperature decreases when pressure increases. This latter trend can have several reasons but the comparison has been made for same liquid velocity and subcooling. For those conditions, water flowing at 14 MPa corresponds to Reynolds number, resp. thermodynamic quality, 4 times, resp. 3 times, larger than water at 0.1MPa. It would be interesting to compare tests with different pressures but similar Reynolds number and thermodynamic quality.

The irradiation or oxidation effect can be observed on the peak cladding temperature but cannot affect the film boiling heat transfer since wettability has no influence on the heat transfer process (liquid cannot contact the wall). But those clad properties can affect the ability of vapour blanketing the wall or the peak heat flux. Therefore increased wettability of the wall delays or inhibits the transition toward film boiling. Sugiyama et al. [23] showed how it can affect the duration of the nucleate boiling phase and this can be illustrated by Figure 5.9. Increase of clad wettability shifts the fuel enthalpy limit toward larger values. Once this limit is over, one recovers the same correlation between further increase of the fuel enthalpy and peak cladding temperature as illustrated on Figure 510. If nucleate boiling had time to release a large energy amount before transition toward film boiling, the peak clad temperature is smaller for the same fuel enthalpy than if it could not.

5.4.3 *Film boiling till quenching*

The film-boiling time follows the same tendency as the peak cladding temperature. It is therefore strongly correlated to this peak cladding temperature itself. During the film boiling phase, temperature measurements clearly indicate a quasi-constant temperature decrease rate till quenching. Therefore, the film boiling duration that is the time to reach quenching conditions scales naturally with the initial temperature of the film boiling phase, namely the peak cladding temperature. This is how the power pulse affects the film boiling phase.

It can be seen that the temperature decrease rate is rather insensitive to the peak cladding temperature and that the film boiling phase of different fuel enthalpy all superimposed if they are time shifted to match a temperature value. Therefore the power pulse does not affect the film boiling heat transfer coefficient during the wall cooling. The same is true when there are variations of the surface properties induced by either oxidation or irradiation that indicates that the film boiling heat transfer is not affected by those clad properties.

The film boiling duration increases naturally with the amount of heat to be released, and therefore the peak fuel enthalpy (or once again the peak cladding temperature). This time is reduced when heat transfer coefficient increases, either by flow rate increase or by subcooling increase, see Figure 5.11.

Since film boiling during a RIA seems rather conform to classical film boiling understanding during the cooling phase, steady state experiments should provide good estimation of the heat transfer coefficient for the cooling phase. Unfortunately, they are still difficult to obtain. Large scattering of the heat transfer coefficient are reported from NSRR tests. This could be analysed by separating values incoming from the heating and cooling phases of the film boiling to see whether transient could affect only a part of the high temperature phase.

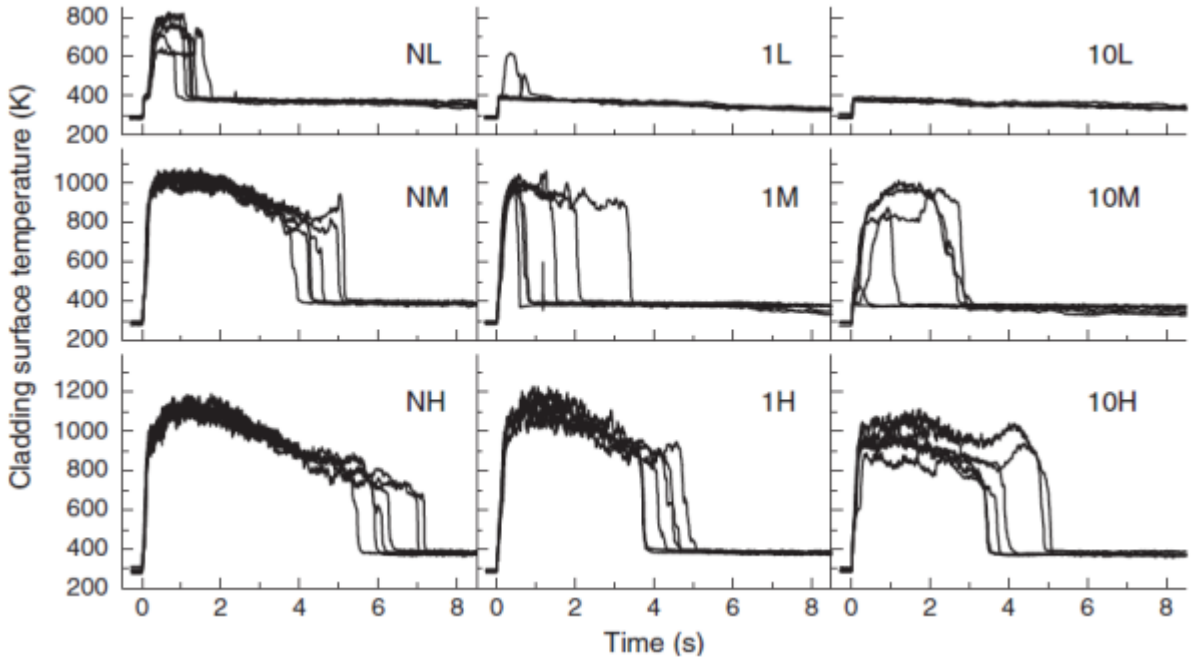

Figure 5.9: Transient records of cladding surface temperature [21]

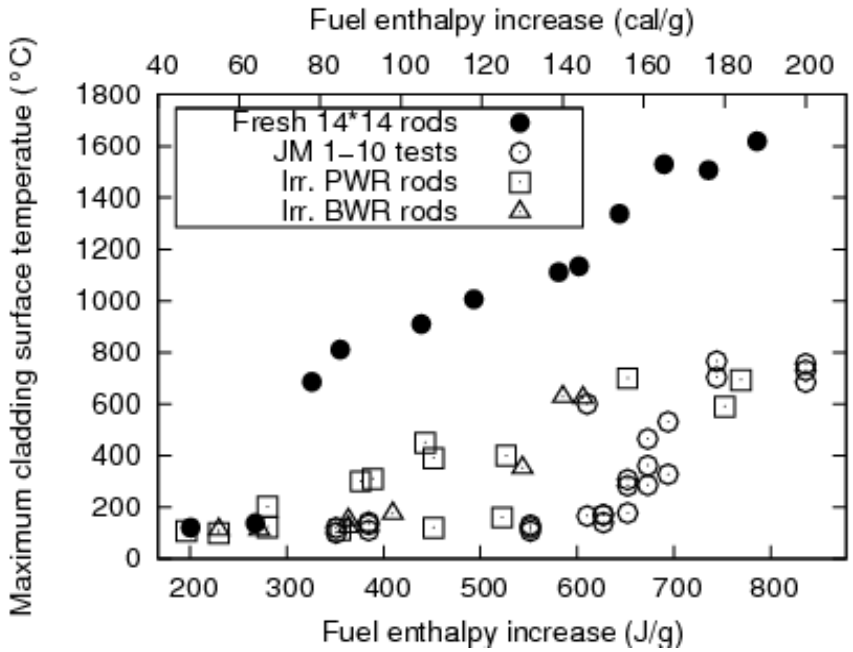

Figure 510: Maximum cladding surface temperature measurements for fresh and irradiated fuels [3]

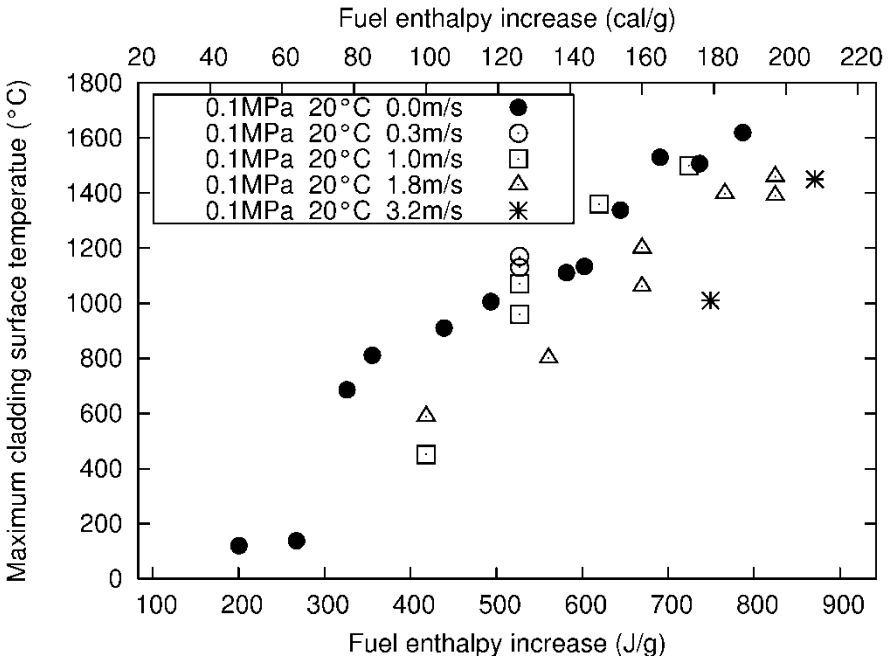

Figure 5.11: Film boiling duration measured for different coolant flow [3]

The quench does not occur for the same wall temperature according to variations of the main parameters. Moreover, there is a variation of the quench time according to the axial location along the rod or when wettability is supposedly affected by either irradiation or oxidation. As pointed out by the authors of [23] for small rods, quench can occur either at the top or at the bottom ends of the rod. For some tests, it

is clear that quench front propagates from bottom to top of the rod. This induces a scattering in the boiling time that is only important for low peak cladding temperature, when the mean boiling time over the rod is short.

5.5 Conclusion

Numerical simulation of the high temperature phase of a RIA requires describing the heat transfer in different boiling regimes. Large variations of the heat transfer coefficient have to be considered as well as criteria for sharp transition between those regimes. The very rapid heating of the fuel clearly impacts how boiling can develop and evolve along the clad. This impacts the heat flux and causes large differences between experimentally measured heat transfer coefficients in RIA-related conditions with respect to some more steady boiling heat transfer cases. To obtain high precision experimental data for realistic thermal hydraulics PWR or BWR conditions is still a challenge and current low level of understanding of the transient boiling processes does not support an accurate modelling of the heat transfer. The present dedicated models still have a large part of empiricism. Nevertheless the analysis of the different phases of the boiling heat transfer help to interpret how the power transient or the thermal hydraulics conditions affect the high temperature transient during a RIA. This raises hypotheses or questions that new in pile or out of pile experiments could help to support or answer in some simpler configurations.

6. CONCLUSIONS AND RECOMMENDATIONS

The objective of this first part of the WGFS RIA fuel codes RIA benchmark Phase II was to compare the results of different simulations on simplified Cases, in order to better understand the differences in modelling of the concerned specific phenomena. Nonetheless, this understanding is forcefully limited by the semi-empiric nature of many codes, which rely on parameters determined when compared to integral tests.

Participation in the RIA benchmark Phase II has been very remarkable: fifteen organizations representing twelve countries have provided analyses for some or all the cases that were defined. In terms of computer codes used, the spectrum was also large as analyses were performed with ALCYONE, BISON, FRAPTRAN, RANNS, SCANAIR, TESPAROD, and TRANSURANUS.

By comparing the results provided by participants, it has been possible to draw the following conclusions:

- Using simplified Cases with fresh fuel leads to very close evaluations of the initial state of the rod (just before the pulse), which was not the case previously during the RIA benchmark Phase I.
- With respect to the fuel thermal behaviour, the differences in the estimation of fuel enthalpies and temperatures are rather limited especially for maximum values of these parameters. However, the agreement is worse for BWR thermal-hydraulic conditions than PWR thermal-hydraulic conditions that lead to water boiling. This seems to be mainly driven by uncertainty in the clad-to-coolant heat transfer.
- Concerning cladding temperatures, considerable scatter is obtained for the cases where water boiling occurs. This scatter is clearly relates to the clad-to-coolant heat transfer modelling. Boiling in RIA conditions is known to be significantly different than in steady-state conditions. Some codes assume that the steady-state correlations are applicable to RIA conditions while other codes use specific fast-transient correlations (for critical heat flux, heat exchange in film boiling, rewetting conditions, etc.). Given the lack of sufficient experimental investigation on boiling in RIA conditions, no sound recommendation can be made as for which correlations are the most suitable ones to use.
- From cases devoted to BWR conditions, it is clear that very few (if any) of the applied computer codes are able to handle the thermal-hydraulic conditions expected in a BWR RIA with large energy injection at cold, zero-power conditions. This is not simply a question of uncertainties in the clad-to-coolant heat transfer modelling; the excessive steam generation expected in the fuel assembly at atmospheric pressure can obviously not be handled by the simple thermal-hydraulic models in the codes.
- With respect to mechanical behaviour, the loading mode of the cladding considered during this benchmark exercise is limited to the PCMI one.
- Although the general behaviour is similar from one case to another, and although the agreement between predictions is reasonable during the heating phase, significant discrepancies are obtained for the maxima of different variables of interest (namely clad hoop strain, fuel and clad elongation

and clad hoop stress), and for long-term evolution of many parameters. The difference between upper and lower values reaches almost 200% (of the mean value) for the clad hoop stress and is between 25 and 75% for clad hoop strain and fuel and clad elongations.

- The reasons for this disagreement can only be partly attributed to model approaches and specific formulations; dependency on key boundary conditions for clad loading, such as the gap closure/opening, is also heavily involved.

Based on the Phase I and Phase II conclusions summed up above, some generic recommendations can be made:

- Fuel and clad thermomechanical models (with the associated material properties) should be further improved and validated more extensively against a sound RIA database.
- Build-up of a comprehensive and robust database consisting of both separate-effect tests and integral tests should be pursued in the short term. In this way, both individual model validation and model integration into codes would be feasible.
- An assessment of the uncertainty of fuel thermo-mechanics is of high interest, which is consistent with the second activity of this RIA benchmark Phase II.

Some more specific recommendations can be also added:

- The clad-to-coolant heat transfer in the case of water boiling during very fast transients is of particular interest, and capabilities related to modelling this phenomenon should be improved. To achieve this target regarding clad-to-coolant heat transfer, more separate-effect tests and experiments seem necessary.
- Models related to the evolution of the gap between fuel and clad should be improved and validated in RIA conditions as this has been shown to have a significant effect on fuel rod response. To reach this objective, in-reactor measurements of cladding strain during RIA simulation tests should be done (or at least attempted).

Finally, as RIA fuel codes are more and more likely to be used for reactor accident studies, particularly for those involving safety analyses, the fuel rod failure criteria (generally used in such analyses) will have to be carefully justified and validated.

Such fuel rod failure criteria can in general be described in terms of:

- thermal variables (e.g., fuel enthalpy, variation of fuel enthalpy);
- mechanical variables (e.g., clad hoop strain, clad hoop stress).

The current RIA fuel failure criteria are mainly based on the fuel thermal variables and the verification is based on “conservative” assumptions for the heat transfer conditions. As all codes give rather consistent evaluations of such variables, it appears possible, taking into account adequate provisions, to derive criteria based on thermal variables from experimental values or from an analytical approach.

However, if in the future more mechanistic modelling is ever to be used to establish fuel-failure criteria based on mechanical variables, the codes will have to be further improved and validated for all the aspects identified above.

The assessment of the uncertainty and sensitivity of the results expected in the second task of this RIA benchmark Phase II will provide more insights on the important input parameters and models to be considered.

7. REFERENCES

[1] NEA/CSNI/R(2013)7, RIA Fuel Codes Benchmark- Volume 1, Nuclear Energy Agency, OECD, Paris, France (2013).

[2] NEA – Nuclear fuel behaviour under Reactivity-initiated Accident (RIA) conditions, State-of-the-art Report – Report NEA No. 6847, ISBN 978-92-64-99113-2, Nuclear Energy Agency, OECD, Paris, France (2010).

[3] Georgenthum V., Trégourès N. and Udagawa Y. – Synthesis and Interpretation of Fuel Cladding Temperature Evolution under Reactivity Initiated Accident in NSRR Reactor – Proceedings of WRFPM 2014 Sendai, Japan, Sep. 14-17, 2014 Paper No. 100097 (2014).

[4] V. Bessiron, T. Sugiyama and T. Fuketa – Clad-to-Coolant Heat Transfer in NSRR Experiments – Journal of Nuclear Science and technology, Vol. 44, pp. 723-732 (2007).

[5] V. Bessiron – Modelling of Clad-to-Coolant Heat Transfer for RIA Applications – Journal of Nuclear Science and technology, Vol. 44, pp. 211-221 (2007).

[6] Udagawa Y., Sugiyama T., Suzuki M., Amaya M. – Experimental analysis with RANNS code on boiling heat transfer from fuel rod surface to coolant water under Reactivity Initiated Accident conditions – Proc. IAEA Technical Meeting, Chengdu, China (2013).

[7] Van Carey P., – Liquid-vapour phase-change phenomena- Taylor and Francis (1992).

[8] Delhaye J.-M., Giot M., Riethmuller M. L. – Thermohydraulics of two-phase systems for industrial design and nuclear engineering – Mc Graw Hill,(1981).

[9] A. E. Bergles, J. G. Collier, J.- M. Delhaye, G. F. Hewitt, F. Mayinger, Two-phase flow and heat transfer in the power and process industries – chap. 10 Post Dryout Heat transfer, Hemisphere publishing Corporation, (1981.)

[10] Baudin N., Colin C., Ruyer P., Sebilleau J. – Experimental study of transient nucleate boiling – 9th Int. Conference on Boiling and Condensation Heat Transfer, Boulder, Colorado, April 26-30 (2015).

[11] Van Houten R. – Fuel rod failure as a consequence of departure from nucleate boiling or dryout – Report NUREG-0562, US Nuclear Regulatory Commission, Washington DC, USA (1979).

[12] Laperriere, A. – An Analytical and Experimental Investigation of Forced Convective Film Boiling, M.Sc. thesis – University of Ottawa, Ottawa, Canada (1983).

[13] Groeneveld D.C., Leung L.K.H., Vasic' A.Z., Guo Y.J., Cheng S.C. – A look-up table for fully developed film-boiling heat transfer, Nuclear Engineering and Design 225 83–97 (2003).

[14] Shiotsu M. Hama K. – Film boiling heat transfer from a vertical cylinder in forced flow of liquids under saturated and subcooled conditions at pressures – Nucl. Eng. Design 200 (2000) 23.

[15] Dhir VK. – Mechanistic Prediction of Nucleate Boiling Heat Transfer: Achievable or a Hopeless Task? – ASME. J. Heat Transfer. 128(1):1-12 (2005).

[16] Bestion D. – From the Direct Numerical Simulation to System Codes – Perspective for the Multi-Scale Analysis of LWR Thermalhydraulics – Nuclear Engineering and Technology, vol.42 no.6 pp. 608-619 (2010).

[17] Visentini R., Colin C. Ruyer P. – Experimental investigation of heat transfer in transient boiling – Experimental Thermal and Fluid Science, 55(0), pp. 95-105, (2014).

[18] Sibamoto Y. et al. – In-pile Experiment in JMTR on the Radiation Induced Surface Activation (RISA) Effect on Flow-boiling Heat Transfer – J. of Nucl. Sci. Technol, 44[2] 183–193 (2007).

[19] Auracher H. Marquardt W. – Experimental studies of boiling mechanisms in all boiling regimes under steady-state and transient conditions – Int. J. of Thermal Sciences, 41(7), pp. 586-598 (2002).

[20] Sakurai A. -Mechanisms of transitions to film boiling at CHFs in subcooled and pressurized liquids due to steady and increasing heat inputs", Nucl. Eng. Design, 197(3), pp. 301-356, (2000).

[21] Hsu Y. – On the size range of active nucleation cavities on a heating surface, – ASME J. of Heat Trans., 84, pp. 207-216 (1962).

[22] M. Ishikawa and S. Shiozawa, A study of fuel behavior under reactivity initiated accident conditons – review, J. Nucl. Mat., 1980, vol. 95, pp. 1-30

[23] Sugiyama T., Fuketa T. – Effect of Cladding Surface Pre-oxidation on Rod Coolability under Reactivity Initiated Accident Conditions – Journal of Nuclear Science and Technology, Vol. 41, No. 11, p. 1083–1090 (2004).

[24] B. Michel, B., Nonon, C., Sercombe, J., Michel, F., & Marelle – Simulation of pellet-cladding interaction with the PLEIADES fuel performance software environment -Nuclear Technology, 182(2), 124-137 (2013).

[25] Sercombe, J., Julien, J., Michel, F., Michel, B., & Fédérici – 3D modelling of strain concentration due to PCI within the fuel code ALCYONE – Proceedings of Top Fuel Conference, Orlando, USA (2013).

[26] Sercombe, J., Aubrun, I., & Nonon, C. – Power ramped cladding stresses and strains in 3D simulations with burnup-dependent pellet–clad friction – Nuclear Engineering and Design, 242, 164-181 (2012).

[27] B. Michel, J. Sercombe, C. Nonon and O. Fandeur, 3.22 – Modeling of Pellet Cladding Interaction – In Comprehensive Nuclear Materials, Pages 677-712 (2012).

[28] Struzik C., Marelle V. – Validation of fuel performance CEA code ALCYONE, scheme 1D, on extensive database – Top Fuel 2012, Manchester, UK (012).

[29] Sercombe J., Fédérici E., Le Saux M., Michel B., Poussard C. – 1D and 3D modelling of PCMI during a RIA with ALCYONE V1.1 – Top Fuel 2010, Orlando (2010).

[30] C. Struzik, V. Blanc, A. Cabrera, V. Garat – LOCA tests IFA 650 analysis through the fuel state at the end of base irradiation and its thermo-mechanical behavior during the experiment – EHPG, Norway (2014).

[31] M. Le Saux, J. Besson, S. Carassou, C. Poussard, X. Averty – A model to describe the anisotropic behavior of fresh and irradiated Zircaloy-4 fuel claddings under RIA loading conditions – Journal of Nuclear Materials, 378 (1), 60-69 (2008).

[32] M. Salvo, J. Sercombe, T. Helfer, P. Sornay, T. Désoyer – Experimental characterization and modeling of UO_2 grain boundary cracking at high temperatures and high strain rates – Journal of Nuclear Materials, 460, 184-199 (2015).

[33] P. Goldbronn, J. Sercombe, B. Michel – Avancées de la simulation du comportement du combustible nucléaire en 3D et en transitoire rapide – Congrès Français de Mécanique, Bordeaux, France (2013).

[34] R. L. Williamson, J. D. Hales, S. R. Novascone, M. R. Tonks, D. R. Gaston, C. J. Permann, D. Andrs, and R. C. Martineau – Multidimensional multiphysics simulation of nuclear fuel behavior. J. Nucl. Mater., 423:149–163 (2012).

[35] J. D. Hales, R. L. Williamson, S. R. Novascone, D. M. Perez, B. W. Spencer, G. Pastore – Multidimensional multiphysics simulation of TRISO particle fuel – J. Nucl. Mater., 443:531–543 (2013).

[36] P. Medvedev – Fuel performance modeling results for representative FCRD irradiation experiments: Projected deformation in the annular AFC-3A U-10Zr fuel pins and comparison to alternative designs – Technical Report INL/EXT-12-27183 Revision 1, Idaho National Laboratory (2012).

[37] N. N. Carlson, C. Unal, and J. D. Galloway – Formulation of the constituent distribution model implemented into the BISON framework for the analysis of performance of metallic fuels with some initial simulation results – Technical Report LA-UR-13-26824, Los Alamos National Laboratory (2013).

[38] P. Medvedev – Summary report on the fuel performance modeling of the AFC-2A, 2B irradiation experiments – Technical Report INL/EXT-13- 30006, Idaho National Laboratory (2013).

[39] K. E. Metzger, T. W. Knight, and R. L. Williamson – Model of U3Si2 fuel system using BISON fuel code. In Proceedings of the International Congress on Advances in Nuclear Power Plants – ICAPP 2014, Charlotte, NC (2014).

[40] D. Gaston, C. Newman, G. Hansen, and D. Lebrun-Grandié – MOOSE: A parallel computational framework for coupled systems of nonlinear equations – Nucl. Eng. Design, 239:1768–1778 (2009).

[41] D. A. Knoll and D. E. Keyes – Jacobian-free Newton-Krylov methods: a survey of approaches and applications – J. Comput. Phys., 193(2):357–397, (2004).

[42] G. Pastore, L. Luzzi, V. Di Marcello, P. Van Uffelen – Physics-based modelling of fission gas swelling and release in UO_2 applied to integral fuel rod analysis – Nucl. Engrg. Design, 256:75–86 (2013).

[43] G. Pastore, L. P. Swiler, J. D. Hales, S.R. Novascone, D. M. Perez, B. W. Spencer, L. Luzzi, P. Van Uffelen, R. L. Williamson – Uncertainty and sensitivity analysis of fission gas behavior in engineering-scale fuel modelling – Journal of Nuclear Materials, 456:398–408 (2015).

[44] G. Pastore, D. Pizzocri, J. D. Hales, S. R. Novascone, D. M. Perez, B. W. Spencer, R.L. Williamson, P. Van Uffelen, L. Luzzi – Modelling of transient fission gas behaviour in oxide fuel and application to the BISON code – In Enlarged Halden Programme Group Meeting, Røros, Norway, (2014).

[45] K.J. Geelhood , W.G. Luscher, C.E. Beyer – FRAPCON-3.4: A Computer Code for the Calculation of Steady-State, Thermal-Mechanical Behavior of Oxide Fuel Rods for High Burnup – NUREG/CR-7022, PNNL-19418, Pacific Northwest National Laboratory, Richland, WA.

[46] M.E. Cunningham, C.E. Beyer, P.G. Medvedev, G.A. Berna – FRAPTRAN: A Computer Code for the Transient Analysis of Oxide Fuel Rods – NUREG/CR-6739, PNNL-13576, Pacific Northwest National Laboratory, Richland, WA.

[47] K.J. Geelhood, W.G. Luscher, C.E. Beyer – FRAPTRAN 1.4 Integral Assessment, NUREG/CR-7023, PNNL-19400, Pacific Northwest National Laboratory, Richland, WA.

[48] W.G. Luscher, K.J. Geelhood – Material Property Correlations: Comparisons between FRAPCON-3.4, FRAPTRAN 1.4, and MATPRO – NUREG/CR-7024, PNNL-19417, Pacific Northwest National Laboratory, Richland, WA.

[49] M. Suzuki, H. Saitou, T. Fuketa – Analysis on pellet-clad mechanical interaction process of high burnup PWR fuel rods by RANNS code in reactivity-initiated accident conditions – Nuclear Technology., Vol. 155, pp. 282-292(2006).

[50] M Suzuki et al – Light Water Reactor Fuel Analysis Code FEMAXI-7; Model and Structure – JAEA-Data/Code 2013-005 (2013).

[51] Moal A, Georgenthum V., Marchand O. – SCANAIR a transient fuel performance code Part one: General modelling description – Nuclear Engineering and Design 280 150-171 (2014).

[52] Georgenthum V., Moal A. Marchand O. – SCANAIR a transient fuel performance code Part two: Assessment of modeling capabilities – Nuclear Engineering and Design 280 172-180 (2014).

[53] K. Lassmann – TRANSURANUS: a fuel rod analysis code ready for use – Journal of Nuclear Materials, Vol. 188 pp. 295-302 (1992).

[54] Cadek F. F., D.P. Dominicis, H.C. Yeh, and R.H. Leyse – PWR FLECHT Final Report Supplement – WCAP-7931 – Westinghouse Electric Corporation, Pittsburgh, PA – 1972.

[55] Rajamäki, M. – TRAB: A Transient Analysis Program for BWR, Part 1. Principles – Report 45. Technical Research Centre of Finland, Nuclear Engineering Laboratory, Helsinki p. 101 + app. p. 9 (1980).

[56] Räty, H., Rajamäki, M. – TRAB: A Transient Analysis Program for BWR, Part 2: User's Manual – Research Notes 1232, Technical Research Center of Finland, Nuclear Engineering Laboratory, Helsinki (p. 105 + app. p. 46) (1991).

[57] Keresztúri, I. Panka, A. Molnár, Á. Tóta -Multi-physics development for the hot-channel calculation of fast reactivity transients – Progress in Nuclear Energy 67 pp 74-81 (2013).

[58] Sakurai, A. et al. – Correlations for subcooled pool film boiling heat transfer from large surfaces with different configurations – Nucl. Eng. Design, 120, pp.271-280 (1990).

[59] F.W. Dittus, L.M. Boelter – Heat transfer in automobile radiators of the tubular type – University of California Publications in Engineering, 2:443 (1930).

[60] F. Kreith – Principles of heat transfer – Intertext press, New York (1973).

[61] V.T. Morgan – The overall convective heat transfer from smooth circular cylinders – volume 11 – T.F. Irvine Jr., J.P. Hartnett (Eds.), Advances in Heat Transfer, New York, (1975).

[62] A. Bishop, R. Sandberg, and L. Tong – Forced convection heat transfer at high pressure after the critical heat flux – Technical Report 65-HT-31, ASME, (1965).

[63] J. Weisman and R. Bowring – Methods for detailed thermal and hydraulic analysis of water-cooled reactors – Nuclear Science and Engineering, 57:255–276, Babcock-Wilcox (1975).

[64] Lienhard J. H. – A Heat Transfer Textbook, Third Edition. Version 1.31.

[65] Mostinski, I.,L. – Application of the Rule of Corresponding States for Calculation of Heat Transfer and Critical Heat Flux – In Teploenergetika, 4, 66, (1963).

[66] D. Schröder-Richter – Analytical Modeling of Complete Nukiyama Curves Corresponding to Expected Low Void Fraction at High Subcooling and Flow Rate. – Fusion Technology, Vol. 29, pp. 468-486 (1996).

8. APPENDIX I: GENERAL DESCRIPTION OF THE CODES

This appendix gives a short description of the codes used by the participants to the RIA benchmark Phase II. The codes are:

- ALCYONE
- BISON
- FRAPTRAN
- RANNS
- SCANAIR
- TESPAROD
- TRANSURANUS

8.1 ALCYONE V1.4

ALCYONE V1.4 is a multi-dimensional PWR fuel application developed at the Atomic Energy Commission (CEA) in Cadarache (France) in the framework of the PLEIADES environment [24] which hosts several other fuel applications. ALCYONE V1.4 contains four schemes [25]: a standard 1.5D description of the fuel rod, a 3D scheme dealing with one quarter of a pellet fragment and associated cladding, a 2D(r,θ) scheme describing the behaviour of the mid-pellet plane of a 3D pellet fragment [26], a 3D multi-pellet fragment scheme where part or the complete fuel rod car be simulated (see Figure 0.1).

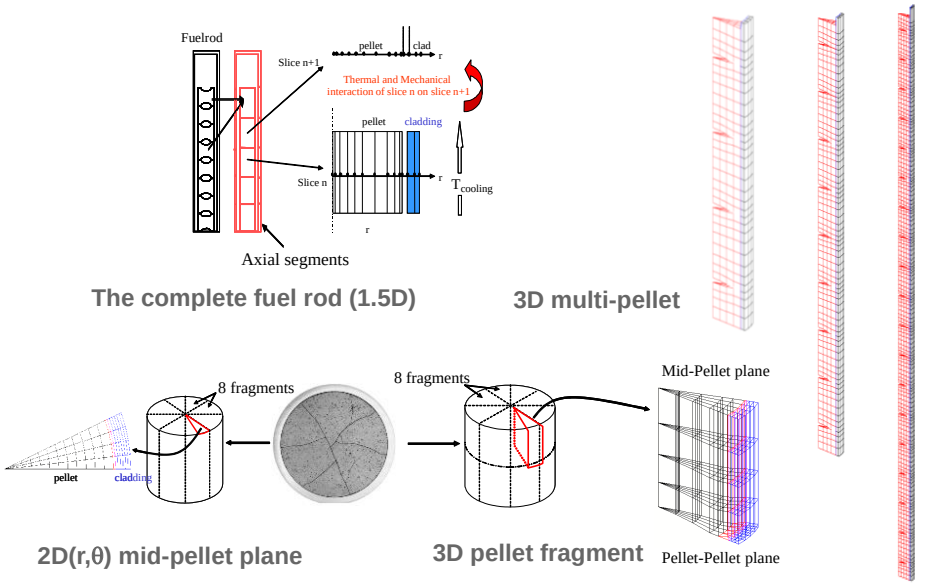

Figure 0.1: ALCYONE – Different schemes

The different schemes use the same Finite Element (FE) code CAST3M to solve the thermo-mechanical pellet-gap-cladding problem and share the same physical material models at each node or integration points of the FE mesh. This makes the comparison of simulated results from one scheme to another possible with no dependency on the constitutive models.

ALCYONE was originally developed for the modelling of fuel rod behaviour during normal (base irradiation) and off-normal (power ramp) loading sequences. The following (main) phenomena are included in the fuel performance code [27]:

- Fuel pellet:
  - Power deposition
  - Heat conduction
  - Creep and fragmentation of the pellet
  - Generation of, diffusion of Fission Gases in the fuel microstructure
  - Fission Gas Release
  - Pellet densification
  - Pellet Fission Gas induced swelling
  - High-Burnup Structure (HBS)
  -
- Cladding:
  - Heat conduction and convection at the clad – coolant interface
  - Irradiation creep, thermal creep and plasticity
  - External corrosion
- Pellet-cladding interface:
  - Heat convection
  - Unilateral contact with friction (2D, 3D)
  - Pressure update (rodlet deformation, FGR)

In ALCYONE, the pre-RIA transient state (t0) is assessed by comparison to an extensive database of base irradiations (200) and ramp tests (50) results on UO_2-Zy4, UO_2-M5® and MOX-Zy4 rods with burnups up to 80 GWd/tM [28]. The experimental data available consist in measures of the clad profilometry, the corrosion thickness, the rod elongation, radial concentration profiles of FG and FG bubbles size, FGR and internal pressure in the rod. The 3D scheme allows one to assess more precisely the local behaviour of the fuel rod by comparing the following experimental and calculated data: the residual clad diameter, the height of pellet-pellet and mid-pellet ridges, the dish filling and the radial-axial cracking of the pellets [25].

- In recent years, ALCYONE capacities have been extended to accidental conditions (RIA [29] and LOCA [30]) with a very limited amount of new developments. By this way, the continuity between nominal (t0) and transient conditions has been ensured. Extension of the fuel code schemes to pulse-irradiation required the following improvements:
- solving the thermal heat balance equation for the pellet-gap-cladding system in non-steady state conditions,

- incorporating material laws describing the non-linear mechanical behaviour of irradiated Zircaloy within large temperature (from 20°C up to 1100°C) and strain rate ranges (from 3.10^{-4} s^{-1} to 5 s^{-1}), representative of the RIA spectrum [31],
- incorporating a material law describing the creep and plasticity of irradiated fuel within large temperature (up to fuel melting) and strain rate ranges (up to 10/s), representative of the RIA spectrum [32],
- solving the thermal and mass balance equations for the sodium coolant in non-steady state conditions [29][33].

Up to now, simulations of RIA transients in ALCYONE have been focused on the CABRI REP-Na [29] and CIP tests [33] where the fuel rod did not fail (UO_2-Zy4, UO_2-M5® and MOX-Zy4). The assessment of the code predictions is based on the numerous measures available: on-line clad elongation, on-line sodium temperature at different axial positions, residual clad profilometry and ridges, radial-axial cracking of the pellets, dish filling. The present calculations are performed without taking into account fission gas induced swelling and grain boundary fragmentation which can however contribute to clad straining during a RIA.

For the calculations performed within the scope of the RIA benchmark Phase II, only the 1D scheme of ALCYONE V1.4 has been used. At this occasion and to extend the modelling capacity of ALCYONE to a water coolant, the clad – water coolant heat exchange correlations proposed by Bessiron for PWR conditions [5] and stagnant liquid water [4] have been implemented and successfully tested.

8.2 BISON

BISON is a nuclear fuel performance code that has been under the development at Idaho National Laboratory (INL) since 2009. BISON is a parallel, finite element-based tool that solves the coupled non-linear partial differential equations associated with nuclear fuel behaviour [34]. The code is applicable to both steady and transient fuel behaviour and is used to analyse 1D spherical, 2D axisymmetric, or 3D geometries and uses implicit time integration, important for the widely varied time scales in nuclear fuel simulation. A software architecture is employed which minimizes the programming required to add new features such as material and behaviour models.

BISON is intended to be a multi-fuels code. Though primarily applied to LWR fuel to date, the code has been used to analyse TRISO-coated particle fuel [35] and metal fuel in rod and plate form [36] [37], design and interpret fuel irradiation experiments [38] and investigate novel fuel concepts [39].

BISON is built using the INL Multiphysics Object-Oriented Simulation Environment, or MOOSE [40]. MOOSE is a massively parallel, finite element-based framework to solve systems of coupled non-linear partial differential equations using the Jacobian-Free Newton Krylov (JFNK) method [41]. This allows modelling of large, computationally expensive problems from a full stack of discrete pellets in a LWR fuel rod up to every rod in a reactor core.

The BISON governing relations currently consist of fully-coupled partial differential equations for energy, species, and momentum conservation. Users can select a subset of these equations (e.g., energy and momentum for thermomechanics analysis) within the input file. The code employs both nonlinear kinematics, which accounts for large deformation, and nonlinear material behaviour.

Focusing principally on UO2 fuel, models are included to describe temperature and burnup dependent thermal properties, solid and gaseous fission product swelling, densification, thermal and irradiation creep, fracture via relocation or smeared cracking, and fission gas production, generation, and release. The coupled fission gas release and fuel gaseous swelling are computed concurrently using a physics-based

model [42] [43]. The model also includes a treatment for the mechanism of rapid fission gas release (burst release) during transients [44].

Focusing initially on Zircaloy as a cladding material, models are available to describe temperature dependent thermal properties, thermal and irradiation creep, instantaneous plasticity and irradiation growth. The plasticity and creep models can be applied simultaneously in Cases where both phenomena are active.

Gap heat transfer is modelled in the traditional manner with the total conductance across the gap computed as a sum of the gas conductance, the increased conductance due to solid-solid contact, and the conductance due to radiant heat transfer. This model is typically applied between the fuel and cladding but can also be used to simulate heat transfer between individual pellets, between a pellet and end cap, or between fracture surfaces.

Mechanical contact between materials is implemented through the use of node/face constraints, which prevent nodes on one side of an interface from penetrating faces on the other side of the interface.

For LWR fuel, the pressure in the gap and plenum is computed assuming a single cavity volume and using the ideal gas law. The moles of gas, the temperature, and the cavity volume are free to change with time. The moles of gas at any time is computed as the original amount of gas (computed based on original pressure, temperature, and volume) plus the amount in the cavity due to fission gas released. The gas temperature is computed based on the fuel surface and cladding interior temperatures. The cavity volume is computed as needed based on the evolving pellet and cladding geometry.

To predict the thermal response of a fuel rod, thermal hydraulic condition of the surrounding coolant needs to be determined. Such condition in modelling the energy transport aspect of the coolant in BISON code is described by a single coolant channel model. This single channel is used mathematically to describe the thermal boundary condition for modelling the fuel rod behaviour. This model covers two theoretical aspects, i.e., the local heat transfer from cladding wall into the coolant and the thermal energy deposition in the coolant in steady state and slow operating transient conditions.

8.3 FRAPTRAN

The ability to predict the performance of light-water reactor (LWR) fuel during irradiation, during both long-term, steady-state operation and during various operational transients and hypothetical accidents, is a major objective of the reactor safety research programme conducted by the U.S. Nuclear Regulatory Commission (NRC). To achieve this objective, the NRC has sponsored not only extensive analytical computer code development, but also in-reactor and out-of-reactor experiments to generate the data necessary for development and verification of the computer codes.

FRAPTRAN (Fuel Rod Analysis Program Transient) is a FORTRAN language computer code developed to calculate the response of a single fuel rod to operational transients and hypothetical accidents. In performing this function, FRAPTRAN calculates the temperature and deformation history of a fuel rod as a function of time-dependent fuel rod power and coolant boundary conditions. The phenomena modelled by FRAPTRAN include a) heat conduction, b) heat transfer from cladding to coolant, c) elastic-plastic fuel and cladding deformation, d) cladding oxidation, e) fission gas release, and f) fuel rod gas pressure. Although FRAPTRAN can be used in “standalone” mode, it is often used in conjunction with, or with input from, other codes.

The FRAPTRAN code is documented in a two-volume publication. Volume 1 describes the code structure and limitations, summarizes the fuel performance models, and provides the code input instructions [46]. Volume 2 provides the code assessment based on comparisons of code predictions to fuel rod integral performance data [47]. The latest version of the code, FRAPTRAN 1.4, is a companion code to the FRAPCON-3 code [45], developed to calculate the steady-state high burn-up response of a single fuel

rod. A separate material properties handbook [48] documents fuel, cladding, and gas material properties used in both FRAPCON-3.4 and FRAPTRAN 1.4.

FRAPTRAN is an analytical tool that calculates LWR fuel-rod behaviour when power or coolant boundary conditions (or both) are rapidly changing. This is in contrast to the FRAPCON-3 code which calculates the time (burn-up) dependent behaviour when power and coolant boundary condition changes are sufficiently slow for the term "steady-state" to apply. FRAPTRAN calculates the variation with time, power and coolant conditions of fuel-rod variables such as fuel and cladding temperatures, cladding elastic and plastic stress and strain, and fuel-rod gas pressure. Variables varying slowly with time, such as fuel densification and swelling, and cladding creep and irradiation growth, are not calculated by FRAPTRAN. However, the state of the fuel rod at the time of a transient, which is dependent on those variables not calculated by FRAPTRAN, may be read from a file generated by FRAPCON-3 or manually entered by the user.

FRAPTRAN is a research tool for: 1) analysis of fuel response to postulated design-basis accidents such as the reactivity-initiated accident (RIA), boiling-water reactor (BWR) power and coolant oscillations without scram, and the loss-of-coolant accident (LOCA); 2) understanding and interpreting experimental results; and 3) guiding of planned experimental work. Examples of applications for FRAPTRAN include defining transient performance limits, identifying data or models needed for understanding transient fuel performance, and assessing the effect of fuel design changes such as new cladding alloys and mixed-oxide (MOX) fuel ((U,Pu)O2) on accidents. FRAPTRAN will be used to perform sensitivity analyses of the effects of parameters such as fuel-cladding gap size, rod internal gas pressure, and cladding ductility and strength on the response of a fuel rod to a postulated transient. Fuel rod responses of interest include cladding strain, failure/rupture, location of ballooning, and cladding oxidation.

The LWR fuel rod analysed by FRAPTRAN consists of oxide fuel pellets enclosed in zirconium alloy cladding. The primary function of the cladding is to contain the fuel column and the radioactive fission products. If the cladding does not crack, rupture, or melt during a reactor transient, the radioactive fission products are contained. During some reactor transients and hypothetical accidents, however, the cladding may be weakened by a temperature increase, embrittled by oxidation, or overstressed by mechanical interaction with the fuel. These events alone or in combination can cause cracking or rupture of the cladding and release of the radioactive products to the coolant. Furthermore, the rupture or melting of the cladding of one fuel rod can alter the flow of reactor coolant and reduce the cooling of neighbouring fuel rods. This event can lead to the loss of a "coolable" reactor core geometry.

Most reactor operational transients and hypothetical accidents will adversely affect the performance of the fuel rod cladding. During an operational transient such as a turbine trip without bypass (for BWRs), the reactor power may temporarily increase and cause an increase in the thermal expansion of the fuel, which can lead to the mechanical interaction of the fuel and cladding and overstress the cladding. During another operational transient such as a loss-of-flow event, the coolant flow decreases, this may lead to film boiling on the cladding surface and an increase in the cladding temperature. During a LOCA, the initial stored energy from operation and heat generated by the radioactive decay of fission products is not adequately removed by the coolant and the cladding temperature increases. The temperature increase weakens the cladding and may also lead to cladding oxidation, which embrittles the cladding.

The FRAPTRAN code can model the phenomena which influence the performance of fuel rods in general and the temperature, embrittlement, and stress of the cladding in particular. The code has a heat conduction model to calculate the transfer of heat from the fuel to the cladding and a cooling model to calculate the transfer of heat from the cladding to the coolant. The code has an oxidation model to calculate the extent of cladding embrittlement and the amount of heat generated by cladding oxidation. A mechanical response model is included to calculate the stress applied to the cladding by the mechanical interaction of the fuel and cladding, by the pressure of the gases inside the rod, and by the pressure of the external coolant.

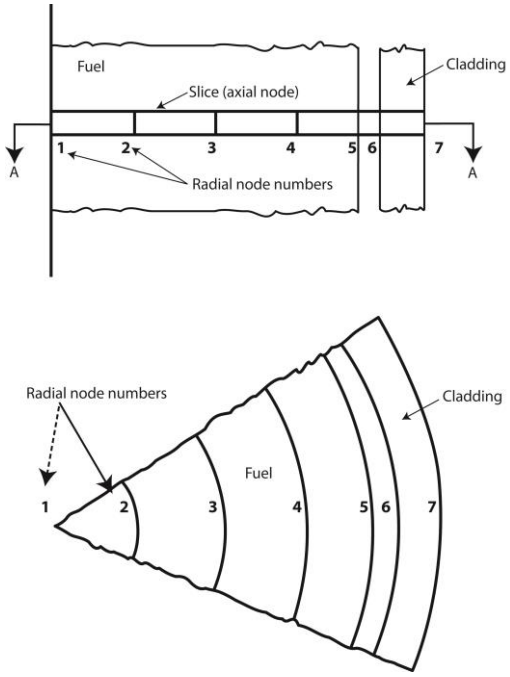

Figure 0.2: FRAPTRAN – Locations at which fuel rod variables are evaluated

The models in FRAPTRAN use finite difference techniques to calculate the variables which influence fuel rod performance. The variables are calculated at user-specified slices of the fuel rod, as shown in Figure 0.2. Each slice is at a different axial elevation and is defined to be an axial node. At each axial node, the variables are calculated at user-specified radial locations. Each location is at a different radius and is defined to be a radial node. The variables at any given axial node are assumed to be independent of the variables at all other axial nodes (stacked one-dimensional solution, also known as a 1-D1/2 solution).

8.4 RANNS

The RANNS code [49] has been developed to analyse thermal and mechanical behaviours of a single fuel rod in RIA conditions based on the light water reactor fuel analysis code FEMAXI-7 [50], which has been developed for normal operation conditions and anticipated transient conditions (see Figure 0.3).

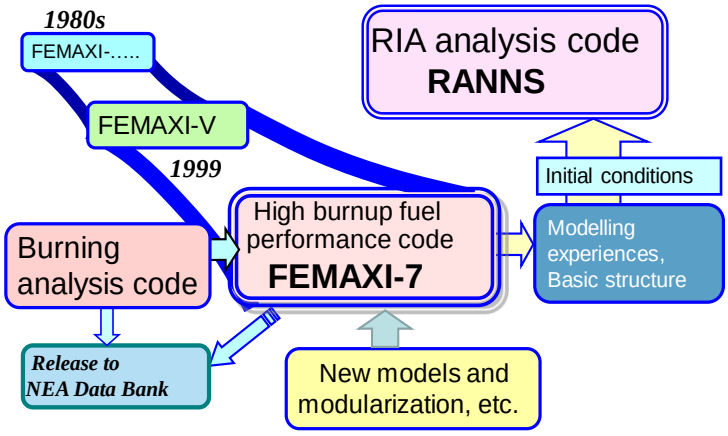

Figure 0.3: Development overview of fuel analysis code in JAEA

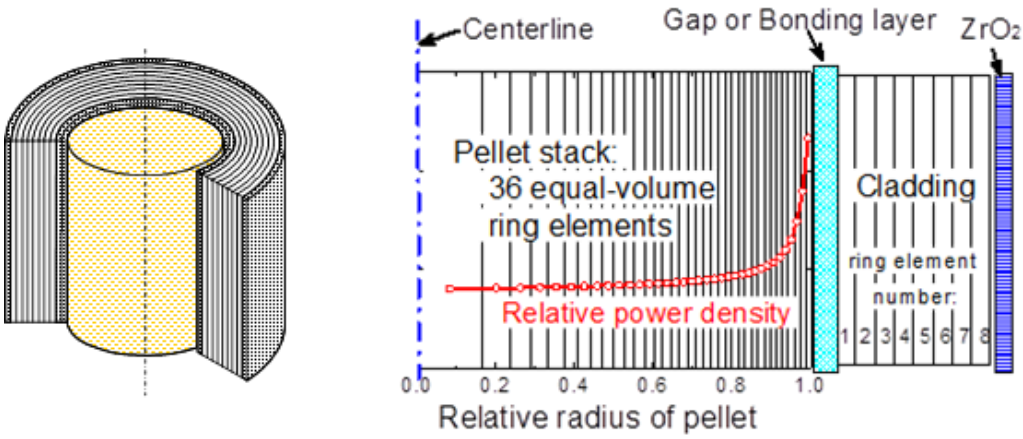

Figure 0.4: FEMAXI – RANNS analytical geometry

The same analytical geometry is applied to both the codes: a single rod can be divided into max. 40 axial segments in a cylindrical coordinate, and thermal analysis and FEM mechanical analysis are performed at each axial segment in which, in the default calculation mode, pellet stack is divided into 36 iso-volumetric ring elements and cladding is divided into 8 iso-thickness ring elements in metal part, 1 oxide element in the inner surface, and 2 oxide elements in the outer surface, as shown in Figure 0.4. In analysis of high burn-up fuels, rod conditions during their base irradiation in commercial reactors are analysed by the FEMAXI-7 code along power histories from BOL to EOL. Then the results of FEMAXI-7 calculations are fed to RANNS code calculation.

8.5 SCANAIR

SCANAIR is a so-called "1.5D code" designed to model a single rod surrounded by a coolant channel and possibly limited by an external shroud. It is also possible to simulate a capsule geometry. SCANAIR is a set of three main modules dealing with thermal dynamics (including thermal-hydraulics in the coolant channel), structural mechanics and gas behaviour [51]. These modules communicate with each other through a database (see Figure 0.5).

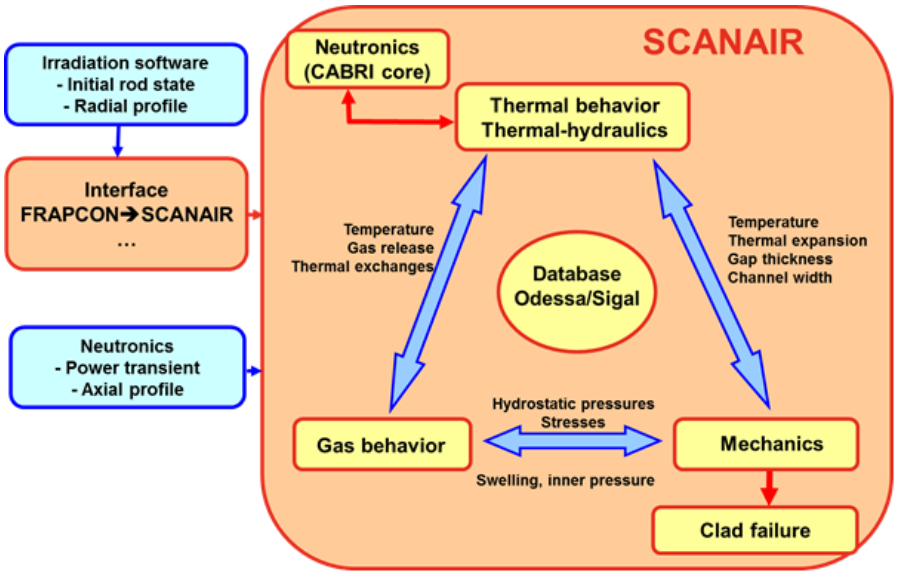

Figure 0.5: Overview diagram of data flow between the different SCANAIR modules

The initial rod state is an input data of the calculation given by an irradiation code. The power transient is an input data computed by neutron kinetics codes or measured from experimental tests.

The validation of the SCANAIR is described in the reference [52].

Structural mechanics

Fuel and clad are assumed to be concentric tubes. The geometry is assumed axisymmetric. The rod can be considered as long cylinders justifying that the crossed derivatives of the displacements are zero. Axial strains tend to be constant over an axial slice. Thanks to these assumptions, strain and stress tensors are diagonal. The equilibrium balance can be separated into radial and axial equilibrium equations.

Total deformation is assumed to be the linear superposition of deformation induced by elementary phenomena. For the fuel material, the total deformation is the sum of elastic, plastic, cracking, thermal, swelling and possibly dishing strains. For the cladding material, the total deformation is the sum of elastic, plastic, viscoplastic and thermal strains. In the brittle oxide layer, an additional cracking strain is considered. The cracking strain is defined as an additional non-elastic strain introduced for relaxing a possible tensile stress to zero.

The contact between the pellet and the clad assumes a perfect sticking.

Several failure criteria are available to predict a possible clad failure based on the fracture mechanics approach, on the Critical Strain Energy Density or the cumulative-strain-damage approach.

Thermal analysis and thermal-hydraulics

Thermal modelling takes into account the rod, the channel and the shroud. Only radial exchanges are computed through the rod and the shroud. Axial coupling is made by the coolant.

Thermal conduction is computed inside the fuel, the clad and the shroud. The fuel-clad gap is modelled by a heat exchange coefficient with contributions of conduction, radiation, and solid-solid contact heat exchanges. Heat exchanges due to free convection in the gap are neglected. Conduction through the gas depends on the nature of the gaseous species mixture, the contact roughness and the gas pressure. Solid-solid heat exchanges depend on the thermal conductance of the material in contact, the contact roughness and the contact pressure.

The thermal-hydraulics module models a one-phase coolant with two conservations equations (mass and energy). Temperatures and flow rates are computed in 1D in the channel. The pressure is assumed constant. The channel width is updated with the clad deformation during the transient. Heat exchanges between the clad and the fluid are modelled thanks to exchange coefficients modelling the different regimes: pre-saturation, nucleate boiling, transition boiling, film boiling and the rewetting stage. A specific modelling takes into account the kinetics effects on the magnitude of the critical heat flux. The boiling curves in PWR conditions or in stagnant water conditions are validated on experimental data from the PATRICIA facility and tests in NSRR.

Gas behaviour

An increase of temperature induces an increase of the volumes occupied by the gas. Thus, the swelling of the pellet can intensify the mechanical loading on the clad during the PCMI stage. Then, the release of fission gases into the free volumes induces an over-pressurization of the rod which may cause clad ballooning if clad temperatures are sufficiently hot.

The gas behaviour models can take into account the gas species inside the fuel and the free volumes (lower and upper plenum, gap, and central hole if any). The fuel is composed of grains bounded by other

grains or by voids. Fission-gas atoms produced during irradiation beside the lattice are not taken into account. Before the transient, they are assumed to have already coalesced into bubbles located inside the grains or at the grains boundary.

Due to thermal gradient and to Brownian motion, the intra-granular bubbles coalesce and migrate to the boundaries to become inter-granular bubbles. Then, the gases inside the inter-granular bubbles may be released into the porosities network. When the stress reaches the grain boundary rupture stress or when the grain boundaries are saturated by inter-granular bubbles, opened porosities allow the communication toward the free volumes. The swelling of the pellet caused by gas expansion in each population of cavities (bubbles and porosities) is modelled.

Coupling between the modules

The coupling between the different modules is strong. During a time step, a first convergence is reached between thermal and thermal-hydraulics solving. Then, using the calculated temperatures, a second iterative loop occurs between the gas behaviour module and the mechanical solving. When the convergence of this second resolution is reached, temperatures are re-calculated and so on until full convergence of the different modules. The time step is automatically reduced in Case of non-convergence.

Physical properties

The cladding mechanical properties such as yield stress and ultimate tensile strength are mainly provided by the PROMETRA experimental programme. Several viscoplastic laws are available for the cladding. The fuel mechanical behaviour is assumed elastic or elasto-plastic. Thermal physical properties such as conductivity depend on temperature, stoichiometry, burn-up and porosity.

8.6 TESPAROD

The fuel rod code TESPAROD represents the fuel rod behaviour in a 1-½-dimensional spatial resolution. It provides the transient radial temperature distribution in a cross-sectional area of a fuel rod while the axial temperature distribution is approximated from an axial power factor which is user input. Characteristic fuel rod volumes like fuel rod plena or gap volume are described with designated volumes. Perfect fission gas communication among these volumes is assumed.

Hoop Stress and Hoop Strain in the Cladding

TESPAROD code's viscous-plastic hoop stress/strain model provides no radial stress resolution within the cladding. The effect of radially localized yielding in the cladding is considered in TESPAROD with the ratio of yield stress to bust stress. This ratio is deduced from the analytical solution of the 3-dimensional viscous-plastic stress/strain relation for thick-walled cylinders. According to this analysis the location of the elastic-plastic transition occurs at the inner cladding surface first, which is associated with yield stress. Finally, the location of the elastic-plastic transition reaches the outer surface, which is associated with both the plastic collapse of the cladding and the burst stress. For ductile cladding behaviour the stress ratio depends on cladding inner diameter and outer diameter. For brittle cladding behaviour the stress ratio is close to unity with 0.985.

In the TESPAROD code the cladding is considered either brittle or ductile depending on the average hydrogen pick-up in the cladding. If cladding behaves partially brittle and partially ductile as observed in the test Cases NSRR VA-1 (60% ductile) and NSRR VA-3 (88% ductile), the stress ratio has to be provided by user input as an interpolation between ductile mode and brittle mode.

Cladding deformation

A pressure difference across the cladding as well as the expansion of a pellet may provoke tensile hoop stresses in the cladding. These stresses may provoke cladding creep and/or cladding plastic deformation. Both effects on the cladding deformation are modelled in TESPAROD code. While plastic deformation affects evenly the circumferential hoop strain, the creep strain can be circumferentially localized depending on the eccentricity parameter provided by user input. All hoop strains result in cladding thinning according to plastic flow rule. Each irreversible deformation contributes to an additional heat-up of the cladding.

If the hoop stress exceeds the hoop burst stress, burst of cladding is assumed. The burst stress in TESPAROD is determined based on the correlation developed at KfK Karlsruhe for Zircaloy-4 in the early 1980s. Recent EDGAR tests showed that this approach is still valid with some modification.

Cladding creep models of the Norton type are available for Zry-4, Zry-2, Duplex, Zirlo®, E110 and M5®. These high temperature creep models also take into account both the hydrogen content and the oxygen content. While increased hydrogen content increases the creep strain rate, the oxygen content reduces the creep strain rate. Furthermore, the creep rate strongly depends on the α-β phase transformation.

Cladding High Temperature Oxidation

The high temperature oxidation of the cladding within steam atmosphere leads to both an uptake of oxygen within the cladding metal layer and a formation of an outer oxide layer. The TESPAROD code applies the weight gain correlations for oxygen uptake and oxide layer formation according to the models of Leistikov. Alternative models like the Baker-Just model or Cathcart-Pawel model are optionally available

Gap Conductance

The gap between the pellet outer surface and the cladding inner surface contains helium and to some extend fission gas. The gap conductance model in TESPAROD predicts the thermal resistance for heat flow depending on the fission gas composition, fission gas pressure and gap size. This model is similar to that model used in the fuel rod code SCANAIR.

Fission-Gas Release

TESPAROD code provides an empirical fission gas release model for the operational fission gas release. This empirical model predicts the fission gas release depending on the fuel rod average burn-up level only. If complex power histories need to be considered, a coupled code version TESPAROD/FRAPCON can be applied optionally.

The transitional fission gas release in TESPAROD is modelled based on both a gas diffusion model for long term transients (in the time range of minutes) and power density model for short term transients (in the time range of milliseconds). The short term transient model considers the transitional fission gas release from inter-granular pellet location. This fission gas release rate is proportional to both the fission gas content at grain boundary. The fission gas release rate is validated with rod internal pressure data of NSRR test LS1.

Pellet Expansion at High Power Densities

In high power transients like RIA transients the pellet expansion is controlled by both the thermal expansion of the pellet and the power density related expansion. The second contribution is a result of a partial amorphous state of the fuel due to the large atomic displacement rate at high power densities. Although the UO_2 crystal cannot reach a permanent amorphous state, a transitional amorphous state can be achieved. Under normal operation the damage accumulation in UO_2 crystals becomes saturated at 10 dpa without reaching a permanent amorphous state, but transitional amorphous state is achievable beyond that 10 dpa with a displacement rate of about 10 dpa/s, e.g. during peak power of RIA transients. The additional fuel expansion associated with the transitional amorphous state is predicted in TESPAROD. Fresh fuel

(fuel with less than 10 dpa) has no damage accumulation in the crystal lattice and therefore, the power density related expansion vanishes.

Fission gas bubble expansion in the fuel is not considered in the TESPAROD code because of an almost complete loss of fission gas at inter-granular locations during the early period of RIA transients predicted by TESPAROD.

Pellet Conductivity

Increasing burn-up reduces the pellet conductivity. The TESPAROD model for fuel thermal conductivity relies on the HALDEN model which provides distinctions for fuel types of UO_2, MOX and Gadolinium.

Radial Power Distribution in Pellet

Because Pu accumulates continuously in the peripheral region of the pellet, the heat release continuously shifts toward the pellet periphery. TESPAROD approximates this power density shift as simple function of burn-up. The heat release at the inner pellet radius (90% of the total radius) is reduced in power density while the outer radius (remaining 10% of total radius) receives the difference thus the average power density across the entire pellet is kept constant. The power density at inner radius is reduced by the factor reduction<1.

Heat Transfer to Coolant

Heat transfer between cladding and coolant can be provided as user input to the code. For RIA transients an extra heat transfer model is optionally available. This heat transfer model predicts DNB if the cladding surface temperature exceeds the DNB temperature deduced from the thermal-mechanical non-equilibrium. The film boiling heat transfer is modelled as a multiple of radiation heat transfer. The multiplier (~9.0) reflects the enhanced heat transfer due to the wavy steam/water interface.

The cladding surface temperature has to fall below the Leidenfrost temperature in order to re-establish both nucleate boiling heat transfer and a cladding surface which is wetted by liquid coolant. Before wetting occurs a pre-cooling effect takes place which is modelled by a quadratic interpolation between film boiling heat transfer and nucleate boiling heat transfer. This interpolation starts if the cladding surface temperature approaches 25% of the Leidenfrost temperature after passing the peak cladding surface temperature.

8.7 TRANSURANUS

TRANSURANUS is a computer program written in FORTRAN95 for the thermal and mechanical analysis of fuel rods in nuclear reactors that is owned by the Joint Research Centre of the European Commission and used by research centres, nuclear safety authorities, universities and industrial partners [53]. The program is generally referred to as a fuel performance code meaning that it solves the equations for the radial heat transfer, the radial displacement along with the stress distribution in both the fuel and the surrounding cladding, and describes the fission product behaviour as a function of time. The equations embody the following phenomena:

- Thermal performance: heat conduction, radiation and convection;
- Mechanical performance: creep, densification, thermal expansion, pellet cracking and relocation, solid and gaseous swelling;
- Actinide behaviour: depletion and build-up of main U, Np, Pu, Am and Cm nuclides, impact on the radial power profile;
- Fuel restructuring: actinide redistribution, grain growth (normal and columnar), central void formation;

- Fission product behaviour: creation in the fuel matrix, diffusion to grain boundaries, release to free rod volume after saturation of grain boundaries, athermal release, formation of High Burnup Structure (depletion and porosity).

The axial and radial discretization of both fuel pellets and cladding are flexible. Once the behaviour of the fuel is computed in each slice, they are coupled in the code via balance equations that regard displacement and axial friction forces. For this reason standard fuel performance codes are so-called 1.5 D codes, while 2D (3D) codes solve the equations simultaneously in two (three) dimensions.

The TRANSURANUS code consists of a clearly defined mechanical–mathematical framework into which physical models can easily be incorporated. The code has a comprehensive material data bank for oxide, mixed oxide, carbide and nitride fuels, Zircaloy and steel claddings and several different coolants. It can be employed in two different versions: as a deterministic and as a statistical code.

Besides its flexibility for fuel rod design, the TRANSURANUS code can deal with a wide range of different situations, as given in experiments, under normal, off-normal and accident conditions, although some models specific for RIA (e.g. plenum temperature) are still under development. Furthermore the code is used for BWRs, PWRs and VVERs. The time scale of the problems to be treated may range from milliseconds to years. Thence complex irradiation experiments can be simulated incl. re-fabricated instrumented fuel rods and changing operating conditions.

9. APPENDIX II: SPECIFIC DESCRIPTION OF THERMAL HYDRAULICS MODELS USED IN CODES

9.1 ALCYONE

The general Gauss-Seidel iterative scheme of ALCYONE has been modified to account for non-steady heat and mass transport in the coolant [29]. The first developments have been focused on a sodium coolant (one-phase coolant) in order to provide a 1D fuel rod scheme able to analyse the CABRI REP-Na tests. Basically, uni-dimensional heat and mass transport along the rod length was assumed in the sodium channel of cross section S. For each fuel rod slice of height (z2 – z1), z being the axial position with respect to the bottom of the rod, the following heat and mass balance equations are solved:

$$\frac{\partial}{\partial t}\left[\int_{z1}^{z2} h\rho S dz\right] + h_2 Q_2 - h_1 Q_1 - \int_{z1}^{z2} \phi \; dz = 0$$

$$\frac{\partial}{\partial t}\left[\int_{z1}^{z2} \rho S dz\right] + Q_2 - Q_1 = 0$$

In those Equations, h_i and Q_i refer respectively to the sodium enthalpy and mass flow rate at an elevation z_i. ρ is the sodium density. ϕ is the linear heat rate received by the fluid from the fuel rod. The physical properties of sodium are assumed constant all over the channel cross section S. The linear heat rate ϕ is estimated as follows from the heat exchange between the cladding external surface and the coolant:

$$\phi = H \left(T_{clad} - T_{Na}\right) \pi D_{clad}$$

where H is the clad-coolant heat exchange coefficient, T_{clad} the clad external temperature, T_{Na} the coolant temperature and D_{clad} the clad external diameter. The heat exchange coefficient H accounts for zirconia thickness and depends also on sodium physical properties. The non-linear system of Equations is solved using a standard upwind method with an explicit time integration scheme. This introduces a constraint on the time step given by the well-known Courant-Friedrichs-Lewy (CFL) condition.

For a water coolant, the correlations proposed by Bessiron for PWR [5] and NSRR [4] conditions (stagnant liquid water) have been implemented in ALCYONE [33]. Water physical properties originate from the CATHARE Thermo-Hydraulics code developed at the CEA.

The PWR correlations are derived from the PATRICIA-PWR experimental programme. The transient boiling curve includes four different regimes [5]:

- forced-convection simulated by the Dittus-Boelter correlation up to the saturation temperature,

- nucleate boiling represented by a linear interpolation up to the Critical Heat Flux (CHF) estimated by the Babcock-Wilcox correlation at the Critical Temperature determined from the PATRICIA experiments (Tsat + 55 K),
- transient and film boiling simulated by an exponential function that first decreases to simulate the transition boiling (up to Tsat + 190 K where the heat flux is minimum) and then tends to the film boiling for high clad surface temperatures The film boiling heat flux is estimated by the Bishop-Sandberg-Tong correlation,
- the rewetting phase is activated for decreasing temperatures lower than the temperature of minimum heat flux. The heat flux is calculated according to the same three previous correlations. This approach differs from the one proposed by Bessiron [5] but was found to have little impact on the results.

In practice, the heat flux derived from the different correlations is prescribed in the thermal calculation. An explicit time integration scheme is used with a strong constraint on the time step, in particular when the CHF is reached.

The correlations for stagnant liquid water conditions were derived by Bessiron from inverse analyses of NSRR tests with the SCANAIR code [4]. The transient boiling curve includes four different regimes:

- Heat conduction in the stagnant liquid water up to the critical temperature (Tsat + 20 K),
- Vaporization of a 30 μm thick layer of water at constant temperature (Tsat + 20 K). This semi-empirical model was introduced to account for the impact of the energy deposition rate on the CHF,
- Transition and film boiling regime are simulated with a heat transfer coefficient that decreases exponentially with the clad temperature up to Tsat + 450 K and then asymptotically tends to the film boiling heat transfer coefficient estimated by Sakurai (with an adjustment coefficient),
- The rewetting phase is activated when the temperature of the minimum heat flux is reached (Tsat + 450 K). The heat flux is calculated according to the same three previous correlations.

The same explicit time integration scheme is used for the simulation of NSRR tests with a stagnant liquid water coolant.

These developments have been tested successfully during this RIA benchmark Phase II.

9.2 BISON

To predict the thermal response of a fuel rod, thermal hydraulic condition of the surrounding coolant needs to be determined. Such condition in modelling the energy transport aspect of the coolant in BISON code is described by a single coolant channel model. This single channel is used mathematically to describe the thermal boundary condition for modelling the fuel rod behaviour. This model covers two theoretical aspects, i.e., the local heat transfer from cladding wall into the coolant and the thermal energy deposition in the coolant in steady state and slow operating transient conditions.

Assumptions and limitations of the coolant channel model are summarized below:

Closed channel

The lateral energy, mass, and momentum transfer in the coolant channel within a fuel assembly is neglected. Therefore, the momentum, mass continuity, and the energy equations are only considered in one-dimension, i.e., the axial direction.

Homogeneous and equilibrium flow

For the flow involving both the vapour and liquid phases, the thermal energy transport and relative motions between the two phases are neglected. This essentially assumes the two-phase flow is in a form of one pseudo fluid.

Fully developed flow

In the application of most heat transfer correlations, the entrance effects are neglected. The heat transfer is assumed to happen in a condition that the boundary layer has grown to occupy the entire flow area and the radial velocity and temperature profiles are well established.

Pressure drop neglected

The pressure drop due to flow induced resistance is not accounted for in the coolant channel model. Instead, coolant pressure as a function of time and axial location can be an input provided by user through a hand calculation or using a computer code.

Depending on the flow rate, flow pattern, and cladding wall surface heat flux, the heat transfer from cladding wall outer surface to coolant can be characterized into different heat transfer regimes.

The heat transfer correlations used to describe the heat transfer condition prior to the point of Critical Heat Flux (CHF) are:

- Dittus-Boelter correlation;
- Jens-Lottes correlation;
- Thom correlation;
- Shrock-Grossman correlation;
- Chen's correlation.

The sub-cooled and saturated boiling can enhance the heat transfer; however at a critical condition when the cladding outer surface is enclosed by vapour film, the heat transfer can deteriorate significantly, the corresponding heat flux is the Critical Heat Flux (CHF). The following correlations are implemented in BISON to calculate CHF, which can be used to estimate the thermal margin in a coolant channel:

- EPRI-Columbia correlation;
- GE correlation;
- Zuber correlation;
- Biasi correlation.

The post-CHF heat transfer regime is divided into transition boiling and film boiling. The transition boiling heat transfer regime occurs when the cladding wall temperature exceeds the Critical Heat Flux (CHF) temperature, but remains below the minimum film boiling temperature. The heat flux decreases significantly with increasing temperature in this regime. Two heat transfer correlations are implemented for the transition boiling regime. The two correlations are McDonough-Milich-King and modified Condie-Bengtson correlations. The film boiling heat transfer regime occurs when the wall temperature reaches the minimum film boiling temperature. Two correlations are provided for the film boiling region. The correlations are Dougall-Rohsenow and Groenveld correlations.

9.3 FRAPTRAN

9.3.1 Standard Version

If the user chooses to model the coolant as water, the fuel rod cooling model calculates the amount of heat transfer from the fuel rod to the surrounding coolant. In particular, the model calculates the heat transfer coefficient, heat flux, and temperature at the cladding surface. These variables are determined by the simultaneous solution of two independent equations for cladding surface heat flux and surface temperature.

One of the equations is the appropriate correlation for convective heat transfer from the fuel rod surface. This correlation relates surface heat flux to surface temperature and coolant conditions. Different correlations are required for different heat transfer modes, such as nucleate or film boiling. The relation of the surface heat flux to the surface temperature for the various heat transfer modes is shown in Figure 0. 1. Logic for selecting the appropriate mode and the correlations available for each mode are shown Table 0.1.

The second independent equation containing surface temperature and surface heat flux as the only unknown variables is derived from the finite difference equation for heat conduction at the mesh bordering the fuel rod surface. A typical plot of this equation during the nucleate boiling mode of heat transfer is also shown in Figure 0. 1 that of the heat transfer correlations determines the surface heat flux and temperature. Neither of the two equations solved simultaneously contains past iteration values so that numerical instabilities at the onset of nucleate boiling are avoided. A separate set of heat transfer correlations is used to calculate fuel rod cooling during the reflooding portion of a LOCA. During this period, liquid cooling water is injected into the lower plenum and the liquid level gradually rises over time to cover the fuel rods. This complex heat transfer process is modelled by a set of empirical relations derived from experiments performed in the FLECHT facility [54].

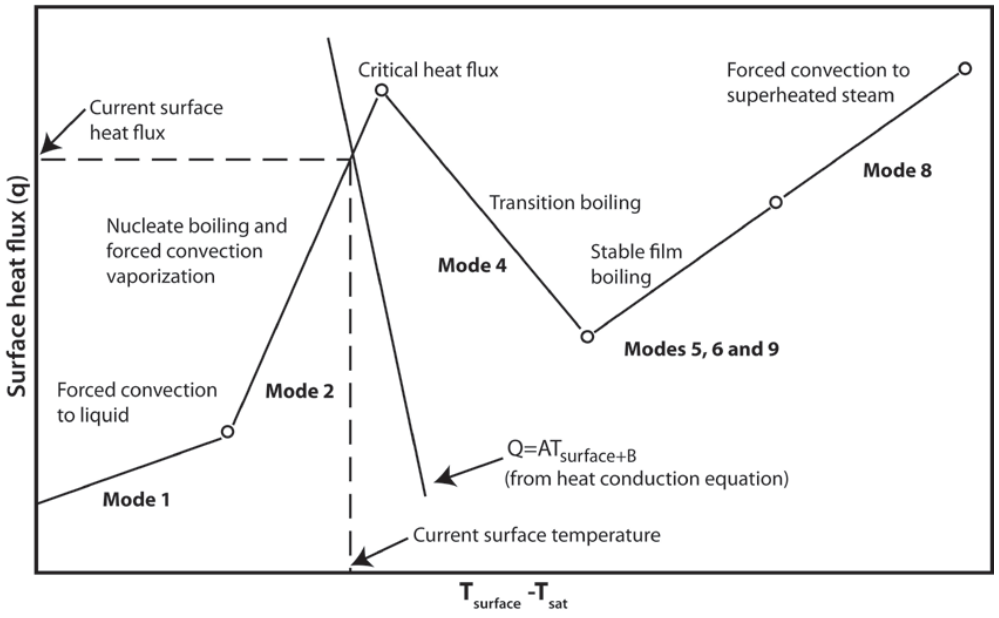

Figure 0. 1: FRAPTRAN – Relation of surface heat flux to surface temperature

Heat Transfer Mode	Range[a]	Default Heat Transfer Correlation[b]	Optional Heat Transfer Correlation(s)
Forced convection to subcooled liquid (Mode 1)	$T_w < T_{sat}$ or $Q_2 < Q_1 < Q_{crit}$	Dittus-Boelter (Dittus and Boelter, 1930) for turbulent flow; constant Nu = 7.86 for laminar flow (Sparrow et al., 1961)	
Subcooled nucleate boiling (Mode 2)	$Q_1 < Q_2 < Q_{crit}$; $T_b > T_{sat}$ $T_w > T_{sat}$	Thom (Thom et al., 1965)	
Saturated nucleate boiling (Mode 3)	$Q_1 < Q_2 < Q_{crit}$; $T_b = T_{sat}$ $T_w > T_{sat}$	Thom (Thom et al., 1965)	Chen (1963)
Post-CHF transition boiling (Mode 4)	$Q_2 > Q_{crit}$; $Q_4 > Q_5$; $G > 200{,}000$	Modified Tong-Young (Tong and Young, 1974)	Bjornard-Griffith (Bjornard and Griffith, 1977) Modified Condie-Bengston (INEL, 1978)
Post-CHF film boiling (Mode 5)	$Q_2 > Q_{crit}$; $Q_5 > Q_4$; $G > 200{,}000$ or $Q_5 > Q_6$	Groeneveld 5.9 (Groeneveld, 1973, 1978; Groeneveld and Delorme, 1976)	Bishop-Sandberg-Tong (1965) Groeneveld-Delorme (1976)
Post-CHF boiling for low flow conditions (Mode 7)	$Q_2 > Q_{crit}$; $Q_6 > Q_5$; $G < 200{,}000$	Bromley (1950)	
Forced convection to superheated steam (Mode 8)	$X > 1$	Dittus-Boelter (Dittus and Boelter, 1930)	

[a]The symbols used are:
Q_i = surface heat flux for i-th heat transfer mode
X = coolant quality
Q_{crit} = critical heat flux
G = mass flux (lbm/hr-ft^2)
T_w = cladding surface temperature
P = coolant pressure (psia)
T_{sat} = saturation temperature of coolant
T_b = local bulk temperature of coolant

[b] Parameter limits describing the range of the heat transfer apply to the default correlation for each mode. The correlation to be used is specified in the input.

Table 0.1: FRAPTRAN – Heat transfer mode selection and correlations

9.3.2 TRABCO coupling

The TRABCO transient thermal hydraulic channel code was used at the MTA EK in the RIA benchmark Phase II for the simulation of the thermal hydraulics phenomena. This code has been originally developed at VTT in Finland [55][56] and it is a sub-channel type code which applies a 4-conservation-equation approximation for a single closed channel in axial direction. In order to close the equations several empirical correlations have been built into the code e.g. for the friction, heat transfer, critical heat flux, vaporisation, condensation, slip ratio. The capabilities of the code have been extended for VVER reactors and nowadays the TRABCO thermal-hydraulic code is usually used at high pressure, at high coolant temperature and velocity.

The TRABCO code has been coupled to the FRAPTRAN 1.3 [57] and later on to the FRAPTRAN 1.4 fuel behaviour codes (FRAPTRAN V1.4+TRABCO). This coupling was made in such a manner that only few modifications have to be built into the original codes. Up to now the two codes (tasks) are running parallel and separately from each other and these parallel tasks are communicating by a shared memory part (see Figure 0.2). In each time steps the FRAPTRAN code gives the heat flux and the cladding outer surface temperature to the TRABCO code and the thermal hydraulics module gives the bulk coolant temperature and the heat transfer coefficient of the coolant to FRAPTRAN.

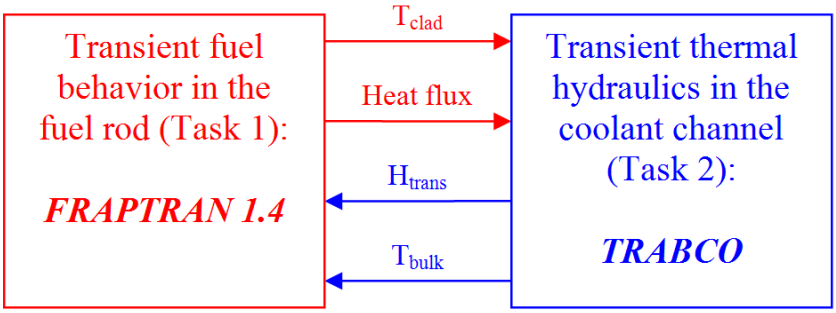

Figure 0.2: TRABCO/FRAPTRAN coupling scheme

In this RIA benchmark Phase II, different heat transfer regimes and heat transfer correlations were used in TRABCO: convective heat transfer ('Dittus-Boelter'), sub-cooled boiling ('Thom'), film boiling ('Groeneveld'). The critical heat flux was calculated by a Russian type correlation ('Smolin') and 11 axial nodes were applied.

9.4 RANNS

In the RANNS code, cladding-surface heat-transfer coefficient is computed by the following equations, assuming heat transfer regimes shown in Figure 9.3. Validation of the model is described in [6].

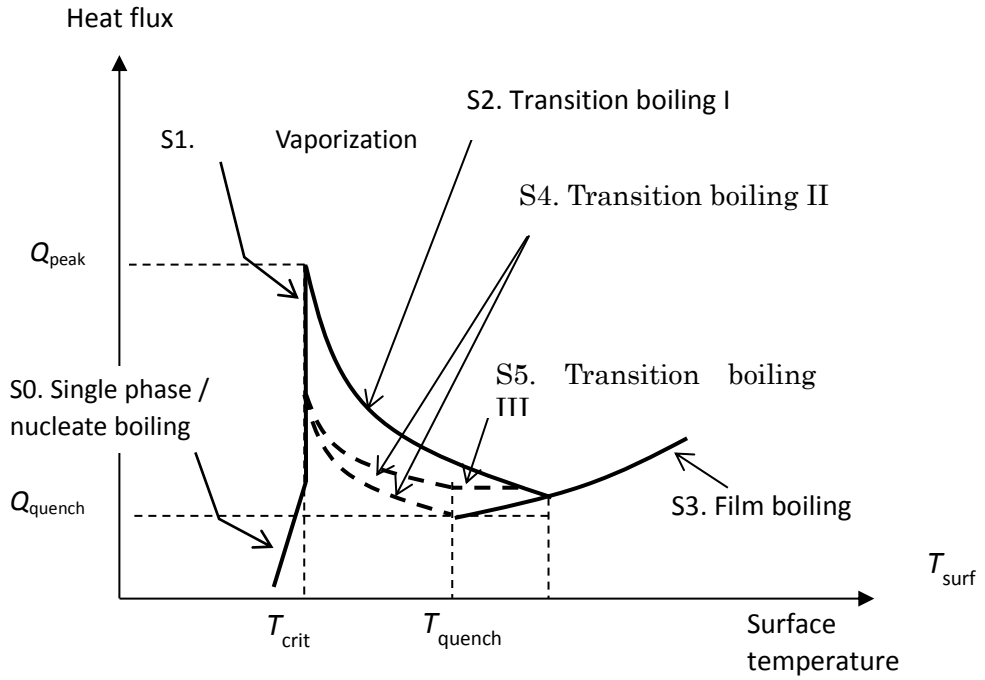

Figure 9.3: Heat transfer regimes assumed in the RANNS model for heat transfer from fuel rod surface to coolant water

Single phase nucleate boiling

Heat transfer coefficient h_{surf} for the regime S0 in Figure 9.3 is computed by Chen's equation or Dittus-Boelter equation.

The heat transfer regime is switched to S1 when the following condition is satisfied:

$T_{surf} >= T_{crit}$

where,

T_{surf} : cladding surface temperature [K]

$T_{crit} = T_{sat} + DNB\_TD\_CRIT$ [K]

T_{sat} : coolant saturation temperature [K]

DNB_TD_CRIT : a model parameter for T_{crit}

Vaporization

Heat transfer coefficient for the regime S1 in Figure 9.3 is given by:

$$h_{surf} = -\frac{k(R_o)\cdot\left(\frac{\partial T}{\partial r}\right)_{r=R_o}}{T_{surf}-T_{cool}}$$

Where:

T : cladding wall temperature [K]

T_{cool} : coolant temperature [K]

$k(R_o)$: cladding thermal conductivity at r=R_o [W·m^{-1}·K^{-1}]

R_o : cladding outer radius [m]

The cladding surface temperature T_{surf} is fixed to T_{crit}

Time evolution of vapour film thickness δ is computed by:

$$\frac{d}{dt}\delta = 10^6 \times \frac{q-h_{DB}(T_{surf}-T_{cool})}{(H_G-H_L)\rho_L}$$

Where:

δ : vapour film thickness [μm]

q : surface heat flux [W·m^{-2}]

h_{DB} : coefficient by Dittus-Boelter equation [W·m^{-2}·K^{-1}]

H_G : (gas state) coolant enthalpy [J·kg^{-1}]

H_G : (liquid state) coolant enthalpy [J·kg^{-1}]

ρ_L : (liquid state) coolant density [kg·m^{-3}]

The heat transfer regime is switched to S0 when the following condition is satisfied: $\delta <= 0$.

The heat transfer regime is switched to S2 when the following condition is satisfied: $\delta > \delta_c$.

Where:

$\delta_c = DNB\_DELTA\_C \times (10 \times P_{cool})^{0.02}$ [μm]

P_{cool} : coolant pressure [MPa]

DNB_DELTA_C : a model parameter for δ_c

Transition boiling I

Heat transfer coefficient for the regime S2 in Figure 9.3 is given by:

$$h_{surf} = \frac{1}{T_{surf}-T_{cool}}\left(b_{S2,1} - a_{S2,1}\frac{1-\exp(-10\times r)}{1-\exp(-10)}\right) \text{(for } x \le x_1$$

$$h_{surf} = \frac{1}{T_{surf}-T_{cool}}\left(a_{S2,2}x + b_{S2,2}\right) \text{(for } x > x_1)$$

$$x = T_{surf} - x_0$$

$$r = \frac{x}{x_2 - x_0}$$

Where:

$x_0 = T_{\text{crit}}$

$x_1 = T_{\text{quench}} - T_{\text{crit}}$

$x_2 = T_{\text{quench}}$

$a_{S2,1} = b_{S2,1} - q_{\text{quench}}$

$a_{S2,2} = 0$

$b_{S2,1} = q_{\text{crit}}$

$b_{S2,2} = q_{\text{quench}} - a_{S2,2}x_1$

$q_{\text{quench}} = q_{\text{quench,base}} + \max(0, dq_{irrad})$

$q_{\text{quench,base}} = h_{\text{quench}}(T_{\text{quench}} - T_{\text{cool}})$

$h_{\text{quench}} = h_{\text{FB},T_{\text{surf}}=T_{\text{quench}}}$

$T_{quench} = T_{sat} + dT_{quench}$

$dT_{quench} = 550 \times \left(1 + \frac{0.002\times dT_{sub}}{P_{cool}}\right)$

$\cdot (1 - 0.04 \times {P_{cool}}^{1.1} V^{0.2}) \cdot (0.1 \times P_{cool})^{0.15}$

$dq_{\text{irrad}} =$

$(1.2 \times 10^6 + 0.4 \times (b_{S2,1} - 7 \times 10^6) + 10^6 \left(\frac{dT_{sub}}{160}\right))(1 - \exp\left(-\frac{\Phi}{10^{24}}\right))\, h_{\text{FB},T_{\text{surf}}=T_{\text{quench}}}$:

h_{FB} at $T_{\text{surf}} = T_{\text{quench}}$ [W·m^{-2}·K^{-1}]

dT_{sub} : coolant subcooling [K]

V : coolant flow rate [m·s^{-1}]

Φ: fast neutron fluence of cladding [m^{-2}]

The values of x_0, x_1, x_2, $a_{S2,1}$,$a_{S2,2}$, $b_{S2,1}$, $b_{S2,2}$ are evaluated at the initiation of the regime S2 (switched from S1).

The heat transfer regime is switched to S3 when the following condition is satisfied:

$T_{\mathrm{surf}} < T_{TBtoFB}$ (T_{TBtoFB} is determined as temperature at which h_{surf} is equal to h_{FB}).

The heat transfer regime is switched to S4 when the following condition is satisfied:

$T_{\mathrm{surf}} < T_{crit}$.

The heat transfer regime is switched to S4 when the following condition is satisfied:

$q_{surf} < 0.5 \times q_{quench}$ [$\mathrm{Wm^{-2}}$].

The heat transfer regime is switched to S5 when the following condition is satisfied:

$T_{\mathrm{surf}} < T_{quench}$ and $dT_{\mathrm{surf}}/dt < 0$.

Film boiling

Heat transfer coefficient for the regime S3 in Figure 9.3 is given by:

$$h_{FB} = h_{Sakurai,cool} \cdot F_{pool} \cdot F_{irr} (\text{for } Q_{pool} < 271.24)$$

$$h_{FB} = h_{Shiotsu,cool} \cdot F_{flow} \cdot F_{irr} (\text{for } Q_{pool} \geq 271.24)$$

$$F_{pool} = 1.5$$

$$F_{flow} = 2.5 - 0.15 \times \arctan(1.5 \times P_{cool} - 4.0)$$

$$F_{irr} = 1.0 + 0.67 \times (1.0 - \exp(-\Phi/10^{24}))$$

Where:

$h_{Sakurai,cool}$: coefficient by Sakurai [$\mathrm{W \cdot m^{-2} \cdot K^{-1}}$] (see [58])

$h_{Shiotsu,cool}$: coefficient by Shiotsu [$\mathrm{W \cdot m^{-2} \cdot K^{-1}}$] (see [14])

F_{pool} : a model parameter for pool boiling

F_{flow} : a model parameter for forced convection boiling

F_{irr} : a scaling factor for irradiation effect

Q_{pool} : coolant mass flux [$\mathrm{kg \cdot m^{-2} \cdot s^{-1}}$]

The heat transfer regime is switched to S4 when the following condition is satisfied:

$T_{\mathrm{surf}} < T_{quench}$.

Transition boiling II

Heat transfer coefficient for the regime S4 in Figure 9.3 is given by:

$$h_{surf} = (x) b_{S2,1} + (1 - x) q_{\mathrm{quench,base}}$$

$$x = (T_{surf} - T_{quench})/(T_{\mathrm{crit}} - T_{quench})$$

The heat transfer regime is switched to S0 when the following condition is satisfied:

$T_{surf} < T_{crit}$ and $q_{surf} < 5 \times 10^5$[$\mathrm{Wm^{-2}}$].

Transition boiling III

Heat transfer coefficient for the regime S5 in Figure 9.3 is given by:

$$h_{surf} = \max(h_{FB}, \frac{a_{S5}T_{\text{surf}}+b_{S5}}{T_{surf}-T_{cool}})$$

$$a_{S5} = 3 \times 10^4)$$

$$b_{S5} = q_{\text{peak}} - a_{S5}T_{\text{peak}}$$

Where:

q_{peak} : surface heat flux at the initiation of the regime S5 [W·m^{-2}]

T_{peak} : surface temperature at the initiation of the regime S5 [K]

The heat transfer regime is switched to S4 when the following condition is satisfied:

$T_{\text{surf}} < T_{quench}$.

9.5 SCANAIR

9.5.1 Standard Version

Usual heat exchange models such as $\phi = H(T_{cl} - T_{co})$ have been made for quasi-steady conditions but have been proved to be unsuitable for fast heating conditions. Indeed in these conditions, the fast clad temperature rise makes the temperature radial gradient very stiff and the temperature radial profile is very different from the shape it would have in quasi-steady conditions (because terms $\rho c_p \frac{\partial T}{\partial t}$ are not negligible any longer). However a usual 1-dimensional approach has been kept, especially for calculation running time reasons, but with adjustments to these conditions. For that purpose an experimental programme PATRICIA has been realised in order to adjust heat exchange coefficients in PWR conditions. These coefficients have also been adjusted for the conditions of the nuclear reactor NSRR: stagnant water at atmospheric pressure and room temperature [3].

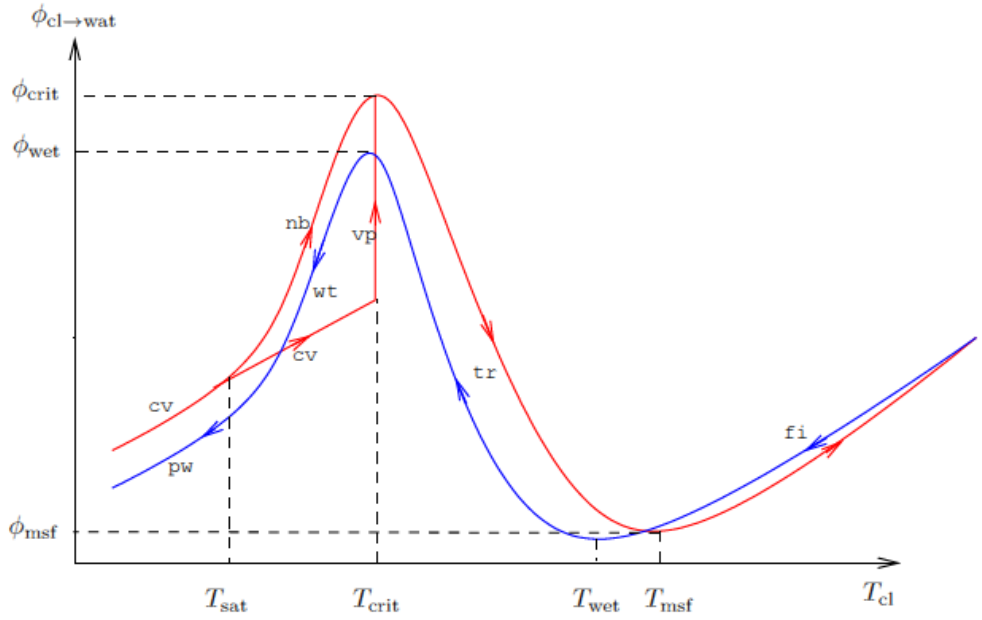

Figure 0.4: SCANAIR – Standard Clad to coolant heat flux phases

Error! Reference source not found. illustrates the evolution of the clad-water heat flux versus the clad surface temperature T_{cl}. Abbreviations (e.g. "cv") are used to mark the different parts of this curve; the red part represents the heat exchanges during the clad temperature rise and the blue one during its cooling.

In the sequel, we describe the different parts of this curve beginning by the pre-saturation phase (cf. §1). The correlations used to calculate the heat exchange coefficient in the nucleate boiling phase or in the vaporisation phase are then presented in §2. The heat transfer occurring in the transition boiling phase are the object of the part §3 while the film boiling phase is discussed in §4. The correlations used in the cooling phase (i.e. the rewetting and post-rewetting phases) are detailed in §5 and, in §6, we detailed the correlations used to compute the critical temperature and the critical heat flux.

1) "pre-saturation" phase "cv"

This part simulates the clad-water heat exchanges during which no vapour is present and when the clad temperature increases. In this case, the heat flux (in W.m^{-2}) is given by:

$$\Phi_{cv} = H_{cv}.(T_{cl} - T_l)$$

where T_{cl} is the outer clad temperature (in K), T_l the coolant temperature and H_{cv} the heat exchange coefficient (in W.m^{-2}.K^{-1}) for which two types of modelling are available.

The first model with heat exchange coefficient simulates the forced convection or the natural convection depending on the coolant velocity. In the former fluid regime, the heat exchange coefficient is calculated by the Dittus-Boelter's correlation [59]:

$$H_{forced} = 0.023.\frac{\lambda_l}{D_h}.\mathrm{Re}^{0.8}.\mathrm{Pr}^{0.4}$$

with $\mathrm{Re} = 0.023.\frac{\rho_l v_l D_h}{\mu_l}$ and $\mathrm{Pr} = \frac{\mu_l c_{pl}}{\lambda_l}$

where the subscript *l* refers to physical properties at the coolant temperature T_l (in K), Re is the Reynolds number, Pr the Prandtl number, v_l the velocity (in m.s^{-1}), D_h the hydraulic diameter (in m), μ_l the dynamic viscosity (in kg.m^{-1}.s^{-1}), C_{p_l} the specific heat (in J.kg^{-1}.K^{-1}), ρ_l the density (inkg.m^{-3}) and λ_l the conductivity (in W.m^{-2}.K^{-1}).

According to [59], the range of validity of this correlation is:

- turbulent regime: Re>10^4,
- vertical tube with $\frac{z}{D_h} > 50$ (*z* is the tube length).

In the natural convection fluid regime, the heat exchange coefficient is calculated according to the Kreith's correlation (see [60][61]):

$$H_{natural} = \frac{\lambda_{fi}}{D_h}.\mathrm{Nu}$$

where λ_{fi} is the coolant conductivity (in W.m^{-2}.K^{-1}) calculated at T_{fi} (defined below) and Nu the Nusselt number. This latter is defined as follow:

$\mathrm{Nu} = 0.555.(\mathrm{PrGr})^{0.25}$ if $\mathrm{PrGr} \leq 10^9$ (laminar flow regime)

$\mathrm{Nu} = 0.021.(\mathrm{PrGr})^{0.4}$ if $\mathrm{PrGr} > 10^9$ (turbulent flow regime)

where Pr and Gr are, respectively, the Prandtl number and the Grashof number written in the following form:

$$\mathrm{Pr} = \frac{\mu_{fi} c_{p,fi}}{\lambda_{fi}}$$

$$\mathrm{Gr} = \max\left(0, \frac{g\rho_{fi}^2 D_h^3 \alpha_{fi} (T_{cl} - T_{fi})}{\mu_{fi}^2}\right) \frac{\rho_l \nu_l D_h}{\mu_l}$$

Here above, the subscript *fi* refers to physical properties at the temperature T_{fi} (in K). This latter is defined by:

$$T_{fi} = \min\left(T_{sat}, \frac{T_{cl} + T_l)}{2}\right)$$

where T_{sat} corresponds to the saturation temperature (in K) and T_{cl} to the outer clad temperature (in K), g is the acceleration due to gravity (in $m.s^{-2}$), α_{fi} the thermal dilation coefficient (in K^{-1}), D_h the hydraulic diameter (in m), μ_{fi} the dynamic viscosity (in $kg.m^{-1}.s^{-1}$) and ρ_{fi} the density (in $kg.m^{-3}$).

The heat exchange coefficient in the pre-saturation phase is calculated as the maximum value of H_{forced} and $H_{natural}$:

$$H_{cv} = \max\left(H_{forced}, H_{natural}\right)$$

The second model computes a thermal radial conduction in water. This one should be used only in stagnant water situations and when the clad temperature rises quickly.

The radial temperature profile in the liquid and the clad-to-coolant heat flux are computed by resolution of the radial heat conduction equation.

This phase is left when the clad temperature becomes higher than:

- the water saturation temperature (T_{sat}) provided that the "vaporisation" modelling has not been selected in the next phase (nucleate boiling phase);
- the water critical temperature (T_{crit}) provided that the "vaporisation" has been selected in the next phase.

At very fast heating rates (~10000 $K.s^{-1}$) this critical temperature corresponds to overheated liquid water: near the clad, the water is still liquid despite the fact that its temperature is above the saturation one because it is in a thermodynamic imbalanced state. This fact has been observed in NSRR experiments during which the clad temperature rises very quickly in stagnant water conditions.

2) "nucleate boiling" phase "nb" or "vaporisation" phase "vp"

Fast transient conditions

In fast rises of the clad temperature, experiments have proved that this micro-convection generated by bubbles has not enough time to take place before reaching the critical heat flux and, as a consequence, the steady state correlations do not allow calculating accurately heat exchanges in these conditions. Moreover, correlations assessing the critical heat flux have to be adjusted also in order to take into account these temperature kinetic effects. To make up for this, an empirical "linear" model validated on experimental results has been implemented. This consists in calculating the heat flux (in $W.m^{-2}$) by the following linear interpolation:

$$\Phi_{nb} = \Phi_{sat} + (T_{cl} - T_l).\frac{\Phi_{crit} - \Phi_{sat}}{T_{crit} - T_{sat}}$$

where Φ_{sat} is the heat flux (in $W.m^{-2}$) calculated in the previous phase when the outer clad temperature is at T_{sat} (in K). Here, the critical temperature T_{crit} (in K) is determined empirically according to the correlations presented in §**Error! Reference source not found.**.

Fast transient and stagnant water conditions

Finally, in NSRR conditions (stagnant water and fast temperature rise ~10000 $K.s^{-1}$), a "vaporisation" model has been implemented and proved to be more suited for these conditions [4][5]. It consists in staying in the pre-saturation phase until the clad temperature reaches the critical one T_{crit} (in K). Then, as explained in [4], the clad temperature is imposed to remain at T_{crit} in order to simulate the temperature plateau preceding the boiling crisis. From a numerical point of view, the heat exchange coefficient in the vaporisation phase H_{vp} (in $W.m^{-2}.K^{-1}$) is set at 10^{16} in order to penalise the clad temperature to the critical one. In [60], the authors also note that imposing a fixed clad temperature leads to an imbalance between the conductive heat fluxes in the clad and in the fluid which corresponds to heat absorbed for the fluid vaporisation. The growth of a vapour film against the clad is, therefore, estimated according to:

$$\frac{\partial \delta_{liq}}{\partial t} = \frac{\Phi_{cl} - \Phi_{cv,crit}}{\rho liq, sat.\Delta H_{sat}}$$

where δ_{liq} is the thickness of liquid (in m) that is vaporised, ΔH_{sat} is the latent heat of vaporisation (in $J.kg^{-1}$), $\rho_{liq,sat}$ the liquid density (in $kg.m^{-3}$) at the saturation temperature T_{sat} (in K), Φ_{cl} the clad-to-coolant heat flux (in $W.m^{-2}$) and $\Phi_{cv,crit}$ the heat flux leaving the vapour film (in $W.m^{-2}$).

This phase is left when:

- the calculated flux is higher than Φ_{crit} or the clad temperature higher than T_{crit}, if the "vaporisation" model has not been selected;
- the calculated flux is higher than Φ_{crit} or the vapour-film thickness higher than an empirical limit, if the "vaporisation" model has been selected.

3) "transition boiling" phase "tr"

In this phase, vapour pockets are periodically in contact with the clad. This type of heat exchange is not well known even in steady-state conditions. Indeed steady-state experiments are generally performed with an imposed heat flux because it is easier to fix the clad heating (electrically) than the clad temperature which needs a feedback control. In the zones where the flux increases with the clad temperature, the temperature is stabilised. But when the flux reaches Φ_{crit}, the clad temperature increases quickly without any control until its new stabilisation in the film boiling phase (zone marked with "fi"). Only controlled-temperature experiments can stabilise the temperature in the transition boiling zone ("tr"). However in steady conditions, modelling precisely this zone is not important because it does not impact the results; this is why a mere interpolation is usually performed between (T_{crit}, Φ_{crit}) and (T_{msf}, Φ_{msf}).

But in transient situations, this phase is more important. For example, the clad temperature can stay in this zone without going in the next one ("*fi*") then decrease. On the basis of the work presented in [4] [5], a quadratic interpolation performed between (T_{crit}, Φ_{crit}) and (T_{msf}, Φ_{msf}), the point at which the minimum heat flux is reached (*cf.* §**Error! Reference source not found.**), is recommended to describe this phenomenon:

$$\Phi_{tr} = \Phi_{msf} + (\Phi_{crit} - \Phi_{msf}).\left(\frac{T_{msf} - T_{cl}}{T_{msf} - T_{crit}}\right)^2 \quad \text{(quadratic interpolation)}$$

This phase is left when the clad temperature reaches the minimum stable film temperature T_{msf} and the next phase is entered (film-boiling phase, §**Error! Reference source not found.**).

4) "film boiling" phase "fi"

When the clad temperature reaches the minimum stable film temperature T_{msf}, the temperature is so high that no liquid water can stay in contact with the clad: a vapour film covers the clad. The heat exchange coefficient is low due to the low thermal conductivity of the vapour. Correlations are available to model this type of heat exchange. They rely on the following relation:

$$\Phi_{fi} = H_{fi}.(T_{cl} - T_{sat})$$

where H_{fi} is the heat exchange coefficient (in $W.m^{-2}.K^{-1}$) in the film boiling phase, T_{sat} the saturation temperature (in K) and T_{cl} the clad temperature (in K). In SCANAIR, H_{fi} is calculated according to Sakurai's correlation for NSRR conditions [58] and to the Bishop-Sanderg-Tong correlation for PWR conditions [62].

Sakurai's correlation

The heat exchange coefficient (in $W.m^{-2}.K^{-1}$) calculated according to Sakurai's correlation is expressed as:

$$H_{fi} = \frac{\lambda_{fi}}{\omega}.\text{Nu} \text{ with } \omega = 2\pi\sqrt{\frac{\sigma_{sat}}{g(\rho_{liq} - \rho_{fi})}}$$

where the subscripts *sat*, *liq* and *fi* refer to properties calculated at the saturation temperature T_{sat} (in K), the liquid temperature T_{liq} (in K) and the steam film temperature T_{fi}, respectively. Here, the liquid temperature is given by:

$$T_{liq} = \frac{1}{2}\left(T_{sat} + T_l\right)$$

The steam film temperature is defined as follow:

$$T_{fi} = \frac{1}{2}\left(T_{cl} + T_{sat}\right)$$

where T_{cl} is the outer clad temperature (in K) and T_l the coolant temperature (in K). Here above, ω is the critical wavelength of the Taylor instability, g the acceleration due to gravity (in m.s^{-2}), λ the conductivity (in W.m^{-2}.K^{-1}), ρ the density (in kg.m^{-3}), σ the surface tension (in N.m) and Nu is a Nusselt number given by:

$$\mathrm{Nu} = 0.82.(\beta_1\beta_2\beta_3)^{0.25}$$

where β_1, β_2 and β_3 are three coefficients which express as:

$$\beta_1 = \frac{1}{\gamma_1}.\frac{g\rho_{fi}(\rho_{liq} - \rho_{fi})\omega^3}{\mu_{fi}^2}$$

$$\beta_2 = \frac{\theta^3}{1 + \theta \big/ \gamma_1 \mathrm{Pr}_{liq}} \text{ with } \theta = (\xi_1 + \xi_3\sqrt{\xi_2})^{1/3} + (\xi_1 - \xi_3\sqrt{\xi_2})^{1/3} + \frac{\gamma_2}{3}$$

$$\beta_3 = \frac{1}{\gamma_1^2\,\mathrm{Pr}_{liq}^2\left(\rho_{fi}\mu_{fi} \big/ \rho_{liq}\mu_{liq}\right)}$$

where μ denotes the dynamic viscosity (in kg.m^{-1}.s^{-1}) and Pr_{liq} the Prandtl number defined by properties computed at T_{liq}. It reads:

$$\mathrm{Pr}_{liq} = \frac{\mu_{liq}c_{p,liq}}{\lambda_{liq}}$$

C_p is the specific heat (in J.kg^{-1}.K^{-1}) and λ the conductivity (in W.m^{-1}.K^{-1}). At this stage, it remains to define the coefficients $\{\gamma_i\}_{i=1,2}$ and $\{\xi_i\}_{i=1,2,3}$. These are written as:

$$\gamma_1 = \frac{c_{p,fi}(T_{cl} - T_{sat})}{\mathrm{Pr}_{fi}\left[\Delta H_{sat} + 0.5c_{p,fi}(T_{cl} - T_{sat})\right]}$$

$$\gamma_2 = \frac{c_{p,liq}(T_{sat} - T_l)}{\Delta H_{sat} + 0.5.c_{p,fi}(T_{cl} - T_{sat})}$$

$$\xi_1 = \frac{\gamma_2^3}{27} + \frac{\gamma_1\gamma_2}{3}.\mathrm{Pr}_{liq}.\left(\frac{\rho_{fi}\mu_{fi}}{\rho_{liq}\mu_{liq}}\right) + \frac{\gamma_1^2}{4}.\mathrm{Pr}_{liq}^2.\left(\frac{\rho_{fi}\mu_{fi}}{\rho_{liq}\mu_{liq}}\right)$$

$$\xi_2 = -\frac{4}{27}.\gamma_2^2 + \frac{2}{3}\gamma_1\gamma_2.\mathrm{Pr}_{liq} - \frac{32}{27}.\gamma_1\,\mathrm{Pr}_{liq}.\left(\frac{\rho_{fi}\mu_{fi}}{\rho_{liq}\mu_{liq}}\right) + \frac{\gamma_1^2}{4}.\mathrm{Pr}_{liq}^2 + \frac{2}{27}.\gamma_2^3.\left(\frac{\rho_{liq}\mu_{liq}}{\rho_{fi}\mu_{fi}}\right)$$

$$\xi_3 = \frac{\gamma_1}{2}.\mathrm{Pr}_{liq}.\left(\frac{\rho_{fi}\mu_{fi}}{\rho_{liq}\mu_{liq}}\right)$$

where ΔH is the latent heat of vaporisation (in J.kg^{-1}) and Pr_{fi} the Prandtl number defined by properties calculated at T_{fi} as follow:

$$\mathrm{Pr}_{fi} = \frac{\mu_{fi}c_{p,fi}}{\lambda_{fi}}$$

Sakurai's correlation has been established in the following conditions:

- Pressure: 101×10^3 Pa
- $T_{cl} - T_{sat}$: 400 K

Bishop-Sanderg-Tong's correlation

The heat exchange coefficient calculated according to the Bishop-Sanderg-Tong's correlation is defined by:

$$H_{fi} = 0.0193.\frac{\lambda_{fi}}{D_{eq}}.\mathrm{Pr}_{fi}^{1.23}.\mathrm{Re}_{liq,fi}^{0.8}\left(\frac{\rho_{vap,sat}}{\rho_{liq,sat}}\right)^{0.068}.\left(\frac{\rho_{vap,sat}}{\alpha\rho_{vap,sat} + (1-\alpha)\rho_{liq,sat}}\right)^{0.68}$$

where the subscripts, *sat*, *liq* and *fi* refer to properties calculated at the saturation temperature T_{sat} (in K), the liquid temperature T_{liq} (in K) and the steam film temperature T_{fi}, respectively. Here, the liquid temperature is set at the coolant temperature T_l (in K) while the steam film temperature is given by:

$$T_{fi} = \tfrac{1}{2}(T_{cl} + T_{sat})$$

where T_{cl} is the outer clad temperature (in K). Here above, α is the void fraction, $\rho_{vap,sat}$ is the steam density (in kg.m^{-3}) at the saturation temperature, $\rho_{liq,sat}$ the liquid density (in kg.m^{-3}) at the saturation temperature, Pr_{fi} the Prandtl number and $\mathrm{Re}_{liq,fi}$ the Reynolds number. These two non-dimensional numbers are given by:

$$\mathrm{Pr}_{fi} = \frac{\mu_{fi}c_{p,fi}}{\lambda_{fi}}$$

$$\mathrm{Re}_{liq,fi} = \frac{\rho_{liq}v_{liq}D_{eq}}{\mu_{fi}}$$

where C_p is the specific heat (in J.kg^{-1}.K^{-1}), λ the conductivity (in W.m^{-1}.K^{-1}), ρ the density (in kg.m^{-3}), v the velocity (in m.s^{-1}), μ the dynamic viscosity (in kg.m^{-1}.s^{-1}) and D_{eq} the heat diameter (in m).

As the thermal-hydraulic modelling assumes a single phase fluid in the channel, the void fraction is an input parameter. For PWR conditions, based on PATRICIA-RIA experiments, the void fraction used in the BST correlation is set at zero during the fast transient stage and is set to grow until 70% during the steady-state stage (i.e., when the time spent in the film-boiling regime exceeds 20 seconds). The value 70% is chosen to reproduce the heat flux magnitude observed in PATRICIA experiments during the post-DNB regime.

The range of validity of the Bishop-Sanderg-Tong correlation is:

- Flux: 3.5×10^5 to 19.2×10^5 W.m^{-2}
- Pressure: 4×10^6 to 22×10^6 Pa
- Mass flow rate: 1193 to 3390 kg.m^{-2}.s^{-1}
- Heat diameter: 2.54×10^{-3} to 8.13×10^{-3}m
- Clad temperature: 621 to 866 K
- Fluid temperature: 523 to 647 K

This phase is left when the clad temperature decreases and becomes lower than T_{wet}. The return to the transition boiling phase occurs when the heat flux is not large enough to sustain a stable film of vapour.

5) "cooling" phases "fi"→"tr"→"wt"→"pw"

When the clad temperature decreases, the different phases described previously are followed in reverse order with some differences:

- The "red" and "blue" curves are not exactly the same in the "*tr*" and "*fi*" phases. Indeed the wetting temperature T_{wet} (temperature at which the vapour film collapses) initially equal to T_{msf} drifts in time according to the time spent in the film-boiling phase, and the same for the rewetting flux Φ_{wet} with the critical flux Φ_{crit}. In practice, as soon as the clad temperature drops below T_{wet}, the clad temperature decrease is particularly fast and the rewetting phase only lasts a few milliseconds.
- The "*nb*" and the "*vp*" phases are followed only during the temperature increase. When cooling, heat exchange mechanisms are not the same and these phases have been replaced by the rewetting phase "*wt*" for which the heat flux Φ_{wt} (in W.m^{-2}) defined similarly to the "linear" modelling of "*nb*" is given by:

$$\Phi_{wt} = \Phi_{sat} + (T_{cl} - T_{sat}).\left(\frac{\Phi_{crit} - \Phi_{sat}}{T_{crit} - T_{sat}}\right)$$

- The post-rewetting phase "*pw*" corresponds to the "*cv*" phase, except that the conduction modelling cannot be activated because it has physical meaning only during a fast temperature rise, and also when the natural convection does not have enough time to work. In these conditions, the heat flux (in W.m^{-2}) is defined by:

$$\Phi_{pw} = H_{pw}(T_{cl} - T_l)$$

where H_{pw} is the heat exchange coefficient (in W.m^{-2}.K^{-1}) calculated as follow:

$$H_{pw} = \max(H_{forced}, H_{natural})$$

6) Critical temperature and critical heat flux

This part focuses on the correlations used in SCANAIR to calculate the critical temperature and critical heat flux.

Critical temperature

The critical temperature T_{crit} (in K) is defined as follows:

$$T_{crit} = T_{sat} + f(\chi)$$

where T_{sat} is the saturation temperature (in K) and $f(\chi)$ a function (in K) of χ which is a kinetic parameter varying in the range [0,1]. It is equal to 0 for steady-state or slow transients and to 1 for fast transients.

This relation is considered when the heat flux in the nucleate boiling phase is calculated by linear interpolation or when the vaporisation phase is studied.

Critical heat flux

In SCANAIR, the critical heat flux can be computed according to:

- Babcock-Wilcox's correlation [63]: it is used to compute the critical heat flux (in W.m^{-2}) in PWR conditions. This is defined as follows:

$$\Phi_{crit} = (1 - 13.873 D_h).\left(\frac{0.3702 \times 10^8 (4.364 \times 10^{-4} Q)^B - 0.04826.\Delta H_{sat} Q}{3.488 (2.254 \times 10^{-3} Q)^A} \right)$$

where the subscripts *sat* and *liq* respectively refer to properties calculated at the saturation temperature T_{sat} (in K) and at the liquid temperature (in K), here set at the coolant temperature T_l. D_h is the hydraulic diameter (in m), ΔH the latent heat of vaporisation (in J.kg^{-1}), Q the mass flow rate per unit surface (in kg.m^{-2}.s^{-1}) and X is the local quality. This latter quality depends on the thermodynamic quality κ as follows:

$$X = \max(\kappa\chi, -1) \text{ with } \kappa = \frac{H_{liq}^{wat} - H_{sat}^{wat}}{H_{sat}^{vap} - H_{sat}^{wat}}$$

where χ is a kinetic parameter varying in the range [0,1], H^{wat} the specific enthalpy of the liquid water (in J.kg^{-1}) and H^{vap} the vapour specific enthalpy (in J.kg^{-1}). It is equal to 0 for steady-state or slow transients and to 1 for fast transients. In the expression of critical flux, it remains to define the two terms *A* and *B*. These are written as:

$A = 0.712 + 0.03006\ (10^{-6}.P - 13.793)$
$B = 0.8304 + 0.09929\ (10^{-6}.P - 13.793)$

where *P* is the pressure (in Pa).

The range of validity of the Babcock-Wilcox's correlation is:

- Quality: -3% to 20%
- Mass flow rate: 1017 to 5425 kg.m-2.s-1
- Pressure: 13.8×10^6 to 16.5×10^6 Pa

- For NSRR conditions the critical heat flux is numerically defined by the value of the heat flux calculated in the nucleate boiling phase at the critical temperature T_{crit}.

9.5.2 QT-COOL Model

QT-COOL is a simple two-phase, one-dimensional single channel thermo-hydraulic module developed by Quantum Technologies AB for use with any computer program intended for thermo-mechanical analyses of light water reactor fuel rods under normal reactor operation or transient conditions. The purpose of QT-COOL is to supply Neumann type boundary conditions for thermal analysis of the fuel rod.

For a certain time step of the fuel rod analysis, the QT-COOL module calculates the changes in coolant properties along the fuel rod, given the current coolant conditions, the coolant inlet conditions and the fuel rod cladding tube surface temperature as a function of axial position. The clad-to-coolant heat transfer coefficient versus axial position along the fuel rod is also determined by the module. A large number of heat transfer correlations for both sub- and supercritical heat transfer are available; see Table 0.2 and Table 0.3. These correlations span a fairly large range of coolant conditions, but it should be borne in mind that they are based on data from experiments performed mainly under steady-state conditions or slow transients, and may not fully capture kinetic heat transfer effects under very fast power-coolant mismatch transients, such as reactivity initiated accidents.

The fundamental assumptions on which the QT-COOL module is based are summarized below:

- Coolant flows in the vertical direction, from the bottom to the top of the fuel rod, by forced convection. The model also works for stagnant conditions (natural circulation), i.e. for a prescribed inlet velocity equal to zero, but not for negative inlet velocities. However, it handles non-prescribed local flow reversals that may occur as a consequence of the heat transfer situation in the coolant channel, for example a flow reversal in the upper part of the channel due to cooling of the bottom part, leading to condensation of steam.
- Lateral cross-flow is not modelled.
- The coolant bulk properties are calculated by use of a homogeneous equilibrium model, which means that the water-steam coolant is treated as a homogeneous pseudo fluid that obeys the usual equations of a single-component fluid. Moreover, the coolant liquid and vapour phases are assumed to have the same velocity and temperature.
- The coolant pressure variation is assumed to be known along the flow channel. By this assumption, the momentum equation becomes superfluous, and only the conservation equations for coolant mass and energy (enthalpy) need be simultaneously solved.
- The coolant flow channel boundary is given by four neighbouring and equally loaded fuel rods. No lateral heat transfer to the surrounding is considered. The cross-sectional area of the flow channel is dependent on the fuel rod deformations, and is therefore continuously updated under the transient.

Heat transfer regime	Correlations	Default correlation
Convection in single-phase liquid	Dittus-Boelter Eckert-Jackson	Default is the maximum heat transfer coefficient predicted by these correlations
Subcooled nucleate boiling	Chen Thom Jens-Lottes	Default if $P \leq 4.0$ MPa or $G \leq 1000$ kg/m^{2}s Default if $P > 4.0$ MPa and $G > 1000$ kg/m^{2}s
Saturated nucleate boiling	Chen Schrock-Grossman	Default for all conditions
Transition boiling	Condie-Bengston McDonough-Milich-King Tong-Young	Default for all conditions
Film boiling	Groeneveld-5.7 Dougall-Rohsenow Sakurai et al.	Default if $P > 0.2$ MPa and $G > 270$ kg/m^{2}s Default if $P \leq 0.2$ MPa and $G > 270$ kg/m^{2}s Default if $G \leq 270$ kg/m^{2}s
Convection in single-phase vapour	Dittus-Boelter	Default

Table 0.2: SCANAIR – cladding-to-coolant heat transfer correlations available in QT-COOL
Here, P and G refer to the coolant pressure and mass flux

Application	Correlations	Default correlation
Forced convection, BWR conditions	EPRI – Columbia Original Barnett Modified Barnett	Default if $G > 270$ kg/m^{2}s
Forced convection, PWR conditions	EPRI – Columbia Babcock & Wilcox BW-2 Westinghouse W-3 Combustion Engineering CE-1	Default if $G > 270$ kg/m^{2}s
Pool boiling	Zuber-Lienhard-Dhir	Default if $G \leq 270$ kg/m^{2}s

Table 0.3: SCANAIR – Correlations for critical heat flux available in QT-COOL
Here, G refers to the coolant pressure and mass flux.

9.6 TESPAROD

Figure 0.5 summarizes heat transfer modes applied in TESPAROD code for RIA transients.

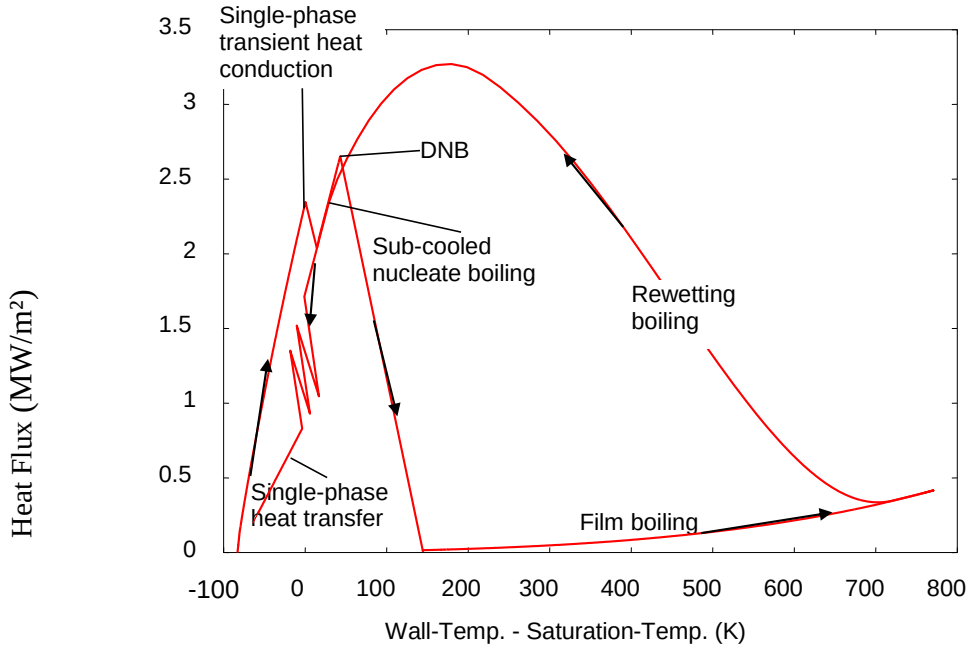

Figure 0.5: Heat Transfer modes of TESPAROD shown in a Nukijama curve

Because the duration of RIA transients is in the range of milliseconds up to a few seconds, conventional steady state heat transfer models are not applicable for this kind transient.

Heat transfer modes under RIA transients follow a sequence of heat transfer mechanisms (see arrows Figure 0.5 starting at a) single-phase transient heat conduction followed by b) sub-cooled nucleate boiling, followed by c) departure of nucleate boiling (DNB), followed by d) film boiling, followed by e) rewetting boiling, followed by f) sub-cooled nucleate boiling (identical to Case b) and finally reaching g) single-phase heat transfer. If DNB will not occur during RIA transient, the heat transfer mechanisms according to Case d) and Case e) are omitted from the heat transfer sequence.

Single-phase transient heat conduction

In the beginning of the RIA transient the temperature of the fuel rod cladding jumps to high temperature levels. The temperature gradient in the cladding toward the cladding surface approaches almost infinite. Therefore the 1-dimensional none-stationary heat conduction equation [64] is evaluated in order to deduce the heat transfer coefficient (HTC). This coefficient is proportional to the heat conductance $b = \sqrt{\lambda \rho c}$ and reciprocal square root of time $\sqrt{1/t}$:

$$HTC = \sqrt{\frac{\lambda \rho c}{\pi\, t}}$$

→ water at 3 bar: $HTC = \sqrt{\frac{2736523}{\pi\, t}}$ [W/m² /K]

This heat transfer mode vanishes after a few milliseconds and is replaced by sub-cooled nucleate boiling.

Sub-cooled nucleate boiling

When cladding surface temperature exceeds fluid's saturation temperature, nucleation of the fluid is assumed. The TESPAROD code applies for sub-cooled nucleate boiling a constant heat transfer coefficient of 19500 W/m²K regardless the actual velocity of the fluid. Fluid's velocity is considered negligible because the radial movement of bubbles due to bubble growth exceeds by far any axial movement of the fluid. Thus the turbulence controlling process is considered in TESPAROD not to be related to the axial flow.

This constant heat transfer coefficient allows reaching heat fluxes at departure of nucleate boiling (DNB) with values up to 2 to 3 MW/m² depending on the power injection ramp. The value of 19500 W/m²K has been quantified based on evaluations of several RIA tests at pressures between 1 and 3 bars. This values increases with system pressures above 3 bars according to Mostinsky's model [65].

$$HTC_{nucleate\ boiling} = 19500\ \frac{10^{-5} p_{system}^3 - 0.0023\, p_{system}^2 + 0.2182\, p_{system} + 3.5657}{4.2}$$

Departure from Nucleate Boiling (DNB)

The identification of departure of nucleate boiling (DNB) is based on the thermal-mechanical non-equilibrium according to Schöder-Richter's deliberations [66]. If super-heating of the cladding surface exceeds a temperature deduced from this thermal-mechanical none-equilibrium, DNB must occur. This critical cladding surface temperature T_{DNB} is approximated in TESPAROD for water by:

$$T_{DNB} = T_{sat} + \begin{cases} 3\, p_{System}\ [bar] + 40\ K & \Longrightarrow\ p_{system} < 20\ bar \\ 100\ K & \Longrightarrow\ p_{system} > 20\ bar \end{cases}$$

Film Boiling

When DNB has been identified, the HTC value reduces roughly by 2 orders of magnitude. The heat transfer is dominated by radiation and convection heat transfer provoked by droplet movement in a steam layer surrounding the fuel rod cladding surface. The heat flux in TESPAROD utilizes the Stefan-Boltzmann law of radiation which is adapted in order to account for the convective heat transfer due to droplet movement. The resulting HTC-value is:

$$HTC_{Film\ boiling} = 9 * 5.6697\ 10^{-8}\ \left[\frac{W}{m^2 K^4}\right] (T_{surface}^2 + T_{Fluid}^2)(T_{surface} + T_{Fluid})$$

Rewetting

The prevailing film boiling heat transfer turns into rewetting heat transfer if both conditions are satisfied, first the cladding surface temperature starts to decrease (culmination of cladding surface temperature is exceeded) and second the cladding surface temperature falls below the rewetting temperature which depends on the Leidenfrost temperature. The Leidenfrost temperature is predicted according to Schröder-Richter's analytical model [66]. The rewetting temperature is predicted in TESPAROD with:

$$T_{rewetting} = 0.75\ T_{culmination} + 0.25\ T_{Leidenfrost}$$

During rewetting the HTC-value increases in accordance to a quadratic temperature interpolation which is given with:

$$\text{Interpolation}_{\text{film boiling}\rightarrow\text{nucleate boiling}} = \left[\frac{T_{\text{rewetting}} - T_{\text{surface}}}{T_{\text{rewetting}} - T_{\text{DNB}}}\right]^2$$

The resulting heat transfer is:

$$HTC_{\text{rewetting}} = HTC_{\text{nucleate boiling}}\text{Interpolation} + HTC_{\text{film boiling}}(1 - \text{Interpolation})$$

9.7 TRANSURANUS

Thermal analysis

The calculation of temperatures in a fuel rod is one of the primary goals of fuel element modelling. The accuracy of these calculations strongly influences temperature-dependent physical phenomena such as fission, gas diffusion and release, restructuring creep, thermal expansion, etc. Due to the numerous non-linearity involved, only numerical solution techniques are possible.

In the TRANSURANUS code thermal analysis of an integral fuel rod is obtained by a superposition of one-dimensional radial and axial energy conservation equations (heat conduction equation for fuel, cladding and structure). Moreover the conservation equations of mass, momentum and energy for the coolant are solved.

The free boundary conditions for the thermal analysis depend on the geometry considered. The geometry is defined by variable ifalll(l) while the option for selecting a structure surrounding the fuel rod is defined by istruk variable. Finally the variable ikuel defines whether the coolant is treated or not. TRANSURANUS code allows the following types of geometrical analysis:

- Analysis of cladding only
- Analysis of fuel only
- Analysis of fuel and cladding
- Analysis of fuel, cladding and coolant
- Analysis of fuel, cladding, coolant and structure

To obtain the desired conditions the user has to select the variables mentioned above during the input file preparation.

From the coolant point of view, two options are available:

- The coolant temperature is prescribed (i.e. is part of the input deck) as a function of the axial position and time (ikuehl = 1).
- The coolant temperature is calculated based on a prescribed coolant inlet temperature and mass flow rate which may depend on the axial position and time (ikuehl = 0).
- For the solids, fuel, cladding and structure in principle temperature (Dirichlet condition) or heat flux (Neumann condition) may be prescribed at a free surface.

Gap conductance: Heat Transfer Coefficient between fuel and cladding

In the TRANSURANUS code the heat transfer coefficient h between fuel and cladding (gap conductance) is calculated by the URGAP model.

By the URGAP model the gap conductance is accurately described for very different conditions, e.g. material pairings (TRANSURANUS can deal with Zircaloy or Stainless Steel as clad and UO_2 or UC or UN as fuel), gas and contact pressure, surface roughness of fuel and cladding, gap width, gas temperature and composition.

The URGAP model is applicable for vacuum (closed gap) conditions, sodium, different gas and gas mixtures. It offers 4 options for gas mixtures:

- ihgap = 0: the thermal conductivity of the gas mixture is calculated according to Lindsay and Bromley, accommodation coefficients are taken into account.
- ihgap = 3: the thermal conductivity of the gas mixture is calculated according to Lindsay and Bromley, accommodation coefficients are not taken into account.
- ihgap = 4: the thermal conductivity of the gas mixture is calculated according to Tondon and Saxena, accommodation coefficients are taken into account.
- ihgap = 5: the thermal conductivity of the gas mixture is calculated according to Tondon and Saxena, accommodation coefficients are not taken into account.

The original URGAP model from 1979 was revised and recalibrated in 1986 using an extended database consisting of approximately 1000 data. This database covers the following reactor conditions:

- Material pairings : UO2-Zircaloy, UO2-steel
- Gas pressure : 0 – 14 MPa
- Contact pressure : 0 – 50 MPa
- Surface roughness fuel : 0.25 – 14.4 µm
- Surface roughness cladding : 0.17 – 4.5 µm

Heat Transfer Coefficient between fuel and coolant

In the TRANSURANUS code the heat transfer coefficient α between the outer fuel rod temperature and the bulk coolant temperature can be calculated (with standard option ialpha = 0) or it can be prescribed by the user (with option ialpha = 1). In the TRANSURANUS code two main geometrical configurations are considered: the annular flow concept and the circular flow concept.

In the annular flow concept the coolant channel is modelled as a concentric annular ring with an inner diameter D_i (which is the outer fuel pin diameter) and an equivalent outer diameter D_0. Thus, annular flow is assumed. The equivalent outer diameter D_0 is calculated by the code for several configurations, selected by the user setting the variable ikueka. The hydraulic diameter dhyd, which characterizes the heat transfer, is given by:

$$d_{hyd} = D_0 - D_i$$

The annular flow configuration is selected by the model option ihydd = 0 in the input file.

In the circular flow concept the coolant channel is treated as a flow in a circular tube. The heat transfer is characterized by an equivalent hydraulic diameter dhyd given by:

$$d_{hyd} = 4A_c/P_w$$

where A_c is the flow area and P_w the wetted perimeter. This thermal hydraulic mode is selected by the model option ihydd = 1 in the input file.

Both concepts give different hydraulic diameters and, therefore, also differ in Reynold numbers. Consequently, the heat transfer coefficients between coolant and cladding differ as well. Although this difference is usually quite small, it may be relevant if temperature sensitive corrosion correlations are used. The user should select the most appropriate according to the concerned analysis.

The heat transfer regions encountered when liquid is flowing along a vertical heated tube, can be subdivided in several regions depending on the temperature. In the lower part there is single phase convective heat transfer, where the clad wall temperature is displaced above the bulk fluid temperature. For fully developed turbulent forced flow of a gas or non-metallic liquid (e.g. water) along a smooth tube, the most widely quoted equation is that of Dittus and Boelter:

$$Nu = 0.023Re^{0.8}\ Pr^{0.4}$$

where the fluid properties are calculated at the bulk coolant temperature.

When the clad wall temperature reaches a certain value a few nucleation sites become available for boiling. However, boiling cannot occur until the tube wall temperature exceeds the saturation temperature, because bubbles that have nucleated and grown by the hot wall move out into the flow until they encounter sub cooled liquid where they collapse.

The amount by which the wall temperature exceeds the saturation temperature is known as the "degree of superheat" (ΔT_{sat}) and the difference between the saturation temperature and the local bulk fluid temperature is known as the "degree of sub cooling" (see Figure 0.6). Once the bulk liquid reaches the saturation temperature bubbles start to move throughout the flow cross section and the bubbly flow regime starts. In the saturated boiling region, the temperature difference and, therefore, the heat transfer coefficient remains constant (at constant heat flux).

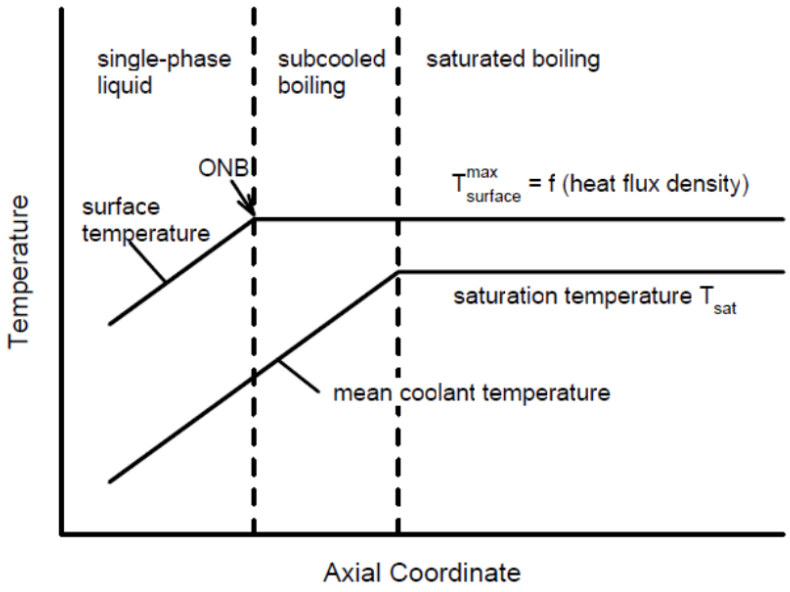

Figure 0.6: Transuranus – Clad surface and liquid temperature distribution in single-phase, subcooled and saturated boiling. ONB = onset of subcooled nucleate boiling

In the nucleate boiling regime a good heat transfer is due partly to the breaking up of the laminar layer of liquid next to the wall by the turbulence associated with the growth and departure of the bubbles, and partly to the evaporation of liquid underneath the growing bubble in contact with the wall, which takes away latent heat.

The Jens-Lottes correlation for fully developed nucleate boiling, adopted in code, is as follow:

$$\Delta T_{sat} = 25\ (q''_{rod,o})^{0.25}\ e^{-p/62}$$

where T_{sat} is the saturation temperature, ΔT_{sat} is the difference between the surface temperature $T_{surface}$ and the saturation temperature, and where q" is in MW/m^2 and p is in bar.

The Jens-Lottes correlation is not given in the form of a heat transfer coefficient. However, according to the simplified model applied in TRANSURANUS for sub cooled boiling or surface boiling (selected by the user through the model option isurfb = 1), an equivalent heat transfer coefficient can be computed by the following equation:

$$\alpha = \frac{(q''_{rod.o})}{(T_{sat} + \Delta T_{sat} - T_c)}$$